PRENOLIN: International Benchmark on 1D Nonlinear SiteResponse Analysis—Validation Phase Exercise

Bulletin of the Seismological Society of America

PRENOLIN: international benchmark on 1D nonlinear site response analysis - Validation phase exercise.

--Manuscript Draft--

Manuscript Number:	BSSA-D-17-00210R1
Article Type:	Article
Section/Category:	Regular Issue
Full Title:	PRENOLIN: international benchmark on 1D nonlinear site response analysis - Validation phase exercise.
Corresponding Author:	Julie Regnier, Ph.D. CEREMA Nice, FRANCE
Corresponding Author's Institution:	CEREMA
Corresponding Author E-Mail:	julie.regnier@cerema.fr
Order of Authors:	Julie Regnier, Ph.D.
	Luis-Fabian Bonilla, Phd
	Pierre-Yves Bard, Phd
	Etienne Bertrand, Phd
	Fabrice Hollender, Phd
	Hiroshi Kawase, Phd
	Deborah Sicilia, Phd
	Pedro Arduino
	Angelo Armorosi
	Dominiki Asimaki
	Daniela Boldini
	Long Chen
	anna Chiaradonna
	Florent Demartin
	Ahmed Elgamal
	Gaetano Falcone
	Evelyne Foerster
	Sebastiano FOTI
	Evangelia Garini
	George Gazetas
	Céline Gélis
	Alborz Ghofrani
	amalia Giannakou
	Jim Gingery
	Nathalie GLINSKY
	Josepth Harmon
	Youssef M.A. Hashash

	Susumu Iai
	Steven Kramer
	stravroula Kontoe
	jozef Kristek
	giuseppe lanzo
	Annamaria Di Lernia
	Fernando Lopez-caballero
	Marianne Marot
	Graeme McAllister
	E Diego Mercerat
	Peter Moczo
	Silvana Montoya-noguera
	Michael Musrgrove
	Alex NIETO-FERRO
	Alessandro Pagliaroli
	FEDERICO PASSERI
	Aneta Richterova
	suwal Sajana
	Maria-Paola Santisi
	Jian Shi
	Francesco Silvestri
	Mahdi Taiebat
	Giuseppe Tropeano
	Didrik VANDEPUTTE
	Luca Verrucci

Abstract:	This article presents the main results of the validation phase of the PRENOLIN project. PRENOLIN is an international benchmark on 1-D non-linear site response analysis. This project involved 19 teams with 23 different codes tested. It was divided into two phases; with the first phase verifying the numerical solution of these codes on idealized soil profiles using simple signals and real seismic records. The second phase described in this paper referred to code validation for the analysis of real instrumented sites. This validation phase was performed on two sites (KSRH10 and Sendai) of the Japanese strong-motion networks KiK-net and PARI, respectively, with a pair of accelerometers at surface and depth. Extensive additional site characterizations were performed at both sites involving in-situ and laboratory measurements of the soil properties. At each site, sets of input motions were selected to represent different PGA and frequency content. It was found that the code-to-code variability given by the standard deviation of the computed surface response spectra is around 0.1 (in log10 scale) regardless of the site and input motions. This indicates a quite large influence of the numerical methods on site effect assessment and more generally on seismic hazard. Besides, it was observed that site-specific measurements are of primary importance and their interpretation needs careful attention when compared with reference results given in the literature. Finally, the lessons learned from this exercise are synthetized, resulting also in a few recommendations for future benchmarking studies, and the use of 1D NL, total stress site response analysis.

Author Comments:	Dear Editor,

	This is the second paper we are publishing on this benchnmark exercice called PRENOLIN. The last paper was published last year in BSSA. As you will see, the co-author list is long and we understand it can come with difficulties for editorial subject but it reflects the number of researchers that participate to this project either as organization team or players of this benchmark. All of the co-authors provided corrections to the manuscript presented here. We were very pleased with the decision of BSSA to agree on that list for the previous paper and we hope that you will provide as well a positive answer for this article. Very kind regards Julie Régnier on the behalf of the PRENOLIN organization team (7 first co-authors)
Suggested Reviewers:	Johnathan Stewart jstewart@seas.ucla.edu
Opposed Reviewers:	
Response to Reviewers:	The response to the reviewers is include in the uploaded files

PRENOLIN: international benchmark on 1D nonlinear site response analysis – Validation phase exercise

Julie Régnier[*]

Luis-Fabian Bonilla IFSTTAR, Paris, France

Pierre-Yves Bard IFSTTAR/ISterre, Paris-Grenoble, France

Etienne Bertrand, CEREMA, Nice, France

Fabrice Hollender, CEA, Cadarache, France

Hiroshi Kawase, DPRI, Kyoto, Japan

Deborah Sicilia, EDF, Aix-en-provence, France

Pedro Arduino, University of Washington, US

Angelo Amorosi, Sapienza University of Rome, Italy

Dominiki Asimaki, Caltech, Pasadena, US

Daniela Boldini, University of Bologna, Italy

[*] *Julie.regnier@cerema.fr,* Cerema, Equipe-Projet MOUVGS, 500 routes des Lucioles, Sophia-Antipolis, F-06903, France

15 Long Chen, Univ. Washington, Seattle, US

16 Anna Chiaradonna, Univ. Napoli, Italy

17 Florent DeMartin, BRGM, Orléans, France

18 Ahmed Elgamal, UC, San Diego, La Jolla, CA, US

19 Gaetano Falcone, Politecnico of Bari, Italy

20 Evelyne Foerster, CEA, Saclay, France

21 Sebastiano Foti, Politecnico di Torino, Torino, Italy

22 Evangelia Garini, NTUA, Athena, Greece

23 George Gazetas, NTUA, Athena, Greece

24 Céline Gélis, IRSN, Fontenay-aux-roses, France

25 Alborz Ghofrani, Univ. Washington, Seattle, US

26 Amalia Giannakou, Fugro, Greece

27 Jim Gingery, UCSD, San Diego, US

28 Nathalie Glinsky, CEREMA, Nice, France

29 Joseph Harmon, Univ. Illinois at Urbana-Champaign, US

30 Youssef Hashash, Univ. Illinois at Urbana-Champaign, US

31 Susumu Iai, DPRI, Kyoto, Japan

32 Steve Kramer, Univ. of Washington, US

33 Stavroula Kontoe, Imperial College, London, England

Jozef Kristek, CUB, Bratislava, Slovakia

Giuseppe Lanzo, Univ. Rome, Rome, Italy

Annamaria di Lernia, Politecnico of Bari, Italy

Fernando Lopez-Caballero, Centrale Supélec Paris, France

Marianne Marot, CEREMA, Nice, France

Graeme McAllister, University of British Columbia, Canada

E.Diego Mercerat, CEREMA, Nice, France

Peter Moczo, CUB, Bratislava, Slovakia

Silvana Montoya-Noguera, Centrale Supélec, France

Michael Musgrove, Univ. Illinois, US

Alex Nieto-Ferro, EDF Lab Paris Saclay, France

Alessandro Pagliaroli, CNR-IGAG, Rome, Italy

Federico Passeri, Politecnico di Torino, Torino, Italy

Aneta Richterova, CUB, Bratislava, Slovakia

Suwal Sajana, Univ. Rome, Rome, Italy

Maria Paola Santisi d'Avila, UNS, Nice, France

Jian Shi, Caltech, Pasadena, US

Francesco Silvestri, Univ. Napoli, Napoli, Italy

Mahdi Taiebat, University of British Columbia, Canada

Giuseppe Tropeano, Univ. Cagliari, Cagliari, Italy

Didrik Vandeputte, EDF, Aix-en-Provence, France

Luca Verrucci, Univ. Rome, Rome, Italy.[*]

[*] The author's list involves first the seven organizers of the PRENOLIN project followed by the participants in an alphabetic order.

Abstract

This article presents the main results of the validation phase of the PRENOLIN project. PRENOLIN is an international benchmark on 1-D non-linear site response analysis. This project involved 19 teams with 23 different codes tested. It was divided into two phases; with the first phase verifying the numerical solution of these codes on idealized soil profiles using simple signals and real seismic records. The second phase described in this paper referred to code validation for the analysis of real instrumented sites.

This validation phase was performed on two sites (KSRH10 and Sendai) of the Japanese strong-motion networks KiK-net and PARI, respectively, with a pair of accelerometers at surface and depth. Extensive additional site characterizations were performed at both sites involving in-situ and laboratory measurements of the soil properties. At each site, sets of input motions were selected to represent different PGA and frequency content. It was found that the code-to-code variability given by the standard deviation of the computed surface response spectra is around 0.1 (in log10 scale) regardless of the site and input motions. This indicates a quite large influence of the numerical methods on site effect assessment and more generally on seismic hazard. Besides, it was observed that site-specific measurements are of primary importance for defining the input data in site response analysis. The non-linear parameters obtain from the laboratory measurements should be compared with curves coming from the literature. Finally, the lessons learned from this exercise are synthetized, resulting also in a few recommendations for future benchmarking studies, and the use of 1D NL, total stress site response analysis.

Introduction

In seismology and earthquake engineering, site effects are widely recognized as an important factor for (mainly) amplifying the resulting surface ground motion. Those site effects are spatially variable depending on the local geomorphology and mechanical properties of the soil; they may vary from one event to the other as the site response to seismic loading is non-linear during strong ground motion (e.g. Amorosi et al., 2016; Bonilla et al., 2005; Gunturi et al., 1998; Zeghal et al., 1995; Ishibashi and Zhang, 1993; Yu et al., 1993; Elgamal et al., 1995; Vucetic and Dobry, 1991; Seed, 1969).

Site-specific analysis of the site response involving its non-linear soil behavior is still very challenging. In low seismicity areas, the lack of strong ground motion recordings limits empirical evaluations. To overcome this limitation, numerical simulations are of primary interest since they allow for simulating strong ground motions beyond the available recordings. In engineering practice, those analyses would, in most of the cases, be limited to methods involving the use of linear or equivalent linear methods in a 1-D site configuration.

As mentioned in the preceding companion paper (Régnier et al., 2016a), previous comparative tests were performed to study 1-D non-linear site response. The first blind tests performed in the late 80's/early 90's, on the Ashigara Valley (Japan) and Turkey Flat (California) sites were very instructive in the linear domain, because of the lack of strong motion recordings at that time. The 2004 Parkfield earthquake, which produced 0.3 g at Turkey Flat site, was the opportunity to launch a new benchmarking exercise for 1D non-linear codes. This also considered a few other sites with vertical array data and large enough ground motion (La Cienega, California; the KGWH02 KiK-net site, Japan;

and a site in Lotung, Taiwan). The results reported in Stewart et al. (2008), Kwok et al. (2008), and Stewart and Kwok (2008, 2009) emphasized the importance of the needed in-situ measurements and of the actual way these codes are used. The origin of the significant mismatch between records and predictions has been attributed to incorrect velocity profiles (despite the redundant borehole measurements), to deviations from 1D geometry (non-horizontal soil layers), and deficiencies in the constitutive models (unsatisfactory match to the actual degradation curves). The 1D codes used for these tests remain, however, extensively used in routine engineering practice for site response estimates, and various developments have been carried out to implement new, or updated, constitutive models, It is therefore needed to repeat such benchmarking activities, notably in other parts of the world which may have different engineering practice, and which were not involved in the previous comparison exercises (which are always good also for young scientists and engineers who never had such a benchmarking experience).

The objective of this two-phase (verification and validation) PRENOLIN exercise is to understand the variability associated to the implementation of the non-linear soil behavior in numerical simulations, and to assess the resulting uncertainties. It was decided to devote the calculations on simple cases focusing on the numerical implementation of the non-linear soil behavior (rheology and soil parameters) to be as close as possible to the standard engineering practice.

In this work we evaluate 1-D wave propagation of SH waves (only one component of motion) having vertical incidence and assuming no pore pressure effects (total stress analysis). These three assumptions mentioned above are not a sensitive issue when dealing with the verification case (although realistic cases were selected to be close to the true physical processes). However, when dealing with validation and comparison with real data, they may have very strong impacts and for most sites and input motions they might be violated to various degrees.

We choose our sites for the validation to minimize the impact of those assumptions.

The verification phase helped to create a synergy between the participants and the organizing teams. We defined a common vocabulary for the implementation of the calculations (as the Non-Linear (NL) communities from different areas of the world may have different practice and a different understanding of the same words). By analyzing the whole set of NL simulations, we found that the code-to-code variability increases with the shear strain level. However, even in the worst case corresponding to large loading and strain levels exceeding 1%, it remained lower than the single-station, random variability of GMPE σ values for PGA. Given the scatter in the nonlinear results, we thus concluded that a realistic analysis should use more than one constitutive model to incorporate at least partially the epistemic uncertainty in site response computations. It was also found that, in order to reduce the epistemic uncertainty, which is partially accounted for by the code-to-code variability, one may need to precisely describe specific input parameters, especially the soil shear strength profile. In addition, the variability between code is considerably reduced when they all used the same loading and unloading process (Masing rules or non-Masing rules, referred to as damping control models) (Régnier et al., 2016a)

To keep this exercise relatively simple, it was decided from the beginning not to deal with the problem of pore pressure effects (e.g. Elgamal et al., 1996; Zeghal et al., 1995). We acknowledge that this hypothesis might not be realistic in saturated soils subjected to strong-motion cyclic loads. One of the chosen PARI sites (Onahama) may have experienced cyclic mobility during the Tohoku-Oki, Mw 9 March 11th, 2011 earthquake (Roten et al., 2013). However, dealing with nonlinear site response increases the number of soil parameters to consider, not only with respect to traditional linear estimates, but also in relation to the complexity of the constitutive model used to describe the soil non-linear behavior. Since soil nonlinear behavior, even in the absence of pore pressure effects, remains a challenge, the main effort of the validation exercise was focused on total stress analysis only, disregarding the simulation of excess pore pressure generation. To verify effects of water pressure build-up on the recordings acceleration time history, some teams used site response analyses with excess pore water pressure generation to compare with the total stress cases and are shown in the electronic supplement (Figure S6 and S7). The recommendations of this report are only for total stress site response analyses.

A detailed presentation of the organization of the project and the participant teams was done in the previous paper related to the verification phase (Régnier et al., 2016a). The table of the participants with description of the methods is thus provided here only in the electronic supplement (Table S1).

The objectives of this paper are to share the experiences on the validation exercise concerning (i) the analysis of data from laboratory and in-situ tests data to define the input soil parameters for the simulations, (ii) the processing and selection of the seismic input motions, (iii) the calculations of the non-linear site response and finally (iv) to quantify the epistemic uncertainty for 1-D nonlinear site response analysis on real sites, both in terms of code-to-code variability and code-to-data distance.

Target sites

Selection criteria

The selection of sites was performed on strong-motion databases involving vertical arrays so that the empirical soil column response (often called transfer function) can be calculated. Considering the hypothesis of the numerical methods and the objective to implement non-linear soil behavior, the sites were selected on the basis of the following requirements:

(1) Availability of both strong and weak motion recordings,

(2) Plausibility of 1-D geometrical soil configuration, i.e. satisfactory agreement between numerical and empirical site responses in the linear / weak-motion range,

(3) The depth of downhole sensor must be less than 300 m.

(4) the possibility to perform complementary investigations in the immediate proximity of the site

To fulfill the first and second criteria, sites that recorded at least two earthquakes with PGAs higher than 50 cm/s^2 at the downhole sensor were selected. Only the KiK-net site configurations identified as fulfilling the 1D criteria proposed by Thompson et al. (2012) and Régnier et al. (2014) were considered. In addition, a visual comparison between the numerical and empirical site response curves was performed and a special attention was given to the matching of fundamental resonance frequency.

The fourth criterion also constrained the site selection, as the nearby urbanization may prevent the drilling of new boreholes or the ability to perform new surface measurements.

Dataset

Presentation

The sites selection was done on the KiK-net and PARI (Port and Airport Research Institute) networks. KiK-net is composed of 688 stations, with high-quality surface and downhole digital 3-component accelerometers. Among the KiK-net sites, 668 are characterized with shear and compressive wave-velocity profiles. These velocity profiles were obtained from downhole or PS logging measurements (depending on the site). Most of the borehole sensors are located between 100 m and 200 m depth. Two thirds of the sites have a Vs30<550 m/s. In the NEHRP and Eurocode 8 regulation, sites with Vs30< 800 m/s are classified as sites prone to site effects, which confirms that the KiK-net database is very interesting for the analysis of these phenomena. The PARI sites are much shallower than the KiK-net sites: the down-hole sensor depth is around 10 m and the corresponding Vs profile is also available.

Data processing

More than 46,000 (six component) recordings were analyzed beforehand (Régnier et al., 2013) to derive the empirical site response (i.e., the transfer function from downhole to surface) at the 688 sites. In addition, on 668 sites with available Vs profiles, the numerical linear site response was also calculated on the basis of the velocity profile provided in the KiK-net data base (see Data and resource section). On the PARI network, only two sites were analyzed: Sendai (30 earthquake recordings), and Onahama (42 earthquake recordings).

The empirical site response is usually evaluated by using a spectral ratio between simultaneous recordings on sediments and on a nearby rock site (the so-called reference site). When this technique is applied, the main issue to overcome is the selection of a reliable reference site. The reference site should not amplify seismic waves, and should be close enough to the studied site so that the travel path from the seismic source remains equivalent for both sites.

Vertical arrays of accelerometers overcome the reference-site issue. Indeed, the down-hole station located at depth represents the reference station. Thus, for each KiK-net (and PARI) sites and each earthquake recording, the Borehole Fourier Spectral Ratio (*BFSR*) were calculated. *BFSR* is the ratio between the Fourier spectra of the horizontal components recorded at the surface and the corresponding ones at depth. Yet we acknowledge that the use of downhole records introduces an additional difficulty in numerical modeling due to the contamination of the control motion by the downgoing wavefield, which is sensitive both to the details of velocity and damping soil profile, and to the complexity of the incoming wavefield (various types of body waves with multiple incidence angles, together with possibility of surface waves, see Bonilla et al., 2002; Régnier et al., 2014).

Before evaluating the *BFSR* a specific data processing procedure was applied that consisted in removing the mean, applying a tapering Hanning window on 2% of the signal, non-causal filtering between 0.1 and 40 Hz, FFT calculation and a Konno-Omachi smoothing (with $b = 40$) before performing the surface to down-hole spectral ratio. The linear site response was obtained by calculating the geometric average of all recordings with a PGA at the surface below 25 cm/s^2.

The empirical site response curves were compared to the equivalent numerical ones ($BFSR_{num}$). The numerical site responses ($BFSR_{num}$ and $OFSR_{num}$, indicating respectively the transfer functions having the reference at the down-hole and at the rock outcrop, respectively) were computed using a Haskell-Thomson 1-D linear method (Haskell, 1953; Thomson, 1950). For the calculation of the transfer function, we also added a Konno-Ohmachi smoothing (*b = 40*) that was applied directly to the transfer function curve (since it is the direct result from the Haskell-Thomson method) and the same frequency sampling as the one dealing with the analysis of earthquake recordings was used.

The soil parameters that are required to compute the numerical transfer functions are the shear wave velocity profile *Vs*, the density profile and the quality factor profile. In the KiK-net (and PARI) database, only the Vs profiles are available. For the density, a constant value along the profile equal to 2000 Kg/m^3 was used. The quality factor (*Q*) was directly derived from the Vs value following the rule of thumb scaling : $Q = Vs/10$ (Olsen et al., 2003) used by many authors when no measurement is available from laboratory data measurements (see section "*From in-situ and lab data to input parameters*"). Others models for the low strain attenuation could have been used as well such as proposed in (Darendeli, 2001; Menq, 2003).

Selected sites

5 KiK-net sites (FKSH14, IBRH13, IWTH04, KSRH10 and NIGH13) passed the selection criteria, together with the 2 PARI sites that were initially chosen. Four KiK-net sites were removed for various reasons: liquefaction susceptibility (FKSH14), rocky geology (IBRH13), mountainous environment (IWTH04) and insufficient nonlinearity (NIGH13). A detailed study on the effects of the topography and non-horizontal layering on waveforms and transfer functions of KiK-net sites can be found in De Martin et al., (2013).

The three remaining sites, i.e., KSRH10, Onahama and Sendai sites were therefore selected for further in-situ investigations for the purpose of the validation phase. Later on, for the Onahama site, it was found that the soil was susceptible to liquefaction (Roten et al., 2013) and clearly show 2D/3D site configuration. Consequently, the calculations performed on this site will not be presented in the present paper, although they were part of the validation phase.

The locations of KSRH10 (Hokkaido region) and Sendai (Tohoku region) are illustrated in Figure 1.

Figure 1

According to the initial available geotechnical data, KSRH10 is mainly composed of clayey soil while Sendai site is composed of sandy soil. KSRH10 site is a deep sedimentary site with 40m of low velocity soil layers; the down-hole sensor is located at a depth of 255m (plot (a) of Figure 2). The site is located on the lower plateaus with about 30m in elevation along the right bank (southern) side of the upper Anebetsu River. The soil column consists of recent Younger Volcanic Ash deposits until 5m at depth, followed by volcanic and Tuffaceous sand until 40m and underlie by an alternation of sandstone and shale.

The Sendai site is a shallow site with 7 m of soft soil deposits and with the down-hole sensor located at 10.4m at depth. According to the Shogama 1:50 000 geological map, the site is in a large flat valley covered by beach ridge deposits (Holocene) consisting of gravel and sand. These surface deposits are underlain by the Pliocene, Geba Formation, forming the northern and eastern hills and consist of gravel stone, sandstone, tuff, tuffaceous siltstone, and lignite.

As illustrated in Figure 2 (plots b and e), empirical weak motion BFSR (surface PGA lower than 25 cm/s^2) and the linear numerical 1-D site response (dotted black line) exhibit a satisfactory similarity, especially for Sendai site. The shallow Sendai site is characterized by a high resonance frequency around 8.2 Hz, while the thicker KSRH10 site is characterized by a lower fundamental resonance frequency of 1.7 Hz; slight differences can be seen however between observations and simulations as to the frequencies of the first two peaks. The numerical simulations (dotted lines) provide site response amplitude much higher at the first two frequency peaks and above 15Hz while it is lower for the third and fourth peaks. This first comparison shows that the sites are close to a 1-D site configuration, but exhibit a more complex behavior than those predicted for a simple soil column subjected to pure vertically incident plane S waves.

When the sites were selected for the validation, one of the requirements was that the sites exhibit some non-linear soil behavior for one or several recordings. In Figure 2 (plots c and f) the BFSR for weak motion is compared to the BFSR calculated from motions with large PGA at the surface. For KSRH10, non-linear soil behavior is significant for the input motions with PGA greater than 47 cm/s^2 at the down-hole station (outside the average ± standard deviation area) and it is even greater for the strongest events (KSRH100411290332 with PGA equal to 81 cm/s2 and KSRH100309260450 with PGA equal to 110 cm/s^2 – table 1). For Sendai, non-linear soil behavior is significant when the downhole PGA exceeds 46 cm/s^2 (outside the average ± standard deviation area) and it is even greater for the strongest event (F-2958 with PGA equal to 252 cm/s2).

Figure 2

Selection of the input motions

A selection of 10 and 9 input motions for KSRH10 and Sendai, respectively was performed among the available earthquake recordings. Their epicenters, magnitudes and peak accelerations at the surface are illustrated in Figure 1 and provided in table 1. The site response computations were performed on 5 input motions at KSRH10 (TS-0-K, TS-1-K, TS-2-K, TS-4-K and TS-9-K) and 4 at Sendai (TS-1-S, TS-2-S, TS-5-S and TS-8-S), numbered from strongest to weakest. Only the results of these input motions are shown in this article. Nevertheless, we provide the information for all available input motions as they may be used for future validation exercises.

The PGA and the frequency content of a recording are two relevant parameters of the input motion for describing the expected degree of non-linear soil behavior (Assimaki and Li, 2012; Régnier et al., 2016b). The input motions for KSRH10 and Sendai sites were selected with 3 different PGA levels (at the downhole sensor), respectively. The PGA was calculated on the acceleration time histories of the geometrical mean of the EW and NS components, filtered between 0.1 and 40 Hz. In each group of PGA level, we quantified the frequency content using the central frequency following Eq 1 (statistical moments order 2 and 0, Sato et al., 1996) but the values were not significantly variable from one event to another. We therefore also considered several magnitudes and epicentral distances couples.

$$Fc = \sqrt{\frac{\int f^2 A^2(f)df}{\int A^2(f)df}}$$

Eq 1

where *Fc* is the central frequency, *f* the frequency, *A(f)* the amplitude of the Fourier Spectrum of the accelerogram. The resulting values exhibit a significant but rather erratic variability, without obvious link to magnitude, epicentral distance or depth. We therefore also considered several magnitudes and epicentral distances couples.

The selected events for the KSRH10 and Sendai sites are listed in the Table 1 along with their main characteristics (Mw, depth, epicentral distance, PGA at the down-hole and at the surface, and central frequency at the down-hole recording). The frequency sampling at KiK-net is between 100 and 200 Hz depending on the event and at Sendai it is 100 Hz. For KSRH10, four input motions with PGA at the down-hole sensor higher than 50 cm/s^2 were available and selected, whereas only 3 were available in Sendai site.

Table 1

Signal to noise ratio

We checked the quality of all events by assuring that their signal-to-noise ratios were high enough (S/N>3) over a broad frequency spectrum of 0.1 to 50 Hz, for all three components.

Orientation of the surface to down-hole sensors

We checked that both surface and down-hole sensors are oriented in a similar way. We rotated anti-clockwise the surface horizontal components with a 1° azimuth increment, starting from the original EW orientation, and we calculated the correlation coefficient with the down-hole EW component. Both signals were filtered between 0.1 and 1 Hz. The angle characterized by the maximum correlation would approximately correspond to the angle between the two EW components of the surface and the down-hole sensors. Correlations are maximum without rotation angles at Sendai and at KSRH10. It is close to the calculations performed by D. Kosaka (PARI) who found a deviation of 7.2° counterclockwise at Sendai also using long period motions correlations. Results are approximately similar to the results of Maeda et al. (2005) who found a deviation of 2.2° clockwise at KSRH10. These values suggest that both surface and down-hole EW-components are mostly oriented parallel one to each other, and even if slight deviations of the order of 7° may occur, it would not impact significantly the soil response functions.

Verification of the verticality of the incident waves

Basic assumptions are made in most 1D simulation codes when propagating a wave through a soil column. One of them is that the wavefield consists of vertically propagating plane S waves; hence the input wave motion at the bottom of the soil column is fully represented by the horizontal components and all vertically propagated towards the surface. However, except for teleseismic (long-distance) events, the seismic waves from local or regional events are very likely to have not only non-vertical incidence (unless located directly underneath the sensor), but also multiple incidence because of crustal scattering

Recording a non-vertical incident wavefield implies that the total seismic energy is distributed all over the three components. Therefore, if only one component of the 3D wavefield is used to represent one type of seismic phase (in our case, the shear wave), then it is highly likely that the wave energy, PGA and strains are underestimated at the down-hole sensor. However, depending on the thickness of the soil column and its characteristics, the upward propagating body waves become increasingly vertical towards the surface and therefore the surface sensor will give a more complete representation of the entire shear wave energy on the horizontal components. Therefore, two consequences can result from this observation:

(1) Although both the numerical and empirical input motions are the same, their transfer functions would be different, since the energy on the horizontal components at the surface will be greater in the empirical observation at KSRH10 than the numerical simulations.

(2) The actual seismic loading at the base of the soil column is underestimated compared to what the soil experiences, and therefore its possible non-linear behavior can also be underestimated.

To determine the direction of propagation of an input motion, we used a polarization analysis based on the 3-component covariance matrix. In the electronic supplement (figure S1) we can see that at KSRH10, the polarization analysis indicates that the waves mostly propagate with a vertical incidence (low incidence angle). At Sendai, except for two recordings, the waves are not linearly polarized; therefore, the calculations of the direction of propagations are not relevant.

From in-situ and laboratory data to input parameters

Identifying the most relevant parameters to be used for simulating the non-linear wave propagation process in a soil deposit was one of the main challenges tackled during the verification exercise. For the elastic and visco-elastic properties, *Vs*, *Vp*, density and low strain attenuation profiles were used. For the non-linear soil properties, the modulus reduction and damping with shear strain curves, with the soil shear strength profile were found to be the key parameters to significantly reduce the code to code site response variability (Régnier et al., 2016). For more complicated non-linear models such as Hujeux (Aubry et al., 1982), more more laboratory measurements are required to define its model parameters, however some of this parameters could be defined using well known soil mechanics correlations.

The challenge for the validation phase was to determine the value of those parameters for a real site. The specifications for the laboratory and in-situ measurements were defined in accordance with the prescriptions coming from the organization team with a few associated geotechnical experts and the participating teams, and bounded by the available budget and the measurement capacity of the local company performing the measurements, together with a few logistical issues linked with the exact location of the vertical array and the surrounding environment.

Site investigation

Measurements performed

To obtain the linear and non-linear soil parameters, in-situ measurements and multiple laboratory measurements were conducted on disturbed and undisturbed soil samples.

The in-situ measurements were subcontracted to Oyo company and consisted in: (1) boring investigation to determine soil stratigraphy and to perform the soil sampling. The diameter of the borehole was 116 mm up to a depth where tripled-tube samplings were used (for sandy soil or relatively stiff clayey soil) then 86 mm; (2) Undisturbed soil samples (80 cm long) were collected using the thin-wall sampler for the soft clay soil and using the tripled-tube samplers for the sand and stiffer clayey soil; (3) Standard

Penetration Tests (SPT); (4) PS logging by suspension method for KSRH10 and down-hole method for Sendai, and (5) multiple MASW (Multichannel Analysis of surface Waves) at the investigated sites to characterize the spatial variability of the underground structure at shallow depth, together with single point ambient vibrations recordings. The laboratory soil tests were conducted on disturbed and undisturbed soil samples. The tests on disturbed samples enable to determine physical characteristics such as particle size distribution, liquid and Atterberg limits. The tests on undisturbed soil samples aim at defining the density and to perform a wide range of laboratory tests such as Undrained and drained tri-axial compressional test, oedometer tests by incremental loading, cyclic undrained and drained tri-axial compression test (undrained for investigating the liquefaction potential) and, for rock samples, unconfined compressional tests. The methods used to perform the laboratory tests are defined by Japanese normative specifications.

For each borehole, the number of undisturbed soil samples was defined according to the expected soil stratigraphy (on the basis of pre-existing KiK-net or PARI information), to ensure at least one sample in each homogeneous soil unit.

The number and location of soil samples are specified in Table 2 together with the down-hole sensor depth and the maximum depth of the complementary drillings. The details of the locations of the laboratory measurements are available in the electronic supplement (Figure S2 to S5). Figure 3 shows the locations of the boreholes having the accelerometers with respect to the boreholes performed for the laboratory measurements and the MASW lines.

Figure 3

Table 2

Uncertainties of soil parameter measurements

Because of the inherent variability of the soil and the systems errors in the measurements and sampling methods, a non-negligible level of uncertainty remains in the soil parameters measured through the laboratory tests. Repeatability of the soil samples and laboratory measurements are a possible way to ensure a reliable definition of the soil parameters. This approach was not applied in this exercise due to budget constraints. We therefore carefully analyzed the data and compared with literature data for similar types of soil.

To minimize the impact of soil spatial variability, the new boreholes were performed as close as possible to the instrumented ones. MASW lines performed between the two boreholes indicate a low spatial variability of the soil parameters for KSRH10 and Sendai (while they did indicate a significant variability at shallow depth for the third site in Onahama, which was also one of the reasons to drop this site for the validation exercise).

Interpretation of the laboratory and in-situ data

Elastic and visco-elastic properties

For the elastic properties, several methods were used to determine the soil parameters. We have preferred the methods that provide the direct in-situ evaluation of the soil properties, yet we did compare the results with alternative techniques characterized by indirect measurements. We used the PS logging to obtain the *Vs* profile and then we use the earthquake recordings to adjust it. As shown in Figure 4, the *Vs* profile was adjusted to improve the fit between the fundamental resonance frequency recorded and predicted for the KSRH10 and Sendai sites.

For KSRH10, the initial *Vs* profile was based on the PS logging investigation down to 50 m depth; beyond this depth, we considered the values of the Vs coming from the KiK-net database, where PS-logging method was used as well. In this project, it was decided to adjust the linear transfer function from Thomson-Haskell predictions to the instrumental observations of surface-borehole spectral ratios, to ensure that the discrepancies between the prediction and the observations during the benchmark were associated to non-linear soil behavior, and not to other causes.

To adjust the numerical linear transfer function to the observation, we modify mostly the *Vs* profile coming from KiK-net for which no information was available on the measurement.

For Sendai, to improve the fit between the weak motion site response calculated with linear site response analysis and computed from weak motions, a gradient type *Vs* profile (Eq 2) was chosen.

$$Vs = Vs_1 + (Vs_2 - Vs)\left[\frac{z - Z_1}{Z_2 - Z_1}\right]^{\alpha}$$

Eq 2

Where, Vs_1 = 140 m/s, Vs_2 = 460 m/s and α=0.7, Z_1 is the depth at which begin the gradient (0 m) and Z_2 (7 m) the depth where it finishes.

The Poisson coefficient (ν) was computed using the PS logging and rounded. To ensure consistency between the values of *Vs*, *Vp* and ν, the *Vp* parameter was obtained from *Vs* and the rounded ν. The density was obtained from the undisturbed soil sample and the low strain attenuation was deduced from the un-drained cyclic tri-axial test, and when not available by using the rule-of-thumb ($Qs = Vs/10$) (Olsen et al., 2003).

Figure 4

Non-linear soil properties

The initial plan was to use only the measured non-linear parameters, i.e., the degradation curves measured in the lab. It had however to be modified to ensure a better fit to the strong motion data: the non-linear soil properties were actually updated during the iterations of calculations, so that three sets of non-linear soil parameters were used. The first one (called SC1) came simply from the use of non-linear degradation parameters defined in the literature, and anchored to elastic soil properties. Here the Darendeli formulation was adopted (Darendeli, 2001). The second (SC2) and third (SC3) soil parameter sets are directly based on interpretations of the laboratory data. One objective of the benchmark was to focus on routine practice with relatively simple models. Furthermore, the participants were also free to build/use their own soil model based on the raw experimental laboratory test. Yet, additional non-linear soil parameters could have been tested as well, such as models that could handle both low and high strain as detailed in Groholski et al. (2016) and Yee et al. (2013).

Darendeli formulation (Darendeli, 2001) was used to define the G/G_{max} and damping ratio curves as a function of shear strain for SC1 soil column. To compute such values, the knowledge of the confining effective stress (σ'), the over consolidation ratio (OCR), the plasticity index (PI) and the damping ratio at low strains (D_{min}) was required.

The SC2 non-linear curves were constructed from the cyclic tri-axial compression test results. We normalized the Young's modulus decay curves (from the lab 5th cycle of loading) by the low strain Young's modulus (E_0). E_0 is the value of the hyperbolic model (Hardin and Drnevich, 1972) that mimics the lab results at 0.0001%. We assimilate this E/E_0 decay curve to the shear modulus G/G_{max} decay curve, with G_{max} associated to the in-situ velocity measurements, i.e., $G_{max} = \rho\ V_S^2$. The shear strain used, γ, was considered equal to 3/2 of the axial strain directly measured during the triaxial test. Indeed, the shear strain is the difference between the axial and radial strain $\gamma = \varepsilon_a - \varepsilon_r$. During the cyclic triaxial test under undrained conditions volumetric changes are zero: therefore, the volumetric strain is null $\varepsilon_v = \varepsilon_a + 2\varepsilon_r = 0$. From the previous two equations we can deduce that: $\gamma = 3/2\varepsilon_a$ (Vucetic and Dobry, 1988).

The elastic shear modulus values from the laboratory tests (G_{max}^{lab}) are generally under-estimated compared to the in-situ measurements (G_{max}^{insitu}), especially for cyclic tri-axial tests (indeed cyclic tri-axial tests are not reliable at low strain, below 10^{-4} %). Tatsuoka et al. (1995) showed that this could be due to sample disturbance where stronger differences are observed depending on the type of shear strain measurement. When local measurements of shear strain are performed using internal gauges (inside the soil sample) compared to external measurements (usual measurement), the discrepancies are much smaller.

When normalizing the shear modulus curve to obtain the $G/\ G_{max}^{lab}$ curve, the G_{max}^{lab} should be corrected. The coefficient of correction to be applied is not well defined but lies between 1.2 and 4 (Lopez-Caballero personal communication, 2015). A correction procedure was set up in this study to partially correct this value (Noguera, 2016). The procedure accounts for the measurements errors when using external measurements instead of local ones but does not consider error due to soil sample disturbance. Considering that this procedure was defined during the project (after the calculations on

Sendai site) it was only applied to the laboratory data for KSRH10 site.

The above-mentioned procedure consists in three steps: (1) to find the maximum shear modulus (G_{max}^{lab}) by fitting the logarithmic equation (Eq 3) proposed by (Nakagawa and Soga, 1995) as measured for intermediate strain values; (2) to compare the G_{max}^{lab} values found with those from other tests or in the literature. Note that this value should not be more than twice the G_{max}^{lab} as it only accounts for the external-to-local strain measurement error; (3) to normalize the fitted decay curve and multiply it by G_{max}^{insitu} value.

$$G/G_{\max}(\gamma) = \frac{1}{1+\alpha|\gamma|^{\beta}}$$

Eq 3

The SC3 model was built using the hyperbolic model (Eq 4 and Eq 5) constrained by the G_{max}^{insitu} and the shear strength (τ_{max}). The latter was estimated from the depth and the cohesion and friction properties according to Eq 6. This formula was derived from the Mohr circle for simple shear test (Hardin and Drnevich, 1972). The shear strength used here is the maximum shear stress not the maximum lateral shear stress, with the effective cohesion (c') and the friction angle (φ') coming from the monotonic compressional test and the coefficient of soil at rest (K_0) coming from Jaky's formula (*1-sin(φ'), Jaky, 1944)*.

$$G/G_{\max}(\gamma) = \frac{1}{1+\gamma/\gamma_{ref}}$$

Eq 4

$$\gamma_{ref} = \frac{\tau_{max}}{G_{max}}$$

Eq 5

$$\tau_{max} = \frac{(1+K_0)\sigma_0' \sin\varphi'}{2} + c'\cos\varphi'$$

Eq 6

The comparison of the non-linear curves is illustrated in Figure 5 and Figure 6 for KSRH10 and Sendai, respectively. For both sites, the SC1 non-linear curves have generally more shear modulus reduction for the same shear strain than those coming from the laboratory data, even after the correction procedure was applied.

The mechanical properties of the KSRH10 and Sendai sites are synthesized in *Table 3*

Table 4

and Table 4, respectively. For KSRH10, three sets of non-linear parameters were tested, whereas only the first two were tested on Sendai site. From in-situ surveys, the water table is located respectively at 2.4 m and 1.45 m below the ground surface for KSRH10 and Sendai site.

Table 3

Table 4

Figure 5

Figure 6

Validation results

Calculations performed

Two iterations of calculations were performed at KSRH10 and Sendai sites. The first iteration was completely blind (i.e. only input motions were given to the participants) while during the second one the surface motions were also provided. Three soil column models were tested for KSRH10 and two for Sendai. Both EW and NS components were used. In addition, the rotated horizontal motion corresponding to the maximum peak acceleration was considered; simulations using this rotated horizontal component were performed. However, the results were not significantly different from those obtained using the EW or NS components. Thus, these computations are not shown here.

All the participating teams were asked to provide the acceleration time histories and the stress-strain curves at different depths in the soil columns. For KSRH10, the acceleration time histories were computed at various ground levels from the surface (GL): 0, -6, -11, -15, -20, -24, -28, -25, -39, -44, -84 and -255 m depth, corresponding to the main soil layers interfaces. The stress-strain curves were computed at GL-3, -8.5, -13, -17.5, -22, -26, -31.5, -37, -41.5, -64 and -169.5 m, which correspond to the middle of the soil layers. For Sendai, the acceleration time history was provided from GL-0 to -8 m every 1 m, while the stress-strain curves from GL-0 . 5 to -7.5 m also every 1 m.

Analysis of results

This article focuses on the analysis of the whole dataset returned from each team to estimate the level of uncertainties associated to NL modelling.

Several sources of uncertainties are involved in 1-D non-linear site response analyses. On one hand, there are epistemic uncertainties coming from the main assumption of the method (1-D, vertical propagation of SH waves), soil parameters measurements (which should however impact all the predictions in the same way), the numerical model and the users. On the other hand, there are random uncertainties coming from the input motions, which are influenced by both the seismic sources and soil heterogeneities. We did use several input motions; however, the number of them is not sufficient to take into consideration all the random uncertainty ranges. The previous verification phase (Régnier et al., 2016) provided an estimation of the code-to-code variability linked to the numerical method such as numerical integration schemes, implementations of damping, constitutive models and users practice. Conversely, the validation phase involves comparison with observations and therefore calculations of residuals. We assume that the residual can be described as a random variable with normal distribution center around a non-necessarily zero mean (models may over or under-predict), with associated standard deviation.

We calculated and compared the misfit between the observations and the computations with the code-to-code variability of the surface response spectra averaged over a period band-width close to the resonance period of the site, namely [0.7 f_0, 1.3 f_0]. The misfit reflects the total uncertainty (epistemic and random) of the results; whereas the code-to-code variability illustrates the part of the epistemic uncertainty associated with the choice of a numerical model. Then, this code-to-code variability is compared to the previous results obtained in the verification exercise done on simplified soil profiles.

An additional analysis was performed to consider the soil column choice in the whole uncertainty assessment. The misfit was calculated for each input motion and all soil columns (SC1, SC2 and SC3) together.

Finally, the results at each site were analyzed, through the distribution of the computed transfer functions and response spectra, using the 25th and 75th percentiles of all computations, and comparing them to the observations. Concomitantly, we also computed and analyzed the distribution of residuals on response spectra to quantify the discrepancy and identify when the observations were under and over-estimated. This operation was carried out at each oscillator period.

Code-to-code variability versus misfit

A first analysis of the code-to-code variability (called hereafter σ_{c2c}) relative to the variability of the residuals between the recording and the simulations (called hereafter *Misfit*) is provided.

To quantify the *Misfit*, we calculate the root mean square distance between each prediction with the observation of the response spectra as proposed in equation Eq 7 and averaging it (geometric mean) over the periods of interest of the site.

$$Misfit = \left(\prod_{i=1}^{n} RMSD_{obs-num}(T_i) \right)^{\frac{1}{n}}$$

$$where$$

$$RMSD_{obs-num}(T_i) = \sqrt{\frac{1}{Nc-1}\sum_{j=1}^{Nc}\left[LSA_{obs}(T_i) - LSA_{num,j}(T_i)\right]^2}$$

Eq 7

Where n is the number period sample between $T_1=1/(1.3f_0)$ and $T_2=1/(0.7f_0)$ of the discrete response spectra SA; $L\overline{SA_{obs}}$ is the logarithmic (to base 10) transformation of the observed SA; $LSA_{num,j}$ is the logarithmic transformation of j^{th} surface predicted SA.

The code-to-code variability (σ_{c2c}) is the standard deviation of the predictions as defined in equation Eq 8, averaged over the same period range as before.

$$\sigma_{c2c} = \left(\prod_{i=1}^{n} RMSD_{num}(T_i)\right)^{\frac{1}{n}}$$

$$where$$

$$RMSD_{num}(T_i) = \sqrt{\frac{1}{Nc-1}\sum_{j=1}^{Nc}\left[L\overline{SA_{num}}(T_i) - LSA_{num,j}(T_i)\right]^2}$$

Eq 8

Where n is the number period sample between $T_1=1/(1.3f_0)$ and $T_2=1/(0.7f_0)$ of the discrete response spectra SA; $L\overline{SA_{num}}$ is the logarithmic (to base 10) transformation of the mean predicted SA; $LSA_{num,j}$ is the logarithmic transformation of j^{th} surface predicted SA.

The considered period range spans an interval of ±30% around the fundamental resonance frequency of the sites (*f_0*) (8.2 and 1.7 Hz for Sendai and KSRH10, respectively). For Sendai it corresponds to the frequency range from 5.47 to 10.66 Hz, equivalent to periods between [0.09-0.18] s. For KSRH10, the adopted frequency interval is [1.19-2.21] Hz, corresponding to periods between [0.45-0.84] s. The periods are log-scale sampled.

Regarding the soil column, the SC1 soil model provided closer results to the observation compared to the SC2 at Sendai. On the opposite, for KSRH10, SC2 and SC3 models led to lower misfit values.

Figure 7 compares the *Misfit* on the East-West component for Sendai and North-South component for KSRH10 (filled markers), with the code-to-code distance σ_{c2c} (empty markers). The simulated component (EW or NS) with less discrepancy with the observations was chosen.

For Sendai, we compared the results for four input motions (1, 2, 5 and 8, for which all calculations were performed) and for the two soil models SC1 and SC2. For KSRH10, it is illustrated for 5 input motions (0,1,2, 4 and 9) and for the 3 soil models (SC1, SC2 and SC3). As expected, the misfit is systematically higher than the code-to-code variability regardless the input motion or site considered: actually they could be equal only if the predictions are unbiased in average, i.e., if $\overline{LSA_{num}}(T_i) = LSA_{obs}(T_i)$ for every period T_i. – which actually never happens... It is also worth observing that the code-to-code variability is quite the same regardless the input motion or the site or the soil columns considered and has a minimum value of 0.06 and a maximum value of 0.15. This suggests that for 1-D seismic response analyses, the epistemic uncertainty related to the choice of the numerical method and soil constitutive model should be considered between 0.06 and 0.15 (in log10 scale). Those values, when compared to well-known uncertainty estimation such as in GMPEs (Ground Motion Prediction Equations), lying between 0.15 to 0.35 (Strasser et al., 2009), are significant and should be taken into account for seismic hazard assessment. One must also keep in mind that such values correspond to a relatively narrow frequency range, and may not be representative of the variabilities in other frequency ranges (as may be seen on Figure 8).

The misfits are generally lower for the weakest input motions regardless the site considered, although slightly more pronounced for the KSHR10 site. This is expected because the predictions are closer to one another and also closer to the observations when the soil response in mainly in the linear range. An exception is observed at Sendai for TS-5-S, for which the misfit is larger for a moderate PGA. The misfits between observations and simulations are found significantly lower at Sendai than at KSRH10. They lie between 0.1 and 0.25 at Sendai, while they are in the interval between 0.08 and 0.35 for KSRH10.

Regarding the soil column, the SC1 soil model provided closer results to the observation compared to the SC2 at Sendai. On the opposite, for KSRH10, SC2 and SC3 models led to lower misfit values.

Figure 7

Comparison between verification and validation epistemic variability

In this section, the variability of the predictions performed during (1) the verification phase on canonical cases (3 profiles P1, P2 and P3 with fundamental resonance frequencies of 3.75, 1.16, 1.58 Hz respectively) and (2) the validation phase on real sites are compared in terms of standard deviation (log10 unit) of the PGA and spectral accelerations at 0.1, 0.3 and 1s at the surface.

We provide the results in Figure 8. For the validation phase, the standard deviation is calculated for KSRH10 for the input motions: TS-9-K, TS-4-K, TS2-K, TS-1-K and TS-0-K. For Sendai it is calculated for the input motions TS-8-S, TS-5-S, TS-2-S and TS-1-S. As far as the verification phase is concerned, we considered only the results for the first profile P1, the rigid substratum case and the non-linear computations. The numerical results depend on the input motion level and on the frequency content (HF stand for High Frequency input motion and LF for Low frequency, see Régnier et al., 2016): the variability increases with the strain level developed in the soil column. It is therefore higher at high PGA and for the low frequency content input motion. The Low Frequency (LF) waveform generates higher strains compared to the High Frequency (HF) waveform, for the same PGA level (black empty triangles). This is because the frequency content of the input motion is close to the resonance frequency of the canonical site. Therefore, strong resonance effects are expected. In the validation phase, the variability is generally larger for the stronger input motions except at KSRH10 site for periods above 0.3s.

Figure 8.

Propagation of the epistemic uncertainty

We built a logic tree similarly to what is done in Probabilistic Seismic Hazard Assessment, to propagate the uncertainty of the numerical simulation and interpretation of the soil data from in-situ and laboratory measurements to the site response and surface response spectra assessment. For each site (Sendai or KSRH10) and each input motion this logic tree is composed of two nodes (as shown in Figure 9). The first node is the soil column (SC1 and SC2 for Sendai, SC1, SC2 and SC3 for KSRH10) and the second node is relative to the team and code couple (from EA-0 - team A with his first code - to

EZ-1 - team Z with his second code). All branches of the tree have the same weight. The uncertainty is quantified by the standard deviation of residuals of the logarithm (log10 unit) of the results (here PGA and response spectra at the surface at 3 periods 0.1, 0.3 and 1s) as defined in Eq 7.

Table 5 synthesizes the standard deviation of the results obtained in the present PENOLIN exercise. It might be noted that the root mean square of residuals (RMSD) are in most cases lower for Sendai compared to KSRH10, except for longer periods (1s). (period close to the KSRH10 fundamental resonance frequency where the fit is good). The fit is generally better for weak input motions, except at Sendai for the response spectra above 0.1s.

Figure 9

Table 5

Comparison of transfer function and response spectra between soil columns

Let us analyze more precisely for each period (frequency) the differences between predictions and observations. The 25% and 75% percentiles of the surface response spectra and the borehole transfer functions are compared to the observations, for a strong and a weak input motion. We selected TS-1-S and TS-8-S for Sendai and TS-1-K and TS-9-K for KSRH10.

Besides, to quantify the discrepancy between observations and predictions the average residuals (R) per period was calculated according to as shown in Eq 9.

$$R(T) = \frac{\sum_{j=1}^{Nc}\left[LSA_{obs}(T) - LSA_{num,j}(T)\right]}{Nc}$$

Eq 9

Where Nc is the number of computations; $L\overline{SA}_{\mathrm{obs}}$ is the logarithmic (base 10) of the observed SA; LSAnum,j is the logarithmic of the jth surface predicted SA.

Sendai

In Sendai, the results of the computations are closer to the observations when using soil model 1 (SC1), which was defined using literature parameters. In Figure 10, the transfer functions are compared, the fundamental resonance frequency (f_0) of the observations for a weak input motion (TS-8-S) is equal to 8.5 Hz, which is well reproduced by the numerical computations using either SC1 or SC2 soil parameters. For the strongest input motion (TS-1-S) f_0 is equal to 7.3Hz in the observations. In the computations, f_0 is similar when using SC1 soil parameters while for SC2, f_0 is slightly above (7.8 Hz), indicating a lower level of non-linearity when using SC2 soil parameters compared to SC1. Similarly, as illustrated in Figure 11, the surface response spectrum is well reproduced by the computations using the two soil columns for weak motion (TS-8-S) while for the strong motion (TS-1-S) the prediction using SC1 is closer to the observation as compared to the SC2 soil column. Those observations are also highlighted in Figure 12, the residuals are close to 0 for the weakest input motion (TS-8-S) for which the two soil columns provide similar estimations. For the strongest input motion we observe an over-estimation below 0.2 s. For TS-5, the under-estimation is observed for both soil columns while for TS-1-S and TS-2-S it is mainly observed for SC2. It shows that the discrepancy between the observations and the predictions for TS-5-S does not depend on the soil column characteristics and may be associated with the input motion specificity.

These first results were somehow disappointing, since site-specific measurements failed in predicting the observations where generic parameters succeeded. We investigate the source of this discrepancy that could come either from a measurement error or a mis-interpretation of the laboratory tests. For Sendai site, there is a large variability between the measured laboratory shear modulus and the in-situ measurement. The shear modulus from the laboratory measurement is equal to 25 MPa at 3.3 m depth, compared to 100 MPa from the *in situ* measurement of Vs (230 m/s) and density values (1890 kg/m^3). This observation suggest that the correction of the laboratory data should have been apply to Sendai site as well.

The procedure to correct the G/G_{max} curves, as indicated previously, has not been applied to the laboratory at Sendai data before the calculations, but it was performed a posteriori.

The comparison of the G/G_{max} curves of SC2 model with G/G_{max} curves from laboratory data did not indicate modifications that could explain the large misfit for SC2 model. We recall that this procedure is supposed to correct only for measurement errors between external and local shear strain devices. Considering the large uncertainty that can lie in the value of the G_{max}^{lab} it is highly recommended that low strain measurements, such as resonant column or bender element should be used in addition to cyclic tri-axial test to define these parameters.

Figure 10

Figure 11

Figure 12

KSRH10

KSRH10 is a deep sedimentary site with down-hole station at GL-255 m. We can observe that the site response (Fourier transfer function) is variable depending on the component of motion and hard to reproduce above the fundamental resonance peak.

In Figure 13, the recorded transfer function is variable from one component of motion to another especially for TS-1-K, where the amplitude of the fundamental resonance peak is equal to 25 for the NS component and only 16 for the EW component. The frequency peaks between 2 to 5 Hz are variable from component to component and event to event and could not be predicted by the 1D assumptions made in this study. For TS-1-K we observe a second and third peaks at 2.3 and 3.3 Hz for the EW component and at 2.7 and 3.2 Hz for the NS component while only one peak is predicted by the numerical simulation with a very high amplitude at 2.7 Hz (high amplitude in the surface Fourier spectrum). For TS-9-K, we observe 3 peaks at 2.3, 3.2 and 4 Hz and only one is predicted by numerical simulations at 2.6 Hz. The fourth peak, close to 7 Hz, is more stable from one component to another, but the frequency is slightly over-estimated and the corresponding amplitude is under-estimated when using the SC1 column.

At high frequencies (above 12 Hz), a de-amplification is observed in the empirical borehole transfer function that is not reproduced by the simulations. One possible explanation is the existence of a noticeable soil-structure interaction at the accelerometer sites: this was proposed by DPRI based on their own experience at several sites and many events. This may also add to some side effects of the low-pass filtering of all KiK-net recordings below 25 Hz. Other possible contributions to this high-frequency reduction may be larger damping (especially for low strains) or scattering from shallow, small size heterogeneities.

For the fundamental resonance peak, we found that SC2 and SC3 soil columns coming from in-situ measurements provided closer results to the observations than the SC1 defined using literature G/G_{max} curves (Darendeli, 2001). As shown in Figure 13, for TS-1-K input motion, the amplitude of the observed resonance frequency peak at 1.4 Hz is around 25 for the NS component, while SC1 column predicted amplitudes (in the 25-75 percentiles envelope) between 12 and 14 only.

As seen in Figure 14, the amplitude of the surface response spectra for the NS component is relatively well reproduced for the weak input motion TS-9-K, but the periods of maximal amplitudes are shifted, creating an over-estimation at 0.13 s and 0.34 s and an under-estimation at 0.18 and 0.25 s. These discrepancies are related to the differences between the observed and computed frequency peaks in the transfer function. For TS-1-K, the amplitude is well reproduced except for SC1 soil column for which the amplitude is significantly under-estimated between 0.1 and 0.34 s. The surface response spectra from the computations using SC2 and SC3 soil columns are closer to the observations.

In Figure 15 we observe the residuals of the response spectra; the recordings are under and over-estimated especially for periods close to 0.35 s for TS-1-K to TS-9-K input motions. The under-estimation amplitude increases with the input motion intensity and is more important for the soil column SC1.

At KSRH10, the site-specific measurements on non-linear properties provide more satisfactory results than the generic curves. The type of soil of KSRH10 was analyzed in detail by one of the participant (Lanzo, personal communication). The non-linear parameters (normalized shear modulus reduction and damping curves) defined in SC2 and SC3 are less non-linear compare to classical literature curves even for similar type of soil (i.e SC1). This observation is consistent with the fact that KSRH10 is composed of volcanic sand, as indicated by site geology. Several authors have shown that volcanic sand exhibits a lower non-linear behavior as compared to classical sand. For example, laboratory experimental tests conducted by Senetakis et al., (2013) show that pumice sands exhibit a slower normalized stiffness decay and a lower dissipative behaviour than classic gravel curves (Rollins et al., 1998). Similar experimental results have been obtained in Italy on volcanic materials such as Colle Palatino tuff in Rome (Pagliaroli et al., 2014), Naples Pozzolana (Papa et al., 1988) and Orvieto (Central Italy) pyroclastic materials (Verrucci et al., 2015). Thus, Darendeli's curves built on "classical" sand data could not necessarily reproduce the non-linear soil behavior at this site. This exercise suggests that one should be careful when using generic soil curves, such as Darendeli (2001) or others: the soil nature is important to evaluate their relevancy in site response analyses.

Figure 13

Figure 14

Figure 15

Discussion and conclusions

Applicability of the calculations

The computations performed in this benchmark are limited by three main assumptions: (1) 1-D wave propagation in horizontally layered media (2) SH waves (only one component of motion) with vertical incidence and (3) total stress analysis.

1-D structure

We succeed to reproduce at both sites the fundamental resonance frequency (for weak and strong motions) but the higher modes remain difficult to reproduce. The sites were chosen (over 688 sites in KiK-net) to fulfill specific criteria warranting limited deviations from a 1-D site configuration. We observe at KSRH10 site that 1-D numerical simulation could not reproduce the observed site response over the whole frequency range, even for weak motions: this is likely to indicate that the site has more complex geometry. The 1-D structure assumption is a very strong one which may not be realistic. However, moving forward for more complex geometries requires more detailed site characterization over a broader area, adequate interpretation of the data and application of 2-D and 3-D numerical simulations (Amorosi et al., 2016; Dupros et al., 2010; Taborda et al., 2010). Benchmarking non-linear numerical codes for 2D or 3D geometries is a real challenge, which should start with a carefully designed verification exercise.

Vertically incident SH waves

Vertically incident SH waves loading implies two distinct assumptions: a) vertically incident plane waves, and b) a uni-directional motion in the whole soil column.

The former has been partially tested through a polarization analysis and has been found only partially fulfilled. In any case, there is not enough information from the two-sensor recordings to constrain the complexity of the incident wavefield, which is an unknown mixture of body waves with varying incidence angles and backazimuths, and surface waves with varying back-azimuths.

Concerning the second assumption, one participant tested a code with an implementation of a 3 Components (3C) non-linear constitutive relation. Using a 3C non-linear constitutive model has been shown to be relevant for strong ground motion prediction with 1D wave propagation models for a large event such as Tohoku 2011 (Santisi d'Avila and Semblat, 2014). The 3D loading path due to the 3C-polarization leads to multiaxial stress interaction that reduces soil strength and increases nonlinear effects.

Therefore, for Sendai site, results of 1D analysis performed using 3 component codes (1D, 3-components) were compared to those obtained by 1D analysis with only one component of motion (1D, 1-component, vertical incidence) see figure S6 in the electronic supplement. Simulations were carried out with reference to the SC2 soil column, which is less non-linear than the SC1, and considering the strongest input motion (TS-1-S).

As illustrated in the electronic supplement figure S6 no significant differences between the two results were observed and cannot explain the discrepancy between the predictions and the observation. Additional research is needed to further explore the impact of 3C motions versus 1C assumption.

Total stress versus effective stress analysis

Even though the exercise was limited to a total stress analysis, and designed accordingly, we thought useful to benefit from the willingness of some volunteer participants to investigate whether the type of analysis (effective or total stress) or the input soil model used could improve the fit. Two teams (W-0 and H-0) performed those calculations at Sendai site. In the electronic supplement, figure S7 presents the borehole transfer function computed for soil columns SC1 and SC2 sorted according to the type of analysis (Total stress analysis, Equivalent linear or effective stress analysis), as compared to the observations for two different input motions (TS-1-S and TS-8-S). We observe that the weak motion effective stress analysis provides results close to total stress analysis, as expected. This is also the case for the strongest input motion when dealing with SC2 soil parameters. However, one team (W-0) succeeds to reproduce the observations even with SC2 soil parameters, when using an effective stress-analysis. That team indicated that the non-linear input data used in this analysis were calibrated directly from the laboratory tests and adjusted to the in-situ measurements of elastic properties. The G/G_{max} curves obtained were closer to the curves used in SC1 rather than SC2. Therefore, no evidence of efficiency of effective stress analysis compared to total stress analysis is available for Sendai site. Additional research is required to further evaluate the conditions under which an effective stress analysis is needed.

Equivalent linear method

In addition to the time domain nonlinear site response analyses limited by these three assumptions, the equivalent linear method (EQL) was also tested. This approach involves a linear computation, coupled to an iterative process that adjusts at each iteration the value of the shear modulus and damping, according to the maximum shear strain calculated at the middle of each soil layer. This method is largely used in earthquake engineering practice since the pioneering work of Schnabel et al., 1972. Three teams used an equivalent linear method (J-1 and Z-0). Team J-1 performed all the calculations, whereas Z-0 provided the results of the equivalent linear method only for the weakest input motions. In the electronic supplement, the figure S7 depicts the results obtained from the equivalent linear method. The EQL results are close to the total stress analysis for the weakest input motion and for the strongest input motion when SC2 soil parameters are considered. However, for the SC1 soil column it should be noted that the shift of the fundamental resonance frequency towards lower values is much higher for the EQL methods and that the high frequencies are largely de-amplified. The strain levels for TS-1-S using SC1 reach 0.3 % and up to 0.7 % for some computations, while for SC2 maximum shear strain values are below 0.2%. For SC1 such high shear strain level implies a decay of shear modulus to 0.1 times the maximum shear modulus. Such results confirm that the EQL approach should not be used beyond strain levels around 0.2 %, consistently with the results presented in Kim et al., (2016) after a comprehensive set of numerical simulations for many different sites, and those also obtained earlier by Ishihara (1996) and Yoshida and Iai (1998).

Main outcomes on NL prediction uncertainties

The present benchmarking exercise allowed to provide some quantitative estimates on the epistemic uncertainty associated to 1D non-linear modeling, which should be considered as lower bound estimates as it is rather rare for practical engineering studies to have as many information as in the present case. Figures 7, 8 11 and 15 indicate that:

- The code-to-code variability is generally in the range 0.05-0.25 (log10 scale), with a slight trend to decrease with increasing period.
- The smaller code-to-code variabilities are found to correspond to the "SC1 case", i.e. here to the Darendeli model, while higher variabilities are found for NL models based on in-situ sampling and dedicated laboratory characterization. We interpret this finding as related to the higher non-linearity level implied by the Darendeli model, resulting in generally weaker motion. The decrease of the uncertainties due to an increase of non-linear soil behavior has been notify in previous studies (Bazzurro and Cornell, 2004; Stewart et al., 2017).
- The misfit (i.e. root mean square average distance to the actual motion) is larger than the code-to-code variability because of model errors (soil parameters, improper 1D assumption, total stress, etc.), and misfit increases with increasing loading level (Figure 7). It may reach values from 0.25 to 0.35 (log10 scale) around the site fundamental frequency where the variability is the highest
- This misfit exhibits a strong frequency dependence, with the lowest values below the fundamental frequency, and largest around f0 and above. Models may over-predict the site response at some frequency, and under-predict it at other frequencies
- The prediction of non-linear site response seems easier for shallow soil deposits than for deeper deposits: the first obvious reason is that the code-to-code variability is mainly visible beyond the site fundamental frequency, which is higher for shallow deposits. In addition, deep deposits not only imply a larger number of sample measurements corresponding to varying depths, but the

wavefield is likely to be more complex, as well as the perturbations due to non 1D layering.

- The widely used, average models such as the Darendeli's ones (SC1), are found to perform rather well for one site (better than the models based on in-situ sampling and laboratory measurements (SC2 and SC3), and less well for the other site. It is impossible to generalize from only two sites, but it is worth mentioning that the first case corresponds to very shallow (depth smaller than 10 m), mainly sandy materials, while the second corresponds to deeper, more clayey material, exhibiting less non-linearity than predicted by Darendeli's model

Finally, one should keep in mind that the results were obtained for rigid base conditions only since they correspond to an input motion recorded at a down-hole sensor. In most practical engineering studies, the "reference motion" corresponds to outcropping rock conditions. The epistemic uncertainty and misfit are then likely to increase especially when the base of the soil column corresponds to much harder bedrock than the "standard" conditions corresponding to a shear wave velocity around 800 m/s: the need for host-to-target adjustments (Campbell, 2003; Van Houtte et al., 2011; Al Atik et al., 2014) then results in increased epistemic uncertainty as recently emphasized by Ktenidou and Abrahamson (2016), Aristizabal et al. (2017) and Laurendeau et al. (2017),

From lessons learnt to tentative recommendations for further benchmarking exercises and NL modelling

This last section intends to provide advices for users of 1-D non-linear site response codes and for next benchmarking exercises, since there is still need for further works, regarding effective stress analysis, NL effect for 2D or 3D media and for more complex incident wavefield as well.

We try to provide an overview of the issues one can encounter when applying those methods and the adapted solutions we found. They are built only partly on the results of this benchmark and refers to several other studies, among which previous recent benchmarks on similar methods (Stewart and Kwok, 2009; Stewart, 2008).

We formulate the following recommendations for applying 1-D nonlinear site response in absence of pore pressure effects.

Preliminary checks

Whatever the numerical method, it is necessary to verify and, if possible, to validate the code used. In particular, if the method used or developed has not been already verified or validated, canonical cases have been uploaded on the Internet for online verification/validation (See Data Resources section).

A verification and validation study, coupled with a documentation of the theory and implementation of a site response method or software, is highly desirable prior to any analyses.

The decision of applying a non-linear analysis rather than a linear or equivalent linear method can follow recommendations for a priori evaluation of differences between EQL and nonlinear site response simulations such as those presented in Kim et al. (2016). EQL results are considered unreliable when the peak strains – or some associated proxies such as PGV/VS30 - exceed some thresholds – which may be frequency dependent (Assimaki and Li, 2012, Kim et al., 2016).

If only one numerical method is used, consider that the variability on the results (standard deviation on pseudo-response spectra) due to the choice of the numerical method is around 0.1 (in log10 scale unit) in average, but may reach values up to 0.2 at short periods or around the site fundamental frequency (Régnier et al., 2016a).

Input data

Input motion

The definition and the processing of the input motion coming from recorded motions (outcrop or within) requires careful attention.

In this study, the input waveforms were processed according to the procedures proposed by Boore and Bommer, (2005), which include the following steps: (1) removing the mean, (2) finding the first and last zero-crossing and then adding zeroes before and after these points over a specific time as a function of the number of poles of the high pass filter to be used (here we added 20 s before and after) and (3) applying a Butterworth high pass filter at 0.1 Hz. This kind of pre-processing is very important when using codes that integrate different input motions (for example, from acceleration, from velocity or from displacement, respectively), in order to ensure having compatible acceleration, velocity and displacement time histories depending of the code's input. In addition, the so prepared input motion has no energy below and above the frequency resolution of the numerical method, which avoids a possible overestimation of permanent surface displacements.

As recommended by Kwok et al., (2007), in linear/equivalent and linear/non-linear site response analyses, two cases can be distinguished: (1) if the reference motion is an outcrop recording, then one should use an elastic base condition with an up-going wave carrying a signal equal to exactly half the outcropping motion; (2) if the reference motion is a within motion recorded by a down-hole sensor, then one should use a rigid base condition without modifying the reference motion or should deconvolve the down-going wave from the within motion and input the up-going wave with elastic base condition.

Soil characterization

It is recommended that a linear analysis be conducted prior to any nonlinear simulations to check that the elastic and visco-elastic properties have been well defined and implemented (check of the expected fundamental resonance frequency if available).

If the site is suspected to have significant lateral variability (Matsushima et al., 2014), then the characterization should involve measurements of the spatial variability of the soil layer (depth and soil properties) and 2D or 3D site response may be needed to capture site effects.

Non-linear parameters, should be defined as a function of depth. The shear modulus reduction and damping curves as functions of shear strain should be associated and compatible with the shear strength and V_S profiles. To find the values of the non-linear parameters, it is recommended to use site specific measurements (e.g. drilling, sampling and laboratory measurements) with comparisons to literature data and relationships for similar materials (e.g. Darendeli, 2001; Ishibashi and Zhang, 1993; Menq, 2003; Roblee and Chiou, 2004; Zhang, 2006).

In this study, it was found that the SC1 model provided good results for one site, but not the other, which was better captured with the SC2 and SC3 soil curves. This was attributed to the unique nature of the geology of the second site. Pre-defined literature curves can produce acceptable estimations of site response, but need to be evaluated based on the site geology. In this study, cyclic-triaxial tests were found to be not always reliable at low strains. Resonant column or blender element tests are useful and can provide complementary measurements to constrain the normalized stiffness decay curves at low strains. Further investigation in future studies, for a larger set of sites and simulations, would greatly help in establishing consensual procedures for bridging in-situ, low-strain and laboratory high-strain measurements. Elastic properties measured in the laboratory should be compared with in-situ measurements; the soil sample size, the soil disturbance and the measurement errors can lead to discrepancies between the measurement in the laboratory and in-situ. The way to adapt the nonlinear curves and elastic properties measured in the lab to elastic properties measured in situ should be detailed and uncertainties on these parameters should be accounted for: the lack of a common, widely accepted procedure is a source of large epistemic uncertainty in the assessment of NL soil properties, and thus in the prediction of site response under strong motion.

Conclusion

This benchmark was limited to 1-D non-linear total stress analysis. This simple case was chosen to ensure an, as clear as possible, identification of the impact of various approaches to implement the non-linearity and the associated parameters. We calculated the variability between predictions and the misfit with observations. The variability between codes indicate that the choice of a non-linear model must be coupled with an uncertainty from 0.05-0.25 (in log10 scale) to reflect the variability from the code, the numerical method, the constitutive model and the user. This uncertainty is generally not considered in any site-specific response analysis. The misfit is even greater than the variability between codes, and is associated to the definition of the soil parameters and intrinsic assumptions of the method (1-D site and vertical propagation of SH waves without pore water pressure effects). The misfit increases with increasing loading level and may reach values from 0.25 to 0.35 (log10 scale) around the site fundamental frequency. It is frequency dependent and can be an over-prediction and an under-prediction depending of the frequency bandwidth.

Further investigations are needed to propose recommendations as for the method to obtain non-linear parameters. Indeed, at Sendai site pre-defined literature curves provided better results, whereas for KSRH10, site specific curves from laboratory tests were closer to the observations.

The experience gained from this thorough benchmarking exercise allows to propose some recommendations for either operational studies or future, more advanced benchmarks. The latter are definitely needed as some issues, in relation to the main assumptions behind the widely used 1D approach, were clearly identified, as potentially impacting the misfit between numerical predictions and instrumental recordings: complexity of the geometry, dimensionality of the input motion and complexity of the wavefield, or constitutive model with or without water pressure. Addressing those issues was much beyond the scope of the present project, but each of them would deserve a dedicated benchmark. We hope that sharing the PRENOLIN experience will contribute to the design of such future studies.

Data and Resources

Time histories used in this study were collected from the KiK-net website www.kik.bosai.go.jp and http://www.kik. bosai.go.jp/kik/ (last accessed November 2011) and from PARI, Port and Airport Institute in Japan .

Some codes used in this work have the following URL links:

ASTER, http://www.code-aster.org (last accessed October 2015);

EPISPEC1D, http://efispec.free.fr (last accessed October 2015);

Real ESSI simulator, http://sokocalo.engr. ucdavis.edu/~jeremic/Real_ESSI_Simulator/ (last accessed October 2015);

OpenSees, http://opensees.berkeley.edu/ (last accessed October 2015);

DEEPSOIL, http://deepsoil.cee. illinois.edu/ (last accessed October 2015);

SeismoSoil, http://asimaki.caltech.edu/resources/index.html#software (last accessed October 2015). The unpublished manuscript by

Verification and validation exercises :

- For 2D/3D linear methods: http://www.sismowine.org (last accessed July 2017)

- for1-D non-linear (PRENOLIN): http://prenolin.org (last accessed July 2017)

References

Amorosi, A., Boldini, D., di Lernia, A., 2016. Seismic ground response at Lotung: Hysteretic elasto-plastic-based 3D analyses. Soil Dyn. Earthq. Eng. 85, 44–61.

Assimaki, D., Li, W., 2012. Site and ground motion-dependent nonlinear effects in seismological model predictions. Soil Dyn. Earthq. Eng. 143–151.

Aubry, D., Hujeux, J.C., Lassoudiere, F., Meimon, Y., 1982. A double memory model with multiple mechanisms for cyclic soil behaviour, in: Proceedings of the Int. Symp. Num. Mod. Geomech. pp. 3–13.

Bazzurro, P., Cornell, allin, 2004. Ground-motion amplification in nonlinear soil sites with uncertain properties. Bull. Seismol. Soc. Am. 94, 2090–2109.

Bonilla, L.F., Archuleta, R.J., Lavallée, D., 2005. Hysteretic and Dilatant Behavior of Cohesionless Soils and Their Effects on Nonlinear Site Response: Field Data Observations and Modeling. Bull. Seismol. Soc. Am. 95, 2373–2395.

Bonilla, L.F., Steidl, J.H., Gariel, J., Archuleta, R.J., 2002. Borehole response studies at the Garner Valley downhole array southern California. Bull. Seismol. Soc. Am. 92, 3165–3279.

Boore, D.M., Bommer, J.J., 2005. Processing of strong-motion accelerograms: needs, options and consequences. Soil Dyn. Earthq. Eng. 25, 93–115.

Darendeli, M.B., 2001. Development of a new family of normalized modulus reduction and material damping curves.

De Martin, F., Matsushima, S., Kawase, H., 2013. Impact of geometric effects on near-surface Green’s functions. Bull. Seismol. Soc. Am.

Dupros, F., De Martin, F., Foerster, E., Komatitsch, D., Roman, J., 2010. High-performance finite-element simulations of seismic wave propagation in three-dimensional nonlinear inelastic geological media. Parallel Comput. 36, 308–325.

Elgamal, A.-W., Zeghal, M., Parra, E., 1996. Liquefaction of reclaimed island in Kobe, Japan. J. Geotech. Eng. 122, 39–49.

Elgamal, A.-W., Zeghal, M., Tang, H.T., Stepp, J.C., 1995. Lotung downhole array. I: Evaluation of site dynamic properties. J. Geotech. Eng. 121, 350–362.

Groholski, D.R., Hashash, Y.M., Kim, B., Musgrove, M., Harmon, J., Stewart, J.P., 2016. Simplified model for small-strain nonlinearity and strength in 1D seismic site response analysis. J. Geotech. Geoenvironmental Eng. 142, 4016042.

Gunturi, V.R., Elgamal, A.-W., Tang, H.T., 1998. Hualien seismic downhole data analysis. Eng. Geol. 50, 9–29.

Hardin, B.O., Drnevich, V.P., 1972. Shear Modulus and Damping in Soils. J. Soil Mech. Found. Div. 98, 667–692.

Haskell, N.H., 1953. The dispersion of surface waves in multilayered media. Bull. Seismol. Soc. Am. 43, 17–34.

Ishibashi, I., Zhang, X., 1993. Unified Dynamic shear moduli and damping ratio of sand and clay. Soils Found. 33, 182–191.

Ishihara, K., 1996. Soil Behaviour in Earthquake Geotechnics. Clarenton Press, Oxford.

Jaky, J., 1944. The coefficient of earth pressure at rest. J. Soc. Hung. Archit. Eng. 78, 355–358.

Kim, B., Hashash, Y.M., Stewart, J.P., Rathje, E.M., Harmon, J.A., Musgrove, M.I., Campbell, K.W., Silva, W.J., 2016. Relative Differences between Nonlinear and Equivalent-Linear 1-D Site Response Analyses. Earthq. Spectra 32, 1845–1865.

Kwok, A.O., Stewart, J.P., Hashash, Y.M., 2008. Nonlinear ground-response analysis of Turkey Flat shallow stiff-soil site to strong ground motion. Bull. Seismol. Soc. Am. 98, 331–343.

Kwok, A.O., Stewart, J.P., Hashash, Y.M., Matasovic, N., Pyke, R., Wang, Z., Yang, Z., 2007. Use of exact solutions of wave propagation problems to guide implementation of nonlinear seismic ground response analysis procedures. J. Geotech. Geoenvironmental Eng. 133, 1385–1398.

Maeda, T., Sasatani, T., Takai, N., Shimizu, G., 2005. Azimuth estimation of KiK-net surface seismometers deployed in Hokkaido, Japan. Geophys Bull Hokkaido Univ 68, 141–152.

Matsushima, S., Hirokawa, T., De Martin, F., Kawase, H., Sánchez-Sesma, F.J., 2014. The effect of lateral heterogeneity on horizontal-to-vertical spectral ratio of microtremors inferred from observation and synthetics. Bull. Seismol. Soc. Am.

Menq, F., 2003. Dynamic properties of sandy and gravelly soils.

Nakagawa, K., Soga, K., 1995. Nonlinear Cyclic Stress-Strain Relations of Soils. Int. Conf. Recent Adv. Geotech. Earthq. Eng. Soil Dyn. Paper 13.

Noguera, S.M., 2016. Assessment and mitigation of liquefaction seismic risk: numerical modeling of their effects on SSI. Université Paris-Saclay.

Olsen, K., Day, S., Bradley, C., 2003. Estimation of Q for long-period (> 2 sec) waves in the Los Angeles basin. Bull. Seismol. Soc. Am. 93, 627–638.

Pagliaroli, A., Lanzo, G., Tommasi, P., Di Fiore, V., 2014. Dynamic characterization of soils and soft rocks of the Central Archeological Area of Rome. Bull. Earthq. Eng. 12, 1365–1381.

Papa, V., Silvestri, F., Vinale, F., 1988. Analisi delle proprietà di un tipico terreno piroclastico mediante prove dinamiche di taglio semplice, in: I National Symposium on Research in Geotechnical Engineering. pp. 265–286.

Régnier, J., Bonilla, L.-F., Bard, P.-Y., Bertrand, E., Hollender, F., Kawase, H., Sicilia, D., Arduino, P., Amorosi, A., Asimaki, D., 2016a. International Benchmark on Numerical Simulations for 1D, Nonlinear Site Response (PRENOLIN): Verification Phase Based on Canonical Cases. Bull. Seismol. Soc. Am. 106, 2112–2135.

Régnier, J., Bonilla, L.F., Bertrand, E., Semblat, J.-F., 2014. Influence of the VS Profiles beyond 30 m Depth on Linear Site Effects: Assessment from the KiK-net Data. Bull. Seismol. Soc. Am. 104, 2337–2348.

Régnier, J., Cadet, H., Bard, P.-Y., 2016b. Empirical Quantification of the Impact of Nonlinear Soil Behavior on Site Response. Bull. Seismol. Soc. Am. 106, 1710–1719.

Régnier, J., Cadet, H., Bonilla, L.F., Bertrand, E., Semblat, J.-F., 2013. Assessing Nonlinear Behavior of Soils in Seismic Site Response: Statistical Analysis on KiK-net Strong-Motion Data. Bull. Seismol. Soc. Am. 103, 1750–1770.

Roblee, C., Chiou, B., 2004. A proposed Geoindex model for design selection of non-linear properties for site response analysis, in: International Workshop on Uncertainties in Nonlinear Soil Properties and Their Impact on Modeling Dynamic Soil Response. PEER Headquarters, UC Berkeley. pp. 18–19.

Rollins, K.M., Evans, M.D., Diehl, N.B., III, W.D.D., 1998. Shear modulus and damping relationships for gravels. J. Geotech. Geoenvironmental Eng. 124, 396–405.

Roten, D., Fäh, D., Bonilla, L.F., 2013. High-frequency ground motion amplification during the 2011 Tohoku earthquake explained by soil dilatancy. Geophys. J. Int. 193, 898–904.

Santisi d'Avila, M.P., Semblat, J.-F., 2014. Nonlinear seismic response for the 2011 Tohoku earthquake: borehole records versus one-directional three-component propagation models. Geophys. J. Int. 197, 566–580.

Sato, K., Kokusho, T., Matsumoto, M., Yamada, E., 1996. Nonlinear seismic response and soil property during strong motion. Soils Found. 41–52.

Seed, H., 1969. 1. M. Idriss, Influence of soil conditions on ground motions during earthquakes, J. Soil Mech Found Div Amer Soc Civ Eng 95.

Senetakis, K., Anastasiadis, A., Pitilakis, K., Coop, M.R., 2013. The dynamics of a pumice granular soil in dry state under isotropic resonant column testing. Soil Dyn. Earthq. Eng. 45, 70–79.

Stewart, J., Kwok, A., 2009. Nonlinear Seismic Ground Response Analysis: Protocols and VerificaBon Against Array Data. PEER Annu. Meet. San Franc.-Present. 84.

Stewart, J.P., 2008. Benchmarking of nonlinear geotechnical ground response analysis procedures. Pacific Earthquake Engineering Research Center.

Stewart, J.P., Afshari, K., Goulet, C.A., 2017. Non-Ergodic Site Response in Seismic Hazard Analysis. Earthq. Spectra. doi:10.1193/081716EQS135M

Strasser, F.O., Abrahamson, N.A., Bommer, J.J., 2009. Sigma: Issues, insights, and challenges. Seismol. Res. Lett. 80, 40–56.

Taborda, R., López, J., Karaoglu, H., Urbanic, J., Bielak, J., 2010. Speeding up finite element wave propagation for large-scale earthquake simulations. Parallel Data Lab. Tech Rept CMUPDL-10 109.

Tatsuoka, F., Kohata, Y., Pesti, D.L., 1995. Deformation characteristics of soils and soft rocks under monotonic and cyclic loads and their relationships.

Thompson, E.M., Baise, L.G., Tanaka, Y., Kayen, R.E., 2012. A taxonomy of site response complexity. Soil Dyn. Earthq. Eng. 41, 32–43.

Thomson, W.T., 1950. Transmission of elastic waves through a stratified solid. J. Appl. Phys. 21, 89–93.

Verrucci, L., Lanzo, G., Tommasi, P., Rotonda, T., 2015. Cyclic and dynamic behaviour of a soft pyroclastic rock. Géotechnique 65, 359–373.

Vucetic, M., Dobry, R., 1991. Effect of soil plasticity on cyclic response. J. Geotech. Eng. 117.

Vucetic, M., Dobry, R., 1988. Cyclic triaxial strain-controlled testing of liquefiable sands, in: Advanced Triaxial Testing of Soil and Rock. ASTM International.

Yee, E., Stewart, J.P., Tokimatsu, K., 2013. Elastic and large-strain nonlinear seismic site response from analysis of vertical array recordings. J. Geotech. Geoenvironmental Eng. 139, 1789–1801.

Yoshida, N., Iai, S., 1998. Nonlinear site response and its evaluation and prediction, in: Proc. 2nd International Symposium on the Effect of Surface Geology on Seismic Motion. pp. 71–90.

Yu, G., Anderson, J.G., Siddharthan, R., 1993. On the characteristics of nonlinear soil response. Bull. Seismol. Soc. Am. 83, 218–244.

Zeghal, M., Elgamal, A.-W., Tang, H.T., Srepp, J.C., 1995. Lotung downhole array. II: Evaluation of soil nonlinear properties. J. Geotech. Eng. 121, 363–378.

Zhang, R.R., 2006. Characterizing and quantifying earthquake-induced site nonlinearity. Soil Dyn. Earthq. Eng. 26, 799–812.

List of captions

Figure 1: Location of the two selected sites for the validation phase with location of the epicenter of the selected events at each site according to their magnitude and surface PGA (cm/s^2 at the station)

Figure 2: The graphs (a) and (d) show the initial Vs profile available at the selected sites for KSRH10 and Sendai. Graphs (b) and (e) illustrates the comparison between 1-D linear site response computed with empirical site response (surface to within motion spectral ratio) calculated with weak motion (PGA at the surface lower than 25 cm/s^2) for KSRH10 and Sendai sites. Graphs (c) and (f) compares the empirical transfer function of weak motions with the strongest ones recoded at KSRH10 and Sendai respectively.

Figure 3: Location of the vertical arrays with respect to the borings for soil parameter measurements and MASW lines (a) for KSRH10 site and (b) for Sendai site.

Figure 4: Modification of the Vs profile with improvements of the surface to within spectral ratio with 1-D linear site response analysis. Graphs (a) and (c): the dashed lines represent the initial Vs profile and the plain line the final Vs profile at KSRH10 and Sendai. Graphs (b) and (d): The dashed lines represent the 1-D linear numerical surface to within spectral ratio with the initial Vs profile and the plain line with the final.

Figure 5: Input parameters for the numerical simulations at KSRH10 site. (a) Vs and elastic attenuation (ξ_0) profiles. The graph (b) illustrates, in the soil layer down to the depth were non-linear soil behavior is defined, the location of the shear modulus decay and attenuation ($G/G_{max}(\Upsilon)$ and $\xi(\Upsilon)$) curves for the soil column 1 (SC1), for the soil column 2 (SC2) and for soil column 3 (SC3) shown in graph (d). For SC3, the locations of

G/G_{max} and damping curves in the soil layers are similar as for SC2. Graph (c) indicates the shear strength profile down to 40m.

Figure 6: Input parameters for the numerical simulations at Sendai site. (a) Vs and elastic attenuation (ξ_0) profiles. The graph (b) illustrates, in the soil layer down to the depth were non-linear soil behavior is defined, the location of the shear modulus decay and attenuation ($G/G_{max}(\Upsilon)$ and $\xi(\Upsilon)$) curves for the soil column 1 (SC1) and for the soil column 2 (SC2) shown in graph (c).

Figure 7: Distance between the recorded and computed surface pseudo-response spectra (Misfit) compare to the code-to-code variability (σ_{c2c}) at Sendai site, using the soil columns SC1 and SC2 for the input motions TS-1-S, TS-3-S, TS-5-S and TS-9-S and at KSRH10 using the soil columns SC1, SC2 and SC3 for the input motions TS-0-K, TS-1-K, TS-2-K, TS-4-K and TS-8-K.

Figure 8: Standard deviation values of the logarithm results (PGA, spectra acceleration at 3 periods) for the verification phase on canonical cases and for the validation phase of PRENOLIN project.

Figure 9: Logic tree for propagation of the epistemic uncertainty.

Figure 10: Comparison of the empirical surface to within spectral ratio of the East-West of the input motion TS-1-S and TS-8-S recorded at Sendai with the envelope of the results represented by the 25 and 75 percentiles of all numerical computations using SC1 or SC2 and only the EW component.

Figure 11: Comparison of the surface response spectra of the East-West components of the input motion TS-1-S and TS-8-S recorded at Sendai with the envelope represented of the 25 and 75 percentiles of all numerical computations using SC1, and SC2.

Figure 12 Comparison of the residuals and associated standard deviation of the surface response spectra of the East-West component of the input motion TS-1-S, TS-2-S, TS-5-S and TS-8-S recorded at Sendai with the envelope represented by the 25 and 75 percentiles of all numerical computations using SC1, and SC2.

Figure 12: Idem Figure 10. For KSRH10, for the input motions TS-1-K and TS-9-K and using the soil columns SC1, SC2 and SC3 for the north-south components.

Figure 13: Idem Figure 11. For KSRH10, for the North-South component of the input motions TS-1-K and TS-9-K and using the soil columns SC1, SC2 and SC3.

Figure 14: Idem Figure 12. For KSRH10, for the North-South component of the input motions TS-0-K, TS-1-K, TS-2-K, TS-4-K and TS-9-K and using the soil columns SC1, SC2 and SC3.

TABLES

Table 1: Selected event characteristics (PGA for EW components)

	EQ	CodeName	Fs* (Hz)	Mw†	Depth‡ (km)	Depi§ (km)	$PGA_{borhole}$ ** (cm/s^2)	$PGA_{surface}$ †† (cm/s^2)	Fc‡‡ (Hz)
KSRH10	**KSRH100309260450**	**TS-0-K**	**200**	**8**	**42**	**180**	**110**	**558**	**6,6**
	KSRH100411290332	**TS-1-K**	**200**	**7,1**	**48**	**32**	**81**	**319**	**4,8**
	KSRH100412062315	**TS-2-K**	**200**	**6,9**	**46**	**44**	**69**	**386**	**4,2**
	KSRH100411290336	TS-3-K	200	6	46	37	64	199	6,0
	KSRH100404120306	**TS-4-K**	**200**	**5,8**	**47**	**43**	**27**	**162**	**5,3**
	KSRH100904282021	TS-5-K	100	5,4	38	69	25	163	4,0
	KSRH100501182309	TS-6-K	200	6,4	50	38	25	125	6,7
	KSRH100912280913	TS-7-K	100	5	85	39	9	58	6,5
	KSRH100805110324	TS-8-K	100	5,1	88	63	8	46	6,2
	KSRH100309291137	**TS-9-K**	**200**	**6,5**	**43**	**105**	**7**	**54**	**4,6**
Sendai	**F-2958**	**TS-1-S**	**100**	**9**	**23,7**	**163**	**252**	**481**	**6,9**
	F-1889	**TS-2-S**	**100**	**7,1**	**72**	**81**	**62**	**244**	**9,0**
	F-1932	TS-3-S	100	6,4	11,9	19	61	208	10,3
	F-2691	TS-4-S	100	6,8	108,1	169	25	89	7,1
	F-3012	**TS-5-S**	**100**	**5.9**	**30.7**	**96**	**25**	**72**	**7.5**
	F-2659	TS-6-S	100	7.2	7.8	83	35	82	7.7
	F-1856	TS-7-S	100	5.9	41.2	95	12	32	7.8
	F-2862	**TS-8-S**	**100**	**6.4**	**34.5**	**208**	**5**	**7**	**3.4**
	F-2730	TS-9-S	100	5.8	47	176	3	12	6.2

* Fs : Sampling frequency

† Moment Magnitude

‡ Hypocentral depth

§ Epicentral distance

** Peak Ground Acceleration at the down-hole station

†† Peak Ground Acceleration at surface station

‡‡ Central Frequency

Table 2: Geological characteristics of the 2 selected sites with locations of the undisturbed soil samples.

Site	Down-hole sensor depth (m)	Max. complementary drilling depth (m)	Type of soil	Number of samples (location)
Sendai	8	10	Sand	2 (3.3 & 5.4 m)
KSRH10	250	50	Sand /clay	6 (3.5, 7.5, 14.5, 22.5, 29,7 & 34 m)

Table 3: Soil properties from the KSRH10 site

Z* (m)	Vs† (m/s)	Vp (m/s)	ρ‡ (kg/m^3)	Qs§	ξ**	Set of G/G_{max} and damping curves	τ_{max}†† (kPa)
6	140	1520	1800	25	0.02	SC1-1,SC2-1,SC3-1	Calculated every 1m. according to Eq 6
11	180	1650	1800	25	0.02	SC1-2,SC2-2,SC3-2	
15	230	1650	1500	25	0.02	SC1-3,SC2-3,SC3-3	
20	300	1650	1500	25	0.02	SC1-4,SC2-3,SC3-3	
24	250	1650	1600	25	0.02	SC1-5,SC2-4,SC3-4	
28	370	1650	1600	25	0.02	SC1-6,SC2-5,SC3-5	
35	270	1650	1800	35	0.0142	SC1-7,SC2-5,SC3-5	
39	460	1650	1800	25	0.02	SC1-8,SC2-6,SC3-6	
44	750	1800	2500	75	0.0066	Linear	
84	1400	3400	2500	140	0.0035	Linear	
255	2400	5900	2500	240	0.0020	Linear	

* Depth of the soil layer

† Shear wave velocity of the soil layer

‡ Density of the soil layer

§ Elastic Damping ratio

** Elastic attenuation

†† Shear strength

Table 4: Soil properties from the Sendai site

Z (m)	*Vs* (m/s)	*Vp* (m/s)	ρ (kg/m^3)	*Qs*	ξ	Set of *G/G*$_{max}$ and damping curves
1	120	610	1850	25	0.02	SC1-1, SC2-1
2	170	870	1850	25	0.02	SC1-2, SC2-1
3	200	1040	1850	7.14	0.07	SC1-3, SC2-1
4	230	1180	1890	7.14	0.07	SC1-4, SC2-2
5	260	1300	1890	7.14	0.07	SC1-5, SC2-2
6	280	1420	1890	7.14	0.07	SC1-6, SC2-2
7	300	1530	1890	7.14	0.07	SC1-7, SC2-2
10.4	550	2800	2480	50	0.01	Linear

Table 5: Standard deviation values of the residuals of the logarithm results for all teams and soil columns (PGA, spectra acceleration at 3 periods).

	Sendai				KSRH10				
	TS-1-S	**TS-2-S**	**TS-5-S**	**TS-8-S**	**TS-0-K**	**TS-1-K**	**TS-2-K**	**TS-4-K**	**TS-9**
PGA	0.16	0.11	0.11	0.09	0.20	0.17	0.17	0.17	0.10
SA(0.1s)	0.10	0.10	0.12	0.10	0.23	0.22	0.23	0.20	0.15
SA(0.3s)	0.11	0.09	0.09	0.09	0.17	0.14	0.15	0.09	0.07
SA(1s)	0.10	0.08	0.09	0.09	0.11	0.06	0.07	0.07	0.11

Mailing address:

- Julie Régnier, CEREMA, Julie Régnier, Cerema, Equipe-Projet MOUVGS, 500 routes des Lucioles, Sophia-Antipolis, F-06903, France.
- Luis-Fabian Bonilla, IFSTTAR, 14-20 Boulevard Newton - Champs-sur-Marne - 77447 Marne-la-Vallée Cedex 2, France
- Pierre-Yves Bard, IFSTTAR and Université Grenoble Alpes ISTerre, CS 40700, 38058 GRENOBLE Cedex 9, France
- Etienne Bertrand, CEREMA, DTer Méditerranée, 56 Bd Stalingrad 06300 Nice, France
- Fabrice Hollender, CEA, DEN, 13108 St Paul lez Durance, France
- Hiroshi Kawase, DPRI, Gokasho,Uji,Kyoto 611-0011 Japan
- Deborah Sicilia, EDF - DPI-CEIDRE, TEGG, 905 av du Camp Menthe,13097 Aix-en-Provence Cedex 2, France
- Pedro Arduino, Department of Civil & Environmental Engineering, University of Washington, Seattle, WA, USA
- Angelo Amorosi, Sapienza, University of Rome, Via Eudossiana 18, 00184 Roma, Italy
- Domniki Asimaki, California Institute of Technology, Campus Address: 1200 E California blvd, Pasadena CA 91125, US
- Daniela Boldini, University of Bologna, Dipartimento di Ingegneria Civile, Chimica, Ambientale e dei Materiali , Via Terracini 28, 40131 Bologna, Italy
- Long Chen, Department of Civil & Environmental Engineering, University of Washington, Seattle, WA, USA

- Anna Chiaradonna, Department of Civil, Architectural and Environmental Engineering, University of Napoli Federico II, via Claudio 21, 80125 Napoli, Italy
- Florent DeMartin, BRGM (French Geological Survey), Direction of Risks and Prevention, 3 Avenue Claude Guillemin, 45100 Orléans, France
- Ahmed Elgamal, University of California, San Diego, Dept. of Structural Engineering, La Jolla, CA 92093-0085, USA
- Gaetano Falcone, Technical University of Bari, Via Amendola 126, 70126 Bari, Italy
- Evelyne Foerster, CEA, DEN/DM2S/SEMT/EMSI and SEISM Institute Paris-Saclay, 91191 Gif-sur-Yvette Cedex, France
- Sebastiano Foti, Politecnico di Torino, Corso Duca degli Abruzzi, 24 - 10129 Torino, Italy
- Evangelia Garini, NTUA National Technical University of Athens, Faculty of Civil Engineering , Geotechnical Department, Iroon Polytechniou 9,Zografou 157 80, GREECE
- George Gazetas, NTUA National Technical University of Athens, Faculty of Civil Engineering , Geotechnical Department, Iroon Polytechniou 9,Zografou 157 80, GREECE
- Céline Gélis, IRSN, 31 Avenue de la Division Leclerc, 92260 Fontenay-aux-Roses, France
- Alborz Ghofrani, Department of Civil & Environmental Engineering, University of Washington, Seattle, WA, USA
- Amalia Giannakou, Fugro Sial, Esentepe mah. Yazarlar sok. No.16 34394 Gayrettepe, Şişli-İstanbul / Turkey
- James R. Gingery, Kleinfelder, Inc., 550 West C Street, San Diego, California, 92101, U.S.A
- Nathalie Glinsky, CEREMA, DTer Méditerranée, 56 Bd Stalingrad 06300 Nice, France

- Joseph Harmon, University of Illinois at Urbana-Champaign, 2230c Newmark Lab, 205 N Mathews, M/C 250, Urbana, IL 61801 , US
- Youssef Hashash, University of Illinois at Urbana-Champaign, 2230c Newmark Lab, 205 N Mathews, M/C 250, Urbana, IL 61801 , US
- Susumu Iai, DPRI, Gokasho,Uji,Kyoto 611-0011 Japan
- Steve Kramer, 132 I More Hall, Department of Civil & Environmental Engineering, University of Washington, Seattle, WA, 98195-2700, US
- Stavroula Kontoe, Imperial College, South Kensington Campus, London SW7 2AZ, UK.
- Jozef Kristek, Comenius University Bratislava Faculty of Mathematics, Physics and Informatics Mlynská dolina F1 84248 Bratislava, Slovakia.
- Giuseppe Lanzo, Sapienza University of Rome, Via A. Gramsci 53, 00197 Rome, Italy
- Annamaria di Lernia, Politecnico of Bari, Via Amendola 126, Bari, Italy Italy
- Fernando Lopez-Caballero, CentraleSupélec, Paris-Saclay University, MSS-Mat CNRS UMR 8579, Grande Voie des Vignes, Châtenay-Malabry 92290, France
- Marianne Marot, CEREMA, DTer Méditerranée, 56 Bd Stalingrad 06300 Nice, France
- Graeme McAllister, Department of Civil Engineering, University of British Columbia, Vancouver, BC, Canada.
- E. Diego Mercerat, CEREMA, DTer Méditerranée, 56 Bd Stalingrad 06300 Nice, France
- Peter Moczo Comenius University Bratislava Faculty of Mathematics, Physics and Informatics Mlynská dolina F1 84248 Bratislava, Slovakia.

- Silvana Montoya-Noguera, CentraleSupélec, Paris-Saclay University, MSS-Mat CNRS UMR 8579, Grande Voie des Vignes, Châtenay-Malabry 92290, France
- Michael Musgrove, University of Illinois at Urbana-Champaign, 2230c Newmark Lab, 205 N Mathews, M/C 250, Urbana, IL 61801 , US
- Alex Nieto-Ferro, Dépt. Analyses en Mécanique Avancée, EDF Lab Paris-Saclay, 7 boulevard Gaspard Monge, 91120 PALAISEAU
- Alessandro Pagliaroli, University of Chieti-Pescara, viale Pindaro 42, 65129 Pescara, Italy.
- Federico Passeri, Politecnico di Torino, Corso Duca degli Abruzzi, 24 - 10129 Torino, Italy
- Aneta Richterova, Comenius University Bratislava Faculty of Mathematics, Physics and Informatics Mlynská dolina F1 84248 Bratislava, Slovakia.
- Suwal Sajana, Sapienza University of Rome, Via A. Gramsci 53, 00197 Rome, Italy
- Maria Paola Santisi d'Avila, UNS, Nice, Campus Valrose, 28 avenue Valrose, 06108 Nice cedex 2, France
- Jian Shi, California Institute of Technology, Campus Address: 1200 E California blvd, Pasadena CA 91125, US
- Francesco Silvestri, Department of Civil, Architectural and Environmental Engineering, University of Napoli Federico II, via Claudio 21, 80125 Napoli, Italy.
- Mahdi Taiebat: Department of Civil Engineering, University of British Columbia, Vancouver, BC, Canada
- Giuseppe Tropeano, Department of Civil, Environmental Engineering and Architecture, University of Cagliari, Piazza d'Armi 09123, Cagliari, Italy.

- Didrik Vandeputte, EDF, A EDF – DIN CEIDRE / TEGG 905, avenue du Camp de Menthe 13097 AIX EN PROVENCE CEDEX 02
- Luca Verrucci, Dipartimento di Ingegneria Strutturale e Geotecnica, University of Rome, via Eudossiana 18, 00184, Rome, Italy.

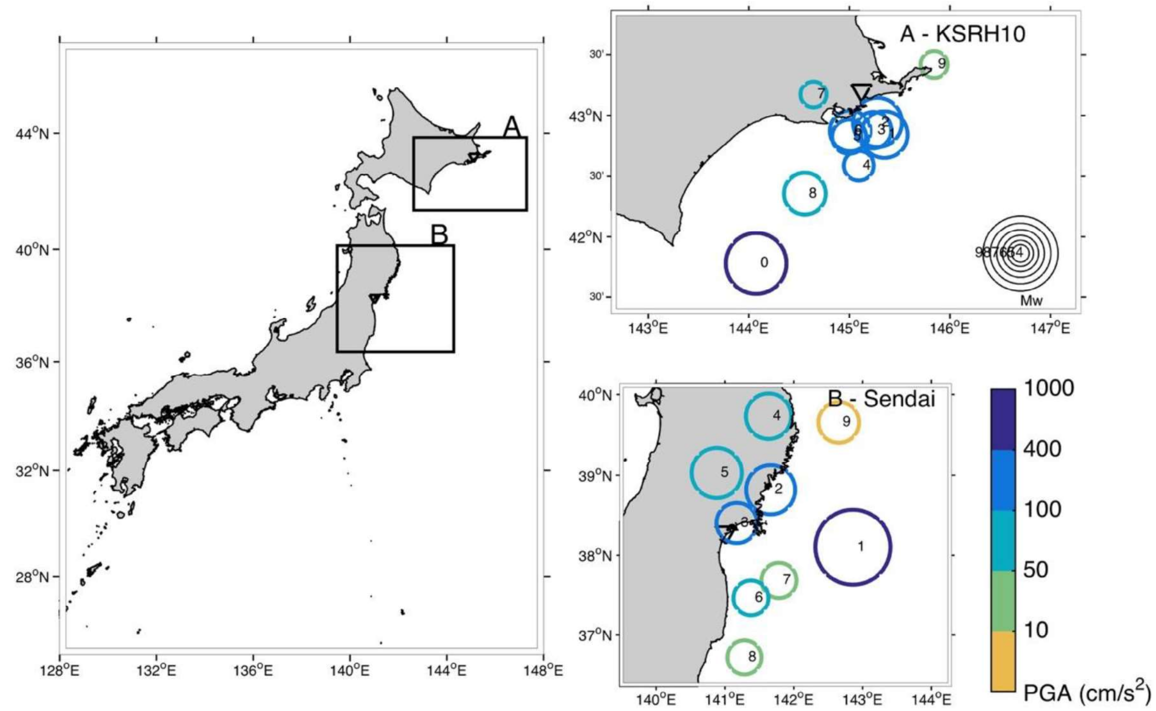

Figure 1: Location of the two selected sites for the validation phase with location of the epicenter of the selected events at each site according to their magnitude and surface PGA (cm/s² at the station)

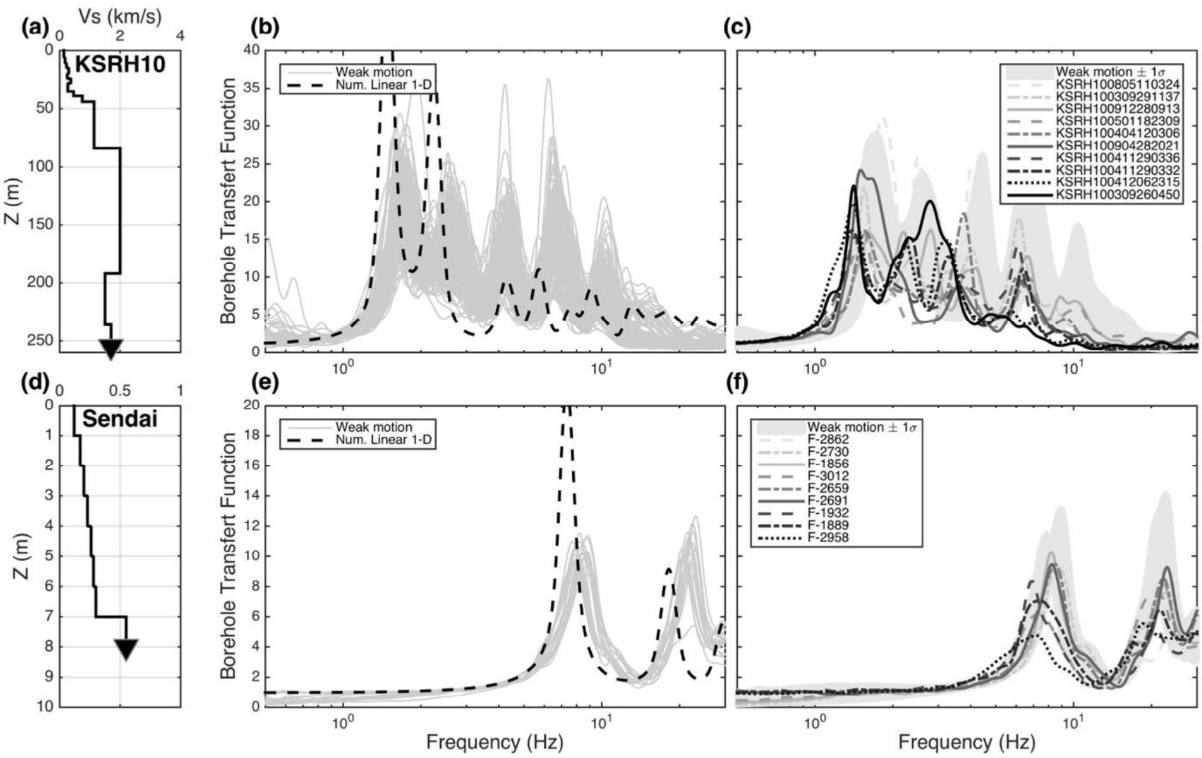

Figure 2: The graphs (a) and (d) show the initial Vs profile available at the selected sites for KSRH10 and Sendai. Graphs (b) and (e) illustrates the comparison between 1-D linear site response computed with empirical site response (surface to within motion spectral ratio) calculated with weak motion (PGA at the surface lower than 25 cm/s²) for KSRH10 and Sendai sites. Graphs (c) and (f) compares the empirical transfer function of weak motions with the strongest ones recoded at KSRH10 and Sendai respectively.

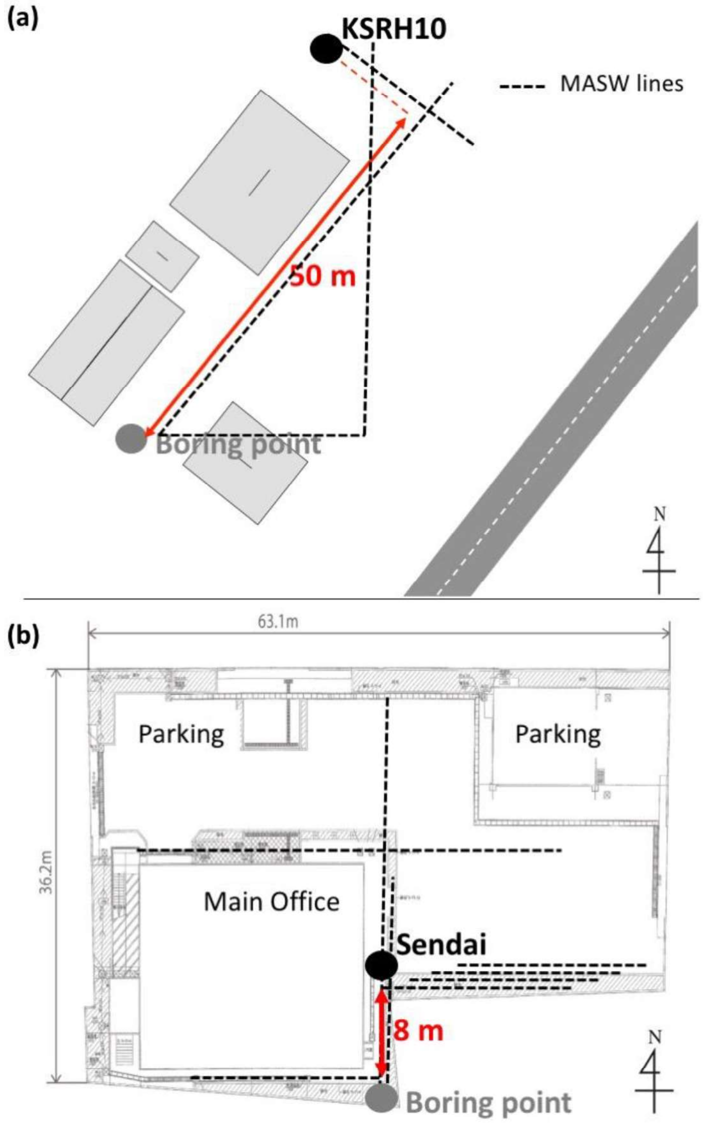

Figure 3: Location of the vertical arrays with respect to the borings for soil parameter measurements and MASW lines (a) for KSRH10 site and (b) for Sendai site.

Figure 4: Modification of the Vs profile with improvements of the surface to within spectral ratio with 1-D linear site response analysis. Graphs (a) and (c): the dashed lines represent the initial Vs profile and the plain line the final Vs profile at KSRH10 and Sendai. Graphs (b) and (d): The dashed lines represent the 1-D linear numerical surface to within spectral ratio with the initial Vs profile and the plain line with the final.

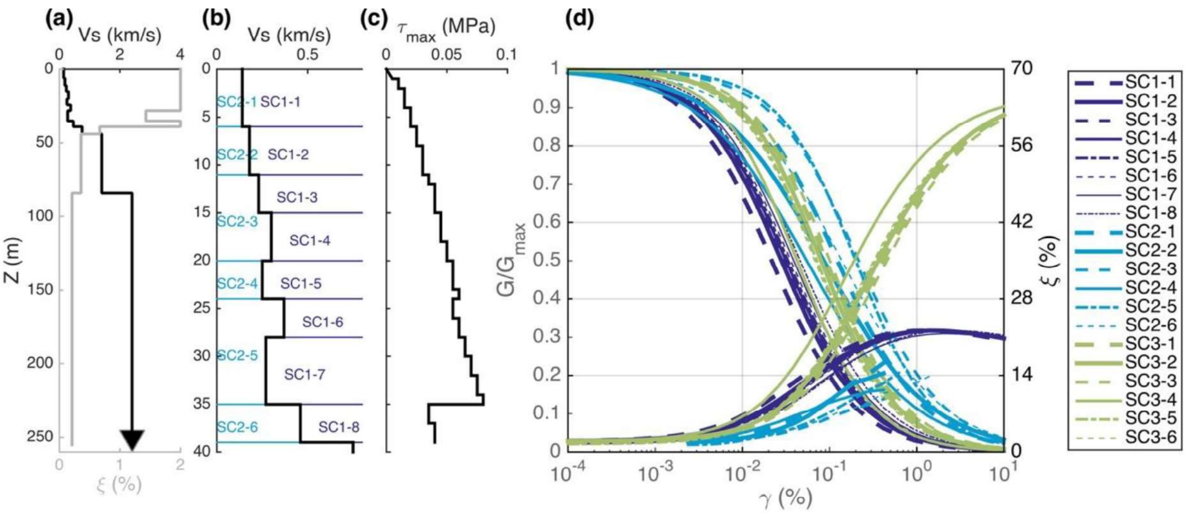

Figure 5: Input parameters for the numerical simulations at KSRH10 site. (a) Vs and elastic attenuation (ξ_0) profiles. The graph (b) illustrates, in the soil layer down to the depth were non-linear soil behavior is defined, the location of the shear modulus decay and attenuation ($G/G_{max}(\Upsilon)$ and $\xi(\Upsilon)$) curves for the soil column 1 (SC1), for the soil column 2 (SC2) and for soil column 3 (SC3) shown in graph (d). For SC3, the locations of G/G_{max} and damping curves in the soil layers are similar as for SC2. Graph (c) indicates the shear strength profile down to 40m.

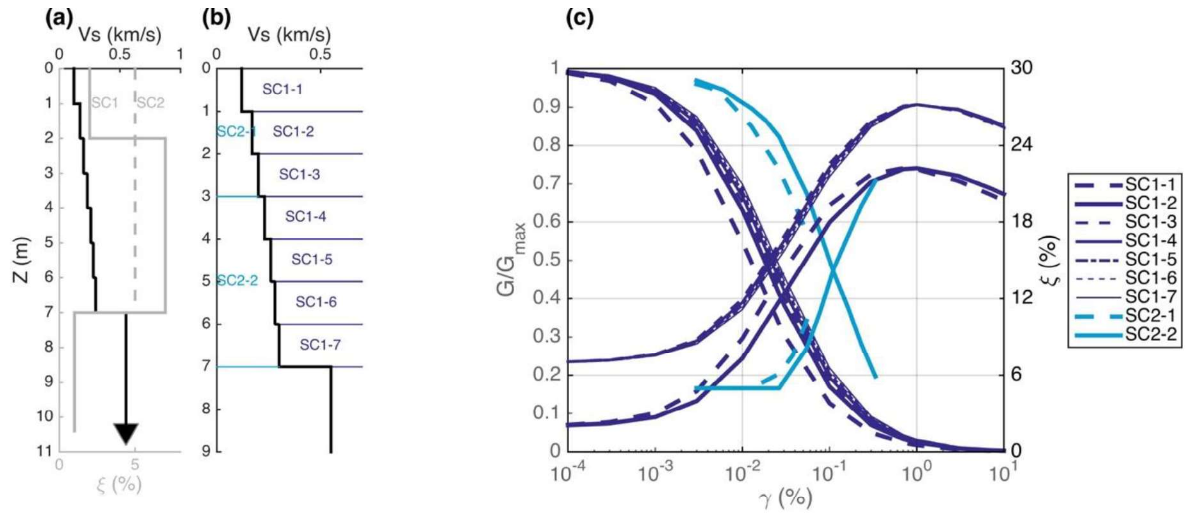

Figure 6: Input parameters for the numerical simulations at Sendai site. (a) Vs and elastic attenuation (ξ_0) profiles. The graph (b) illustrates, in the soil layer down to the depth were non-linear soil behavior is defined, the location of the shear modulus decay and attenuation ($G/G_{max}(\Upsilon)$ and $\xi(\Upsilon)$) curves for the soil column 1 (SC1) and for the soil column 2 (SC2) shown in graph (c).

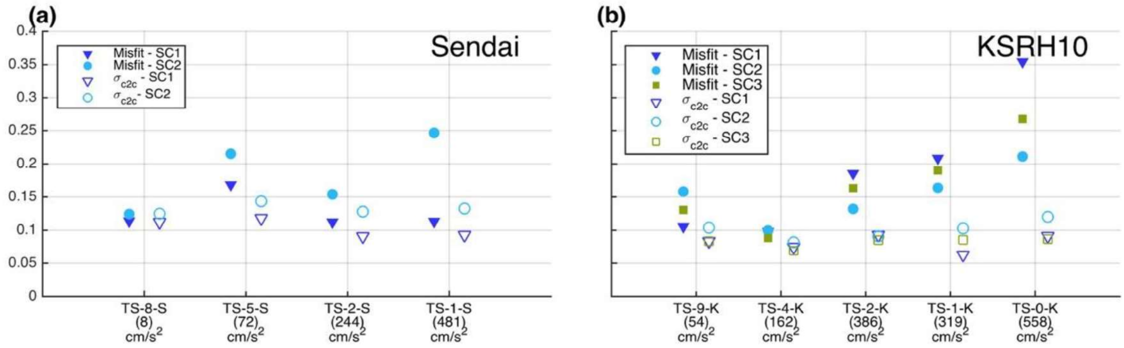

Figure 7: Distance between the recorded and computed surface pseudo-response spectra (Misfit) compare to the code-to-code variability (σ_{c2c}) at Sendai site, using the soil columns SC1 and SC2 for the input motions TS-1-S, TS-3-S, TS-5-S and TS-9-S and at KSRH10 using the soil columns SC1, SC2 and SC3 for the input motions TS-0-K, TS-1-K, TS-2-K, TS-4-K and TS-8-K.

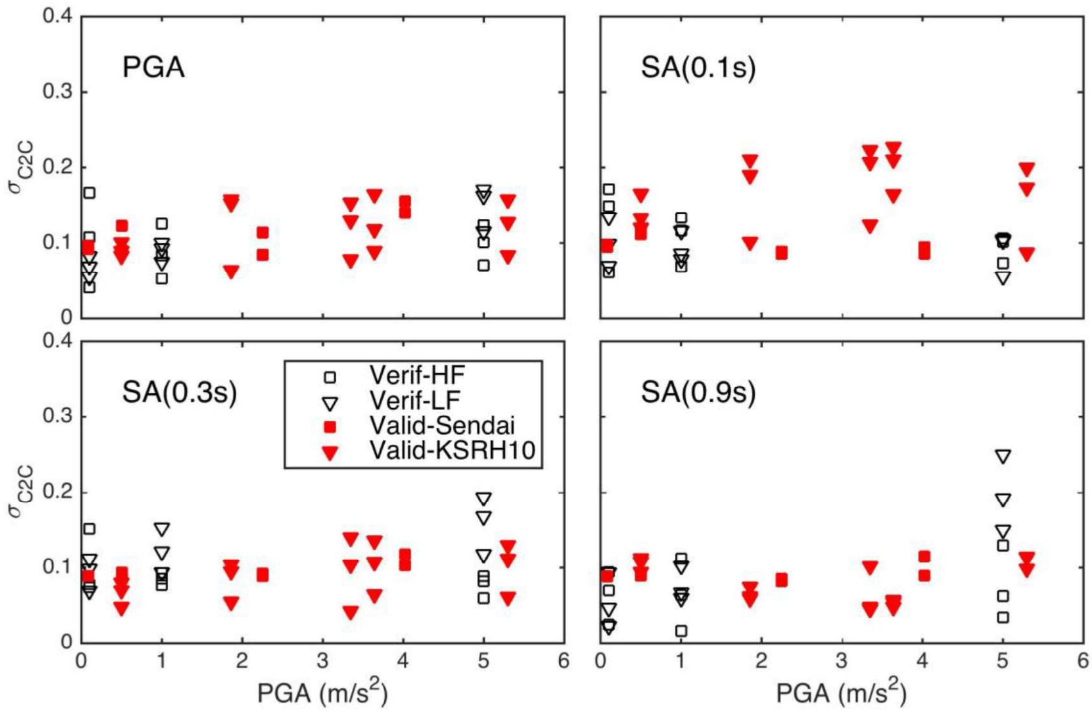

Figure 8: Standard deviation values of the logarithm results (PGA, spectra acceleration at 3 periods) for the verification phase on canonical cases and for the validation phase of PRENOLIN project.

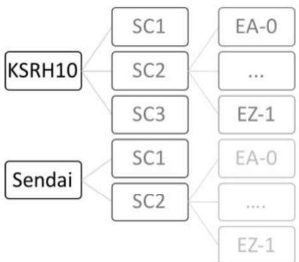

Figure 9: Logic tree for propagation of the epistemic uncertainty.

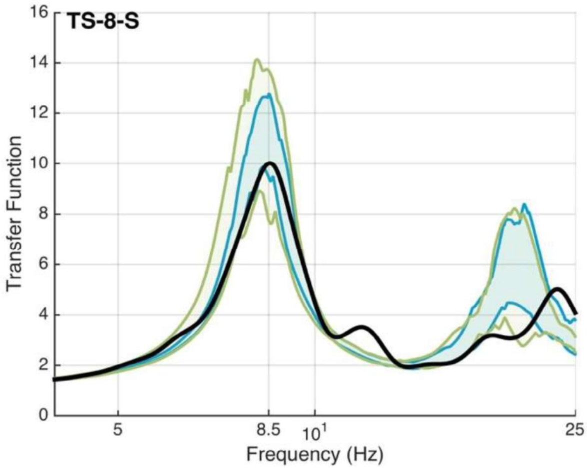

Figure 10: Comparison of the empirical surface to within spectral ratio of the East-West of the input motion TS-1-S and TS-8-S recorded at Sendai with the envelope of the results represented by the 25 and 75 percentiles of all numerical computations using SC1 or SC2 and only the EW component.

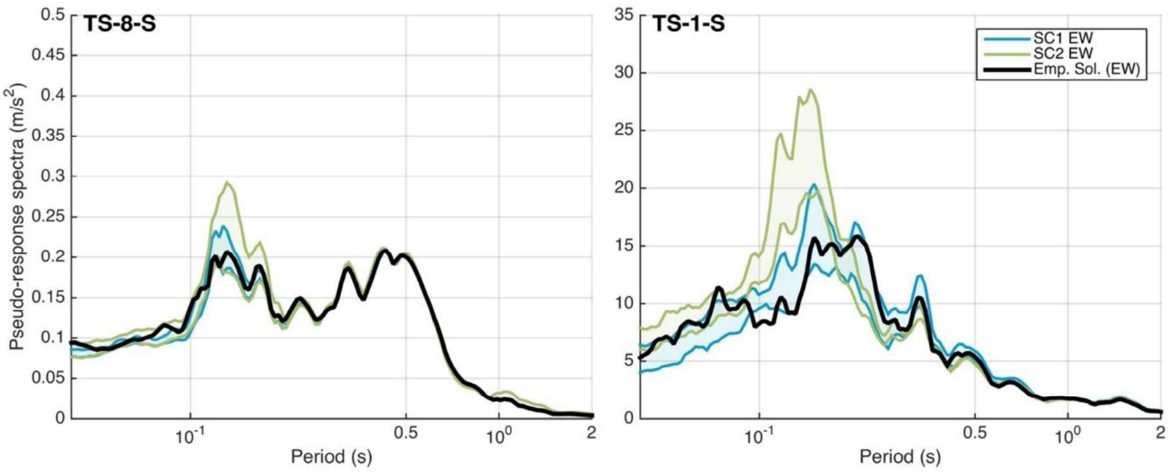

Figure 11: Comparison of the surface response spectra of the East-West components of the input motion TS-1-S and TS-8-S recorded at Sendai with the envelope represented of the 25 and 75 percentiles of all numerical computations using SC1, and SC2

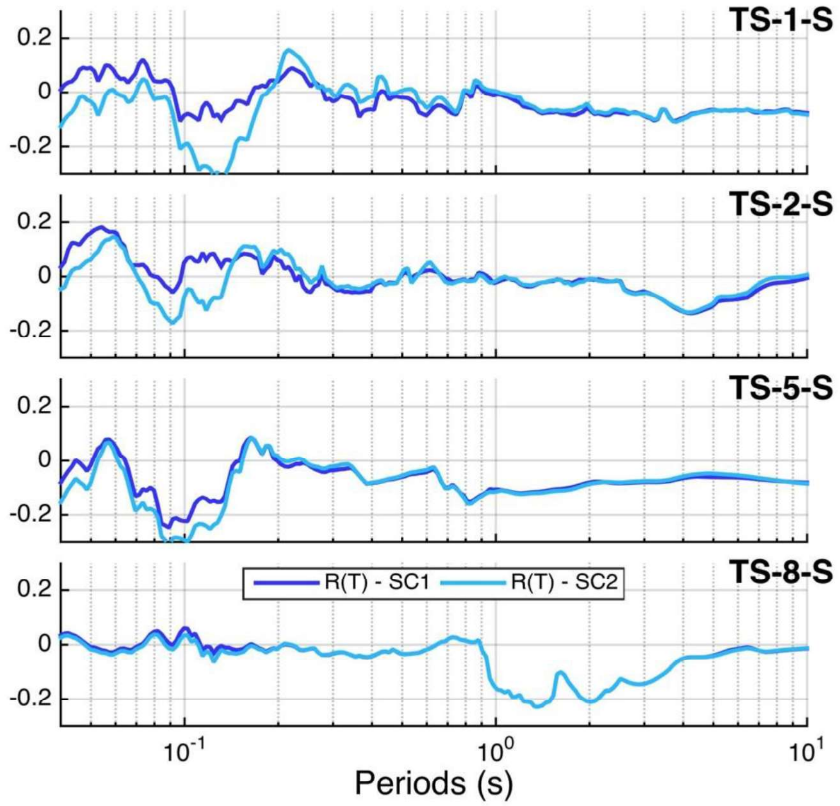

Figure 12: Comparison of the residuals and associated standard deviation of the surface response spectra of the East-West component of the input motion TS-1-S, TS-2-S, TS-5-S and TS-8-S recorded at Sendai with the envelope represented by the 25 and 75 percentiles of all numerical computations using SC1, and SC2.

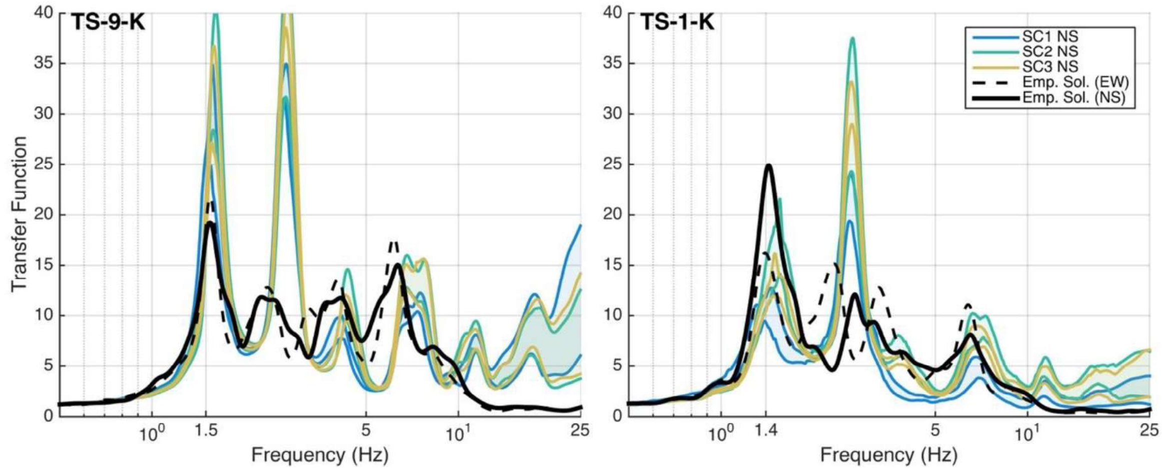

Figure 13: Idem Figure 10. For KSRH10, for the input motions TS-1-K and TS-9-K and using the soil columns SC1, SC2 and SC3 for the north-south and east-west components.

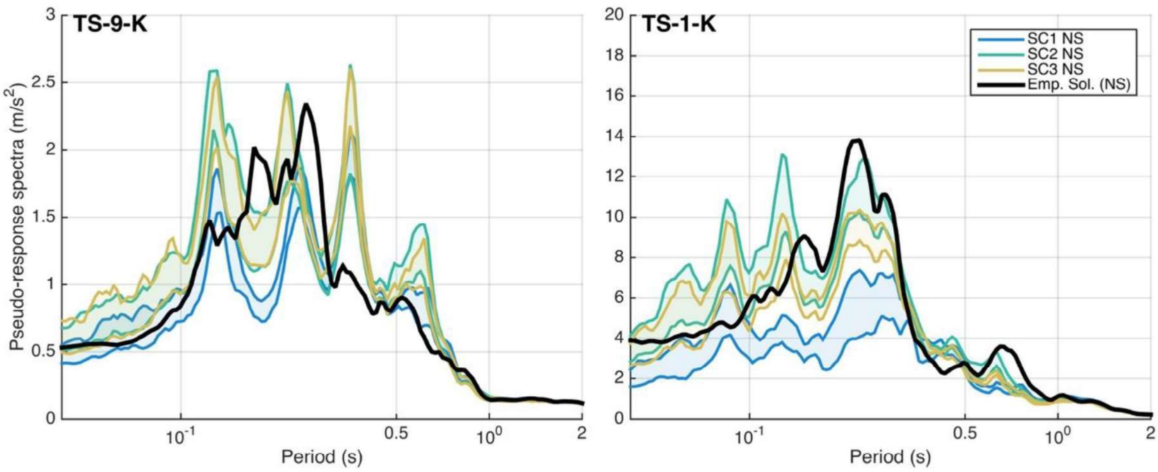

Figure 14 Idem Figure 11. For KSRH10, for the North-South component of the input motions TS-1-K and TS-9-K and using the soil columns SC1, SC2 and SC3.

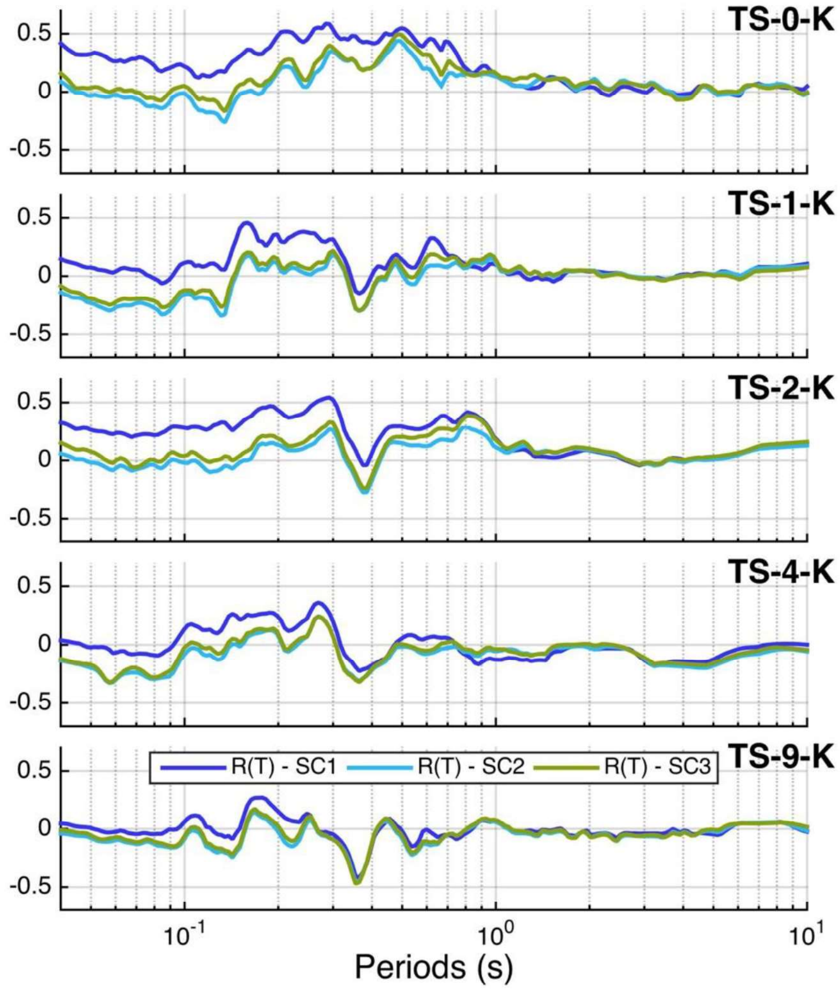

Figure 15 Idem Figure 12. For KSRH10, for the North-South component of the input motions TS-0-K, TS-1-K, TS-2-K, TS-4-K and TS-9-K and using the soil columns SC1, SC2 and SC3.

Figure 1

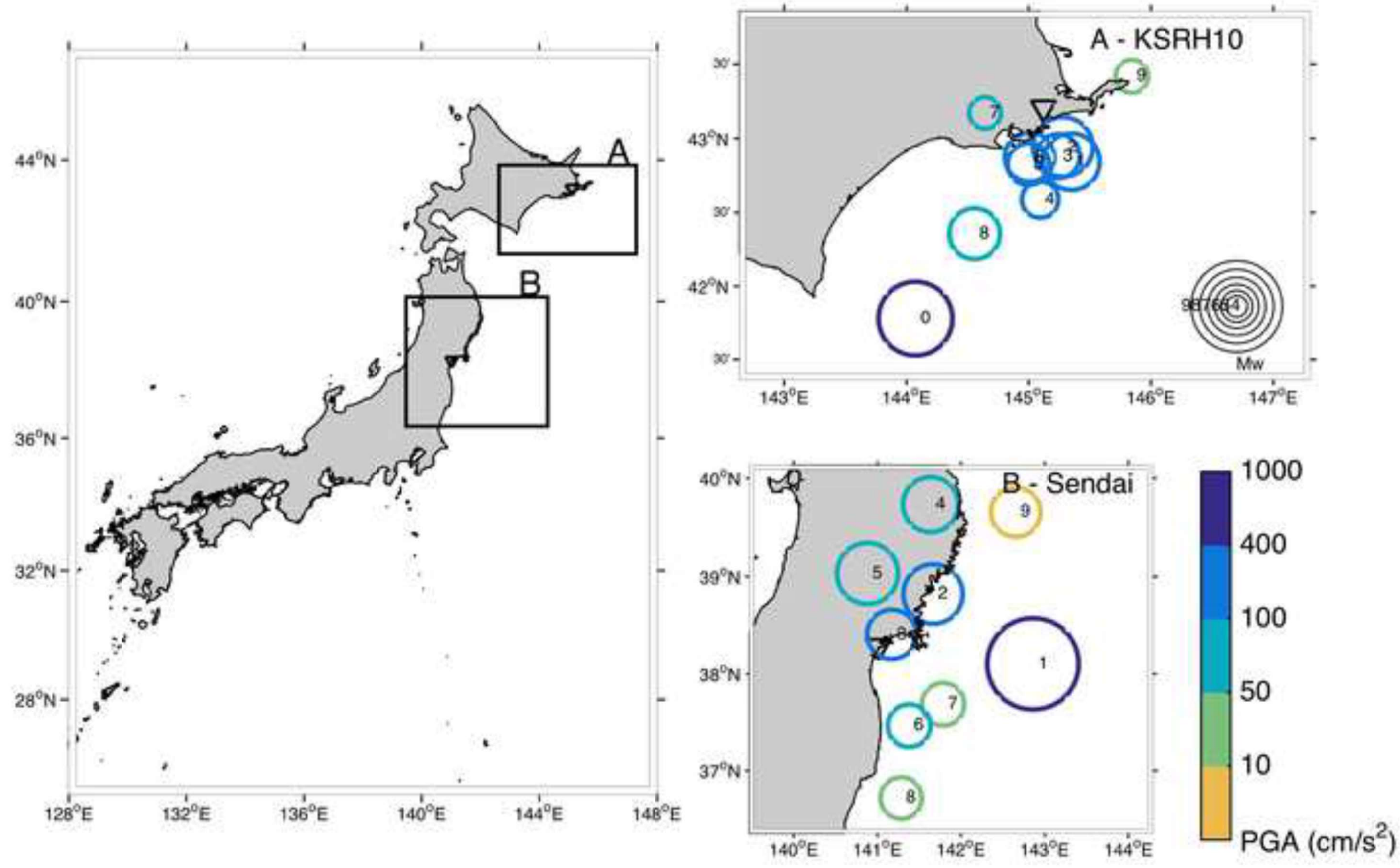

44°N
40°N
36°N
32°N
28°N
128°E
132°E
136°E
140°E
144°E
148°E
A
B
A - KSRH10
43°N
42°N
30'
143°E
144°E
145°E
146°E
147°E
Mw
B - Sendai
40°N
39°N
38°N
37°N
140°E
141°E
142°E
143°E
144°E
1000
400
100
50
10
PGA (cm/s²)

Figure 2

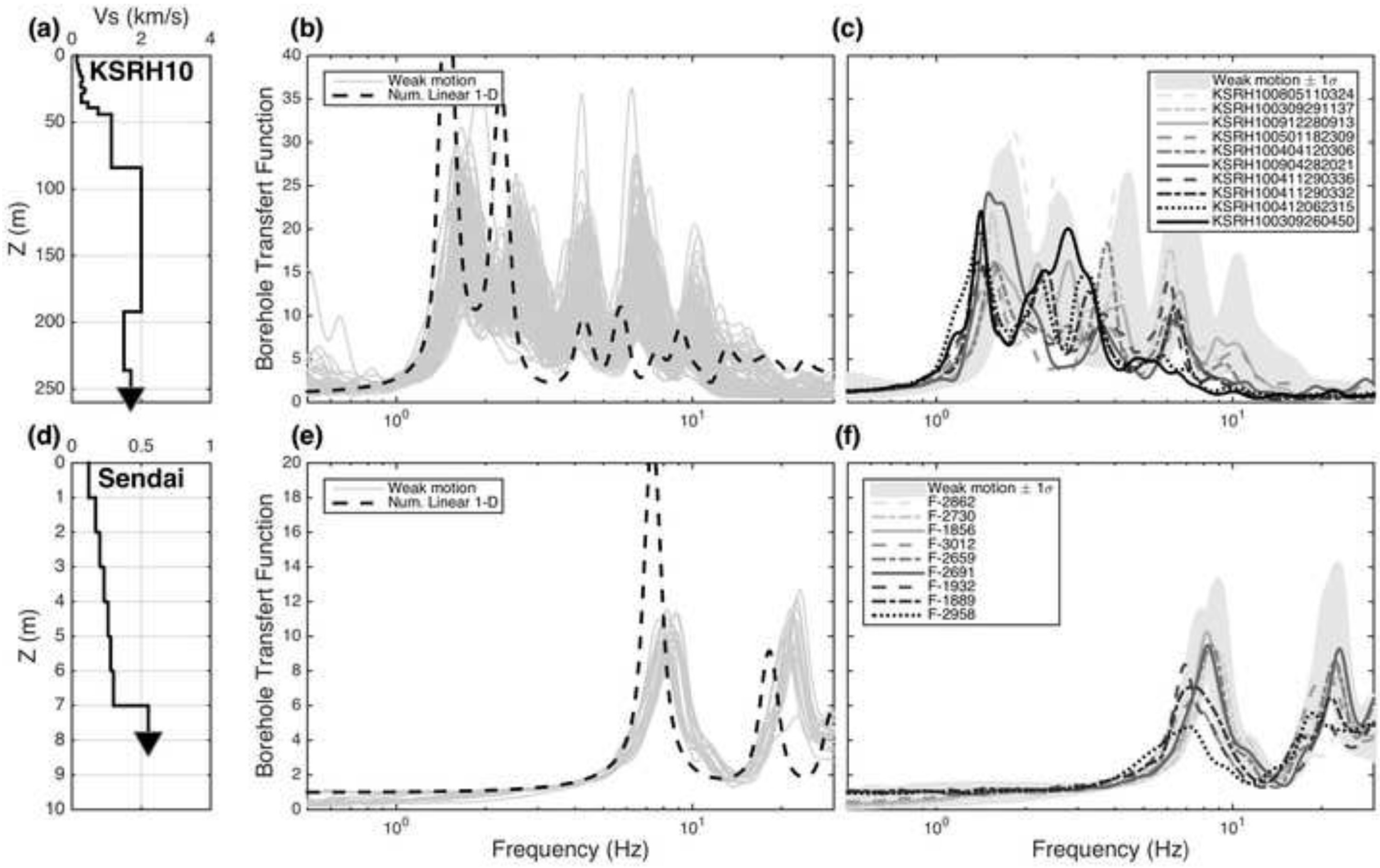
(a)
Vs (km/s)
Z (m)
KSRH10
(b)
Borehole Transfert Function
Weak motion
Num. Linear 1-D
(c)
Weak motion ± 1σ
KSRH100805110324
KSRH100309291137
KSRH100912280913
KSRH100501182309
KSRH100404120306
KSRH100904282021
KSRH100411290336
KSRH100411290332
KSRH100412062315
KSRH100309260450
(d)
Z (m)
Sendai
(e)
Borehole Transfert Function
Weak motion
Num. Linear 1-D
Frequency (Hz)
(f)
Weak motion ± 1σ
F-2862
F-2730
F-1856
F-3012
F-2659
F-2691
F-1932
F-1889
F-2958
Frequency (Hz)

Figure 3

Click here to download Figure Fig_3_loc_station_boring.jpg

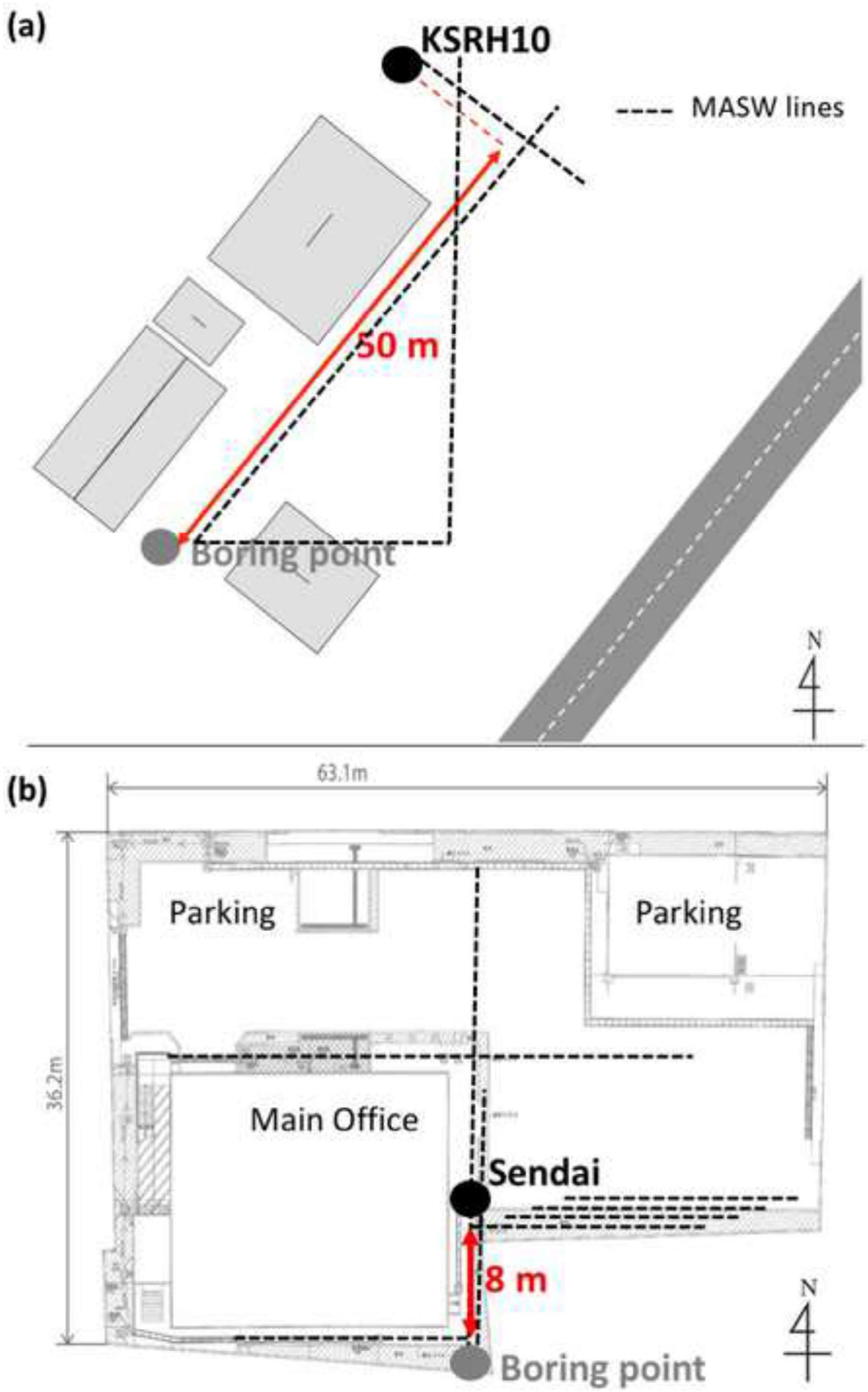

Figure 4

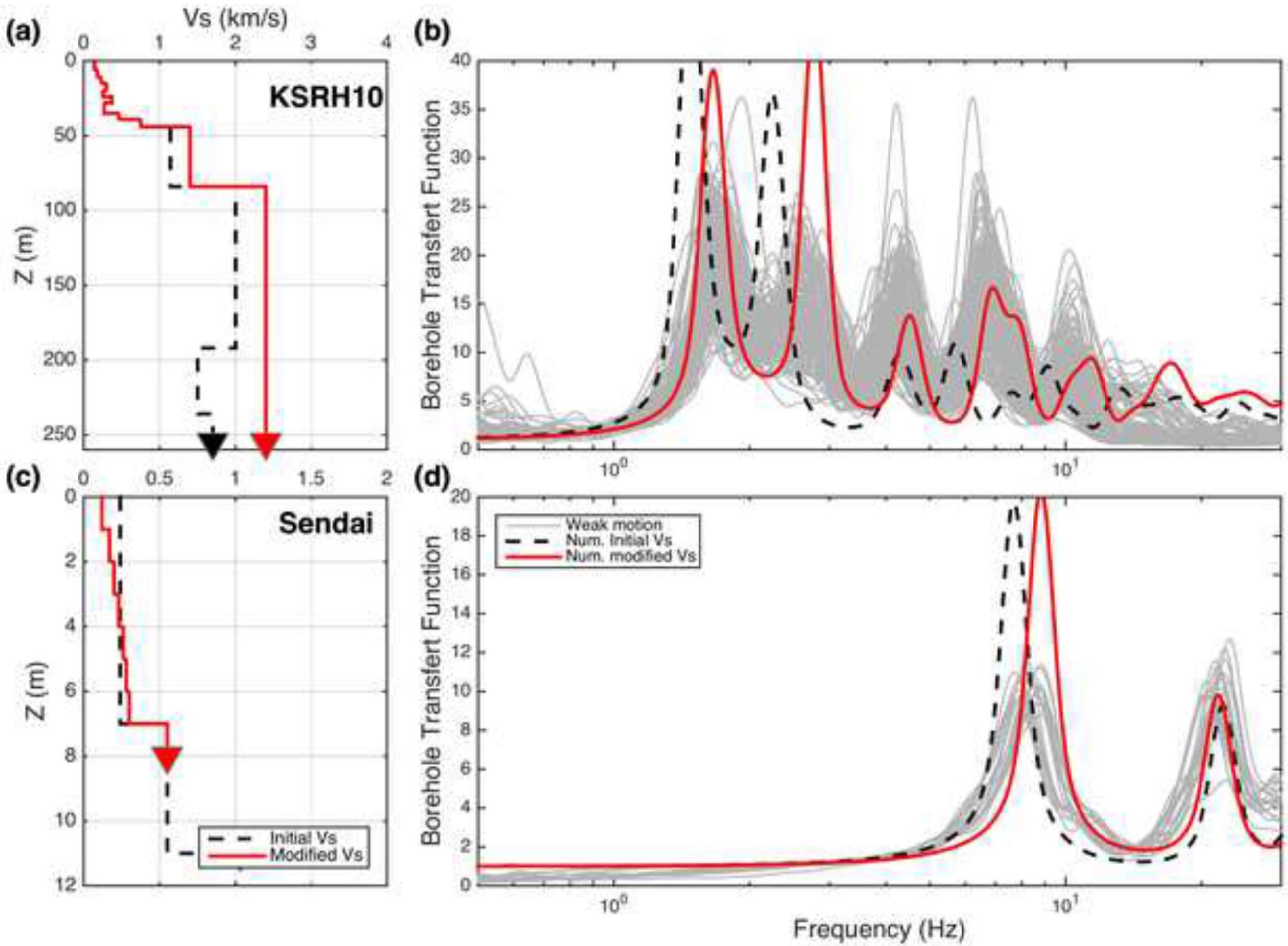
(a)
Vs (km/s)
KSRH10
Z (m)
(b)
Borehole Transfert Function
(c)
Sendai
Z (m)
Initial Vs
Modified Vs
(d)
Borehole Transfert Function
Weak motion
Num. Initial Vs
Num. modified Vs
Frequency (Hz)

Figure 5

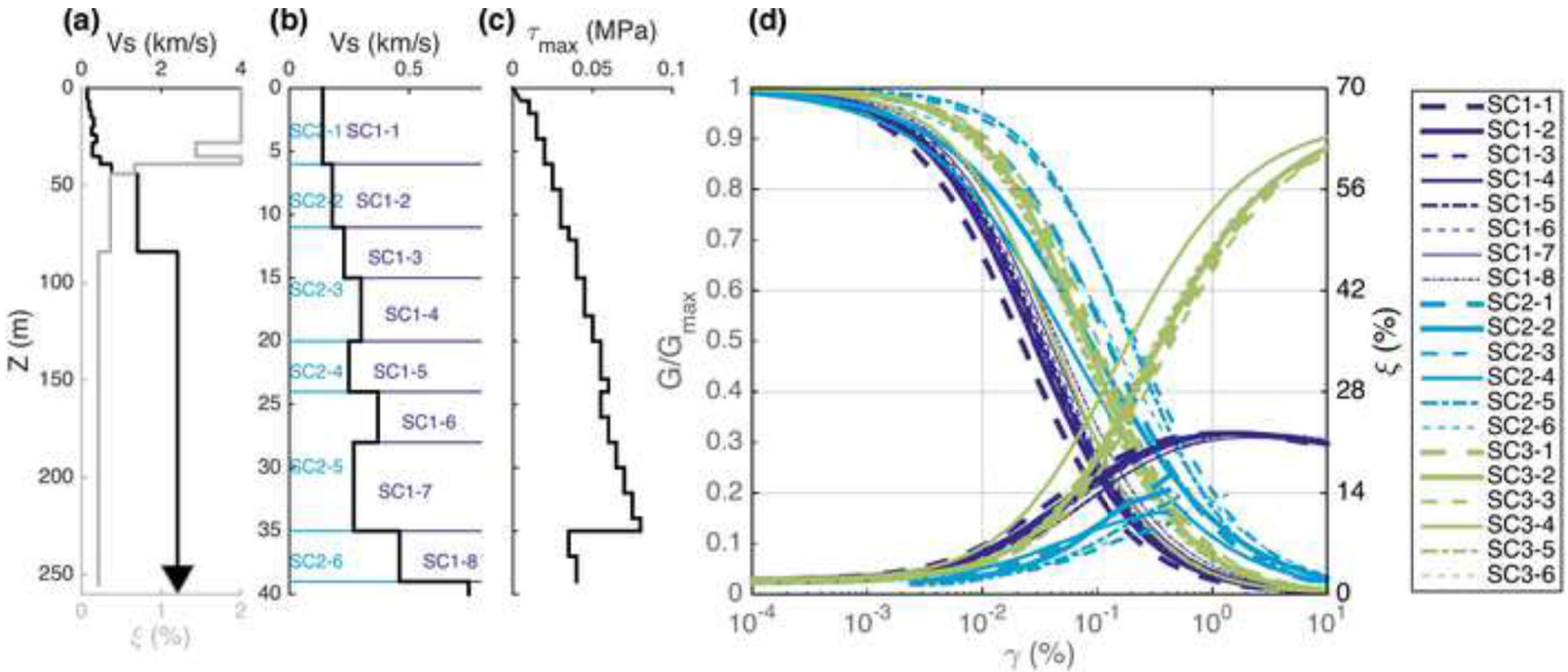

(a)
Vs (km/s)
0
2
4
Z (m)
0
50
100
150
200
250
0
1
2
ξ (%)
(b)
Vs (km/s)
0
0.5
0
5
10
15
20
25
30
35
40
SC1-1
SC1-2
SC1-3
SC1-4
SC1-5
SC1-6
SC1-7
SC1-8
SC2-2
SC2-3
SC2-4
SC2-5
SC2-6
(c)
τ_{max} (MPa)
0
0.05
0.1
(d)
G/G_{max}
1
0.9
0.8
0.7
0.6
0.5
0.4
0.3
0.2
0.1
0
10^{-4}
10^{-3}
10^{-2}
10^{-1}
10^{0}
10^{1}
γ (%)
70
56
42
28
14
0
ξ (%)
SC1-1
SC1-2
SC1-3
SC1-4
SC1-5
SC1-6
SC1-7
SC1-8
SC2-1
SC2-2
SC2-3
SC2-4
SC2-5
SC2-6
SC3-1
SC3-2
SC3-3
SC3-4
SC3-5
SC3-6

Figure 6

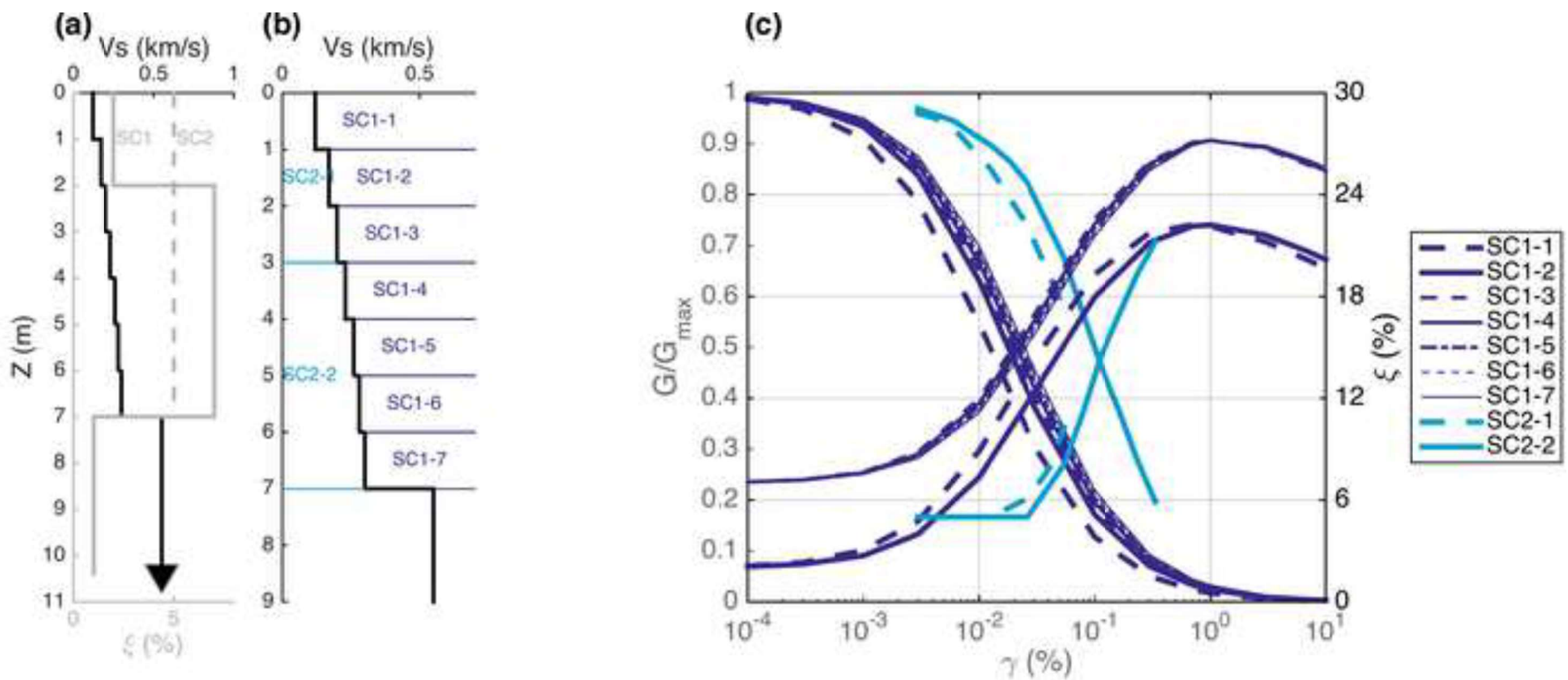
(a)
Vs (km/s)
0
0.5
1
Z (m)
SC1
SC2
ξ (%)
(b)
Vs (km/s)
SC1-1
SC1-2
SC1-3
SC1-4
SC1-5
SC1-6
SC1-7
SC2-1
SC2-2
(c)
G/Gmax
γ (%)
ξ (%)
SC1-1
SC1-2
SC1-3
SC1-4
SC1-5
SC1-6
SC1-7
SC2-1
SC2-2

Figure 7

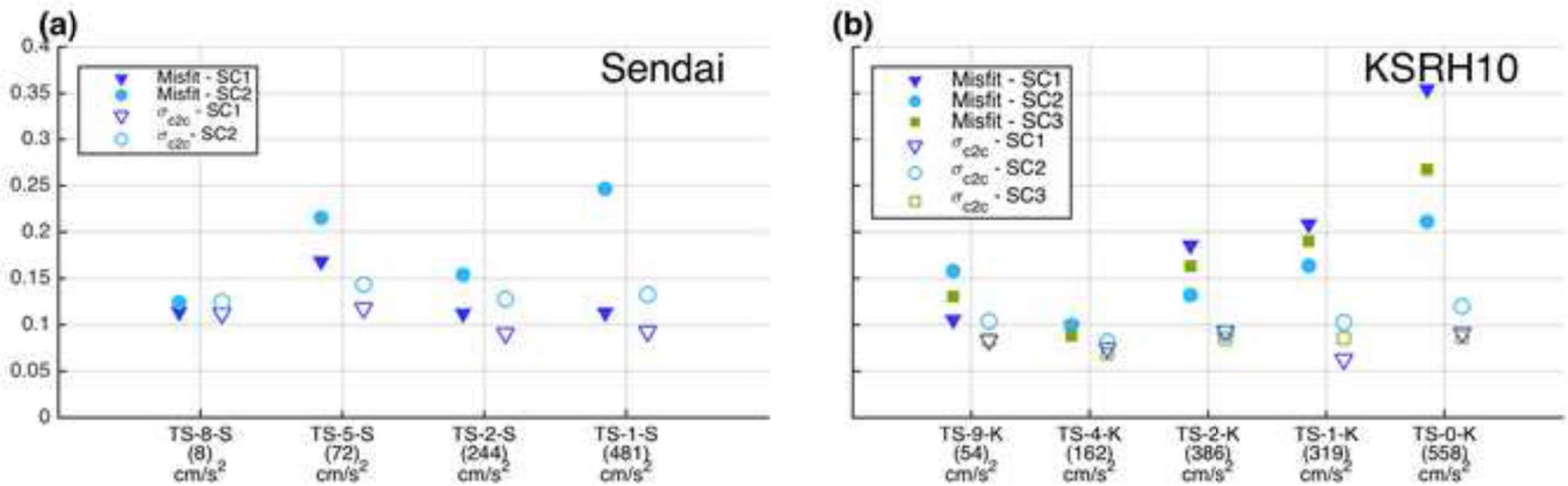
(a)
Sendai
Misfit - SC1
Misfit - SC2
σc2c - SC1
σc2c - SC2
0.4
0.35
0.3
0.25
0.2
0.15
0.1
0.05
0
TS-8-S (8) cm/s2
TS-5-S (72) cm/s2
TS-2-S (244) cm/s2
TS-1-S (481) cm/s2
(b)
KSRH10
Misfit - SC1
Misfit - SC2
Misfit - SC3
σc2c - SC1
σc2c - SC2
σc2c - SC3
TS-9-K (54) cm/s2
TS-4-K (162) cm/s2
TS-2-K (386) cm/s2
TS-1-K (319) cm/s2
TS-0-K (558) cm/s2

Figure 8

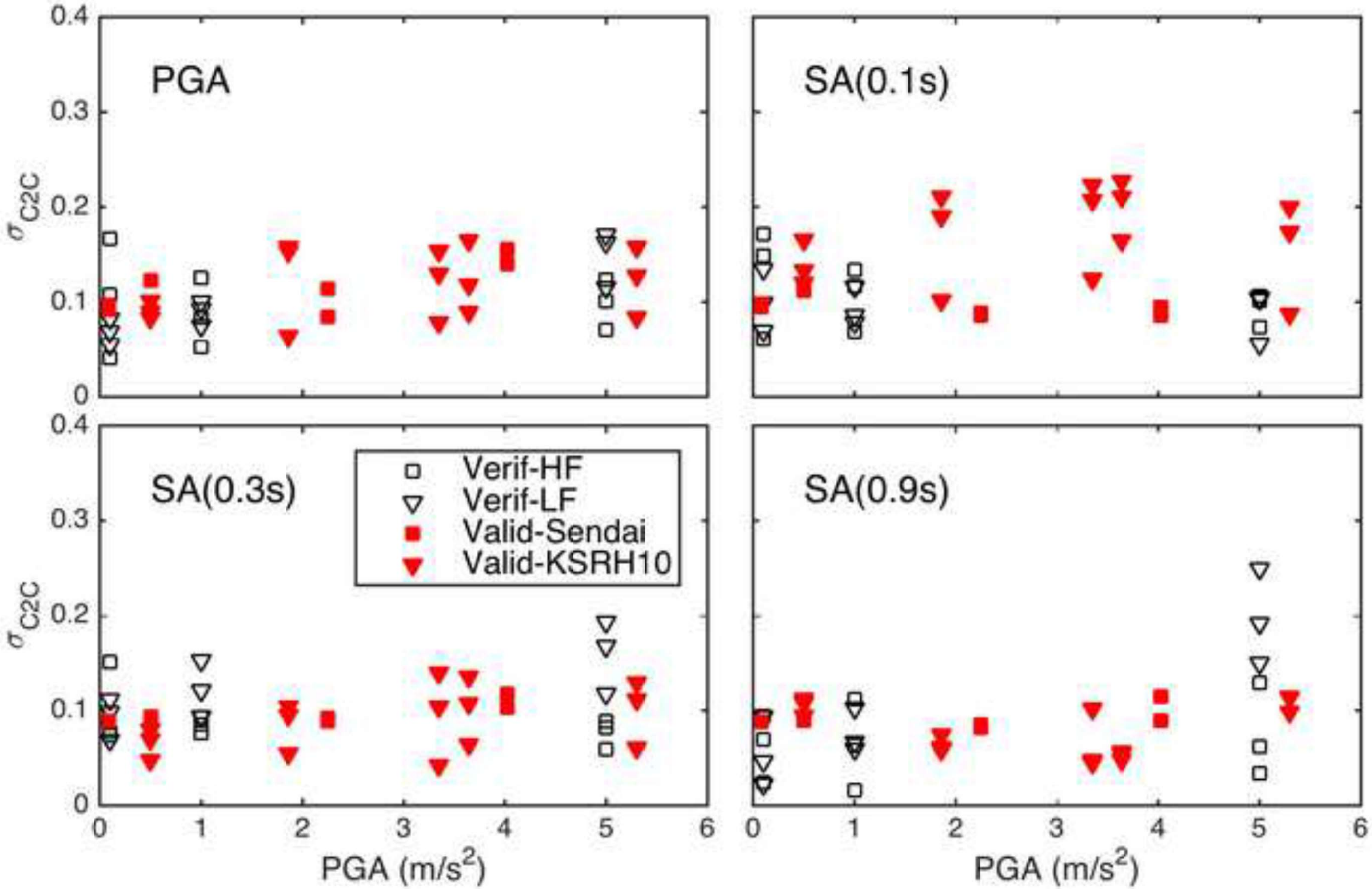
PGA
SA(0.1s)
SA(0.3s)
SA(0.9s)
Verif-HF
Verif-LF
Valid-Sendai
Valid-KSRH10
σ_{C2C}
0
0.1
0.2
0.3
0.4
0
1
2
3
4
5
6
PGA (m/s^2)

Figure 9

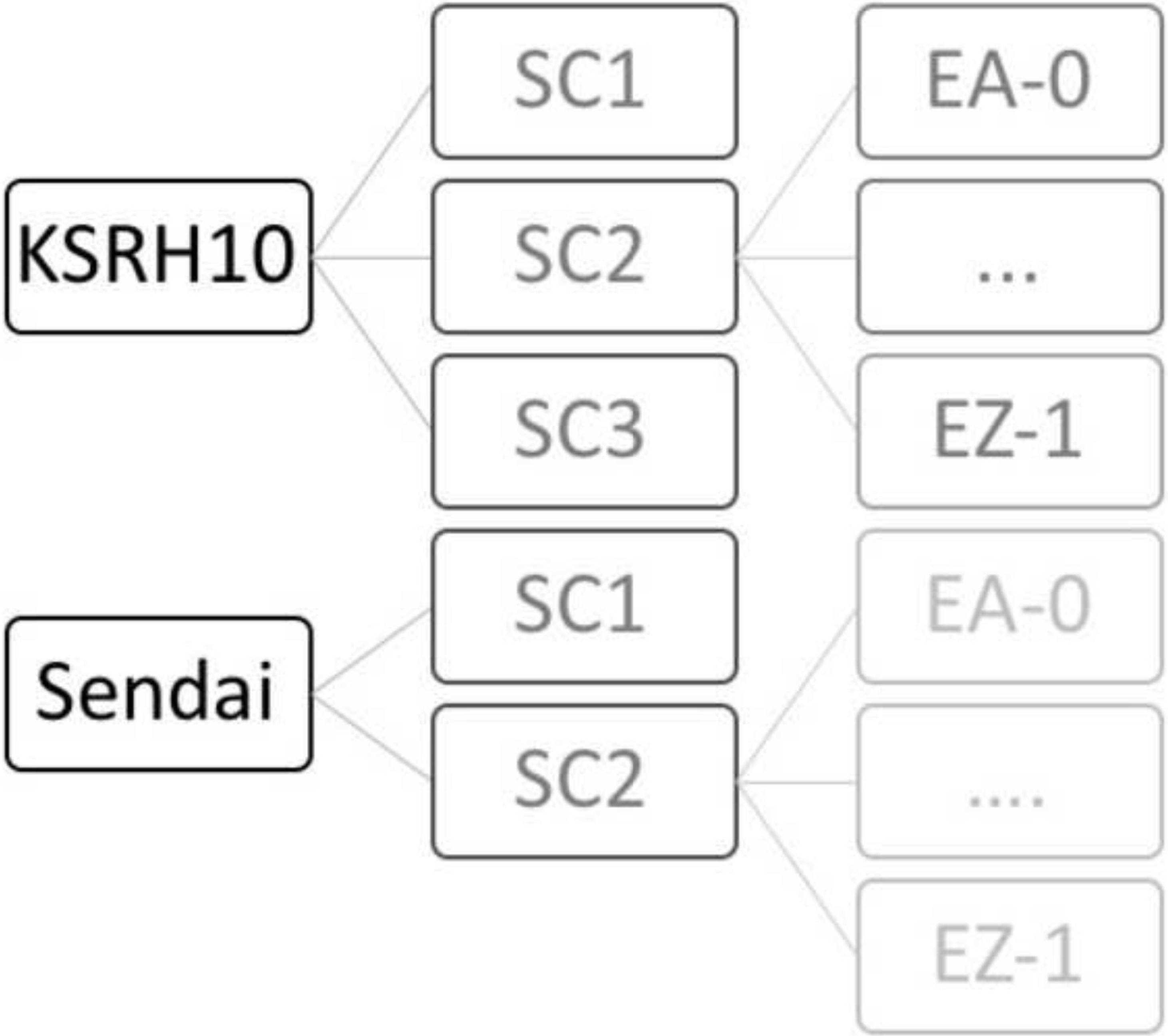

Figure 10

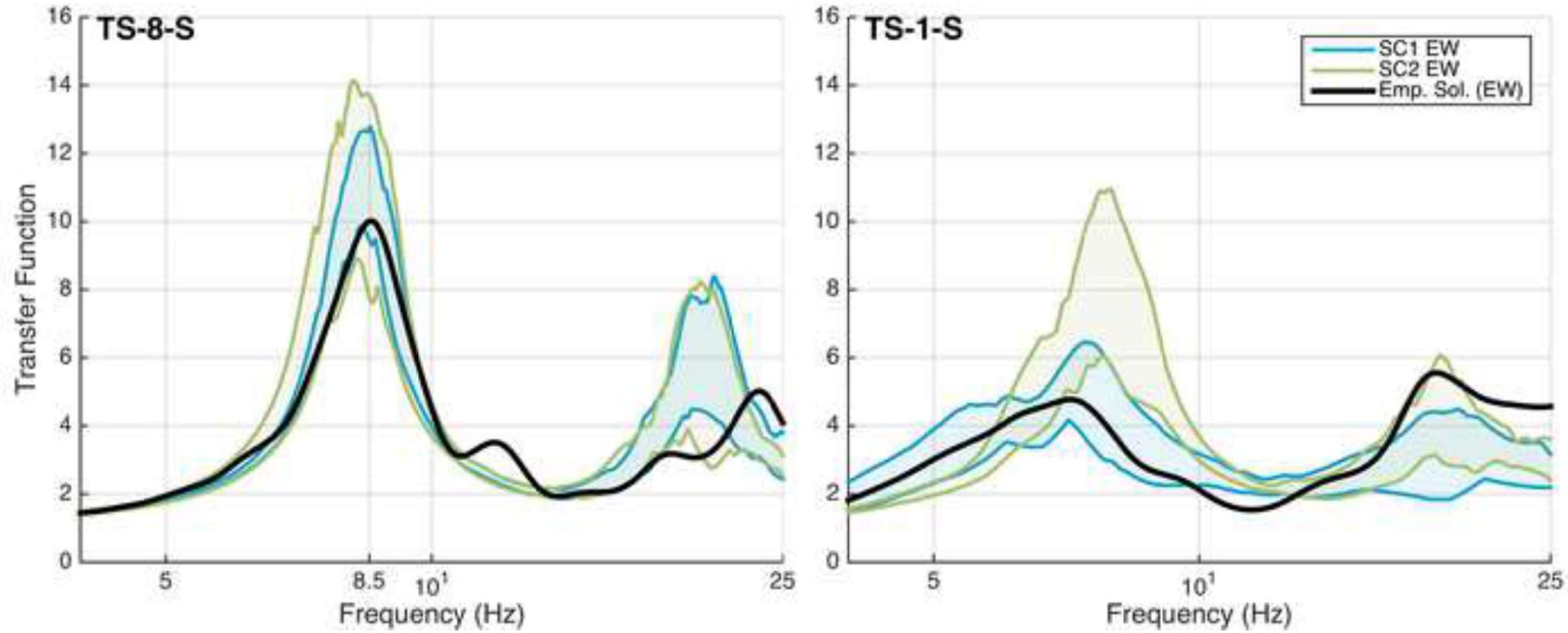
TS-8-S
TS-1-S
SC1 EW
SC2 EW
Emp. Sol. (EW)
Transfer Function
Frequency (Hz)
Frequency (Hz)
0
2
4
6
8
10
12
14
16
5
8.5
10^1
25

Figure 11

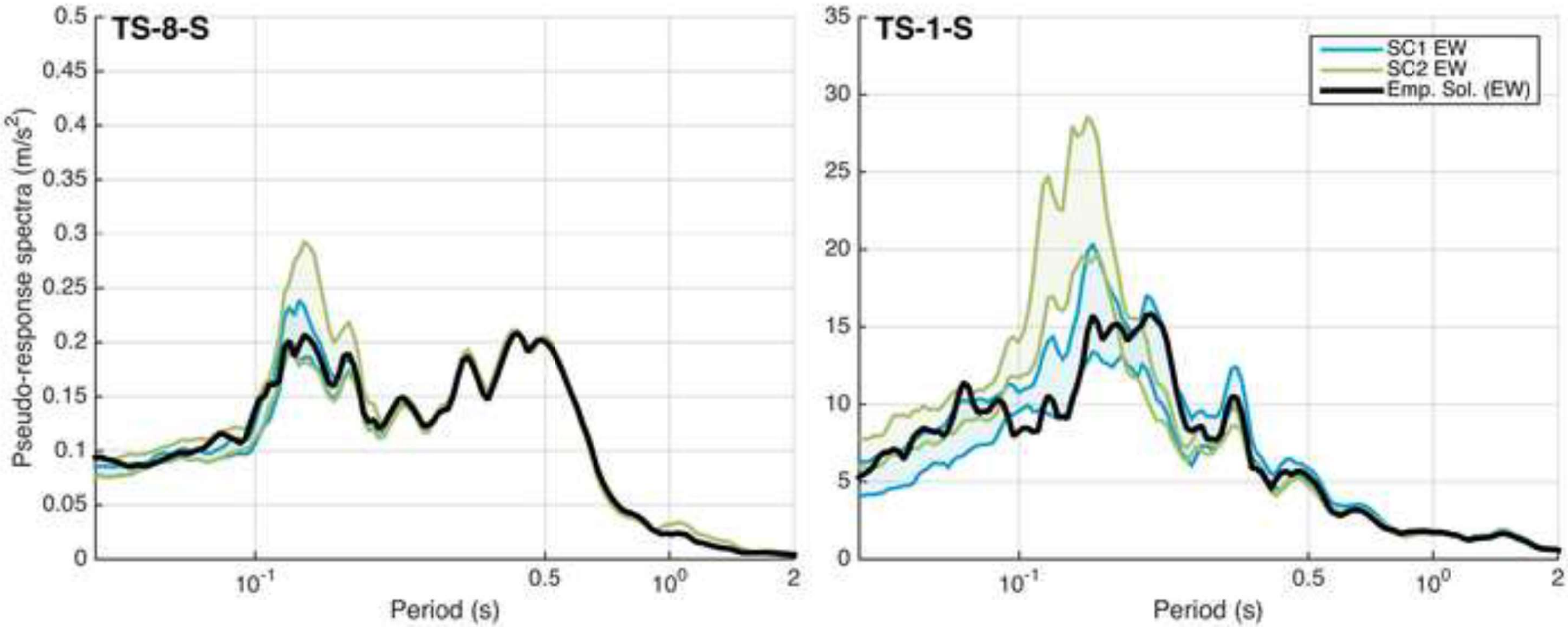
TS-8-S
TS-1-S
Pseudo-response spectra (m/s^2)
Period (s)
SC1 EW
SC2 EW
Emp. Sol. (EW)
0.5
0.45
0.4
0.35
0.3
0.25
0.2
0.15
0.1
0.05
0
35
30
25
20
15
10
5
10^{-1}
10^{0}
2

Figure 12

Click here to download Figure Fig_12_Misfit_period_average_sendai.jpg

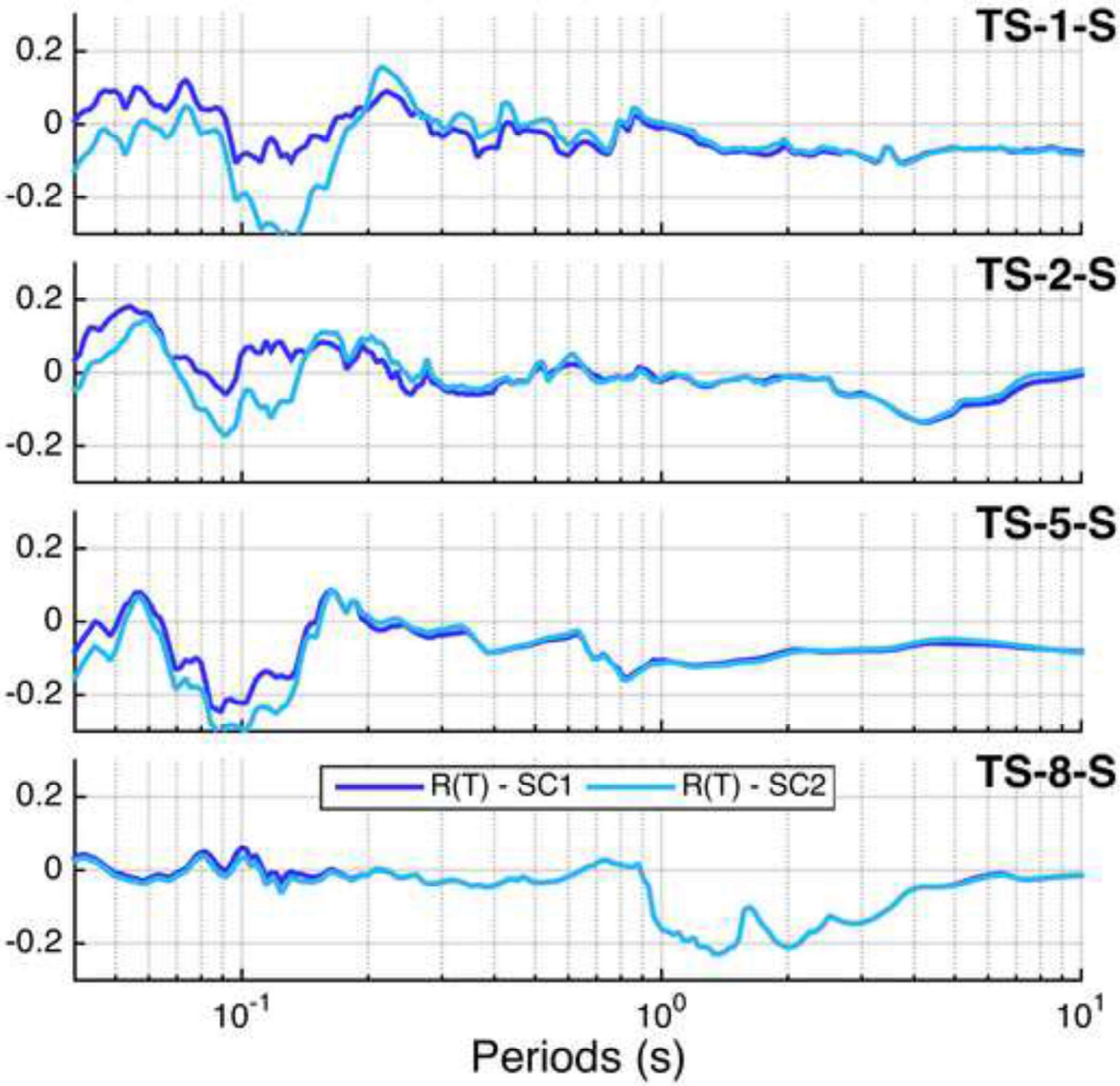

Figure 13

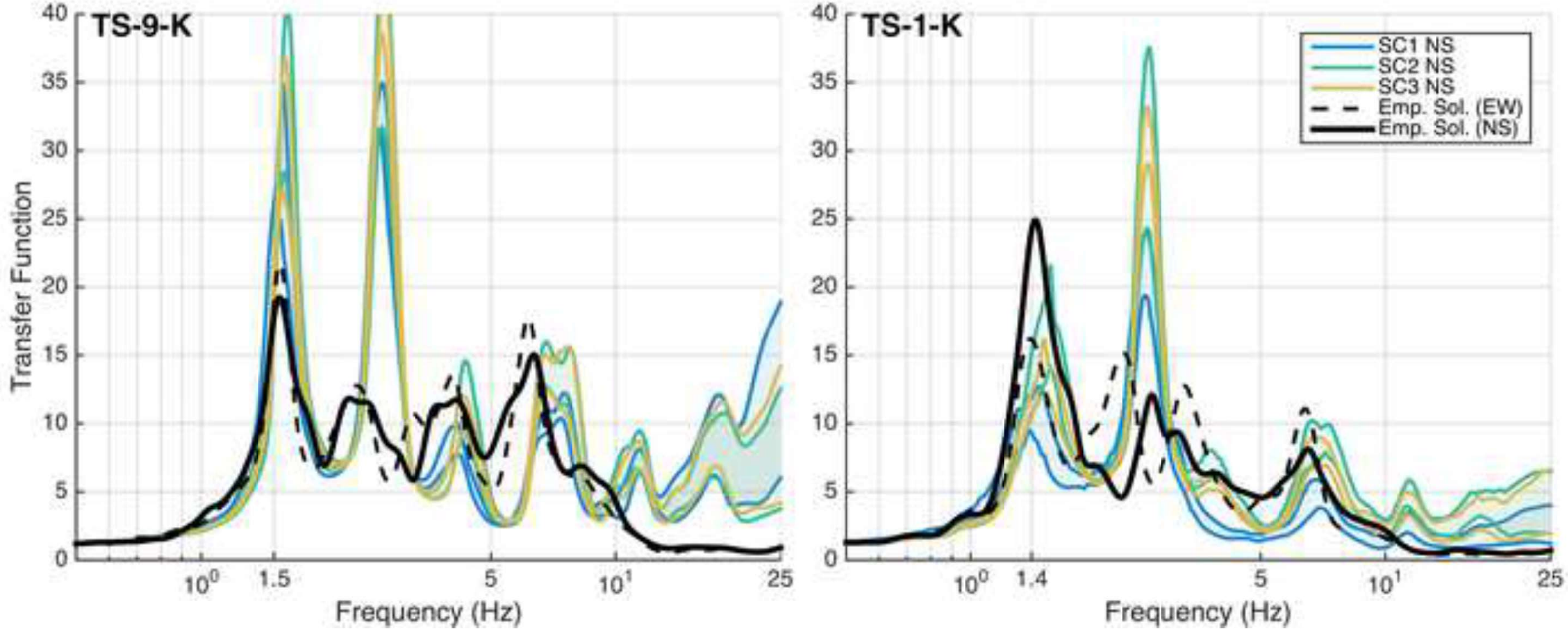
TS-9-K
TS-1-K
Transfer Function
Frequency (Hz)
Frequency (Hz)
SC1 NS
SC2 NS
SC3 NS
Emp. Sol. (EW)
Emp. Sol. (NS)
0
5
10
15
20
25
30
35
40
10^0
1.5
1.4
5
10^1
25

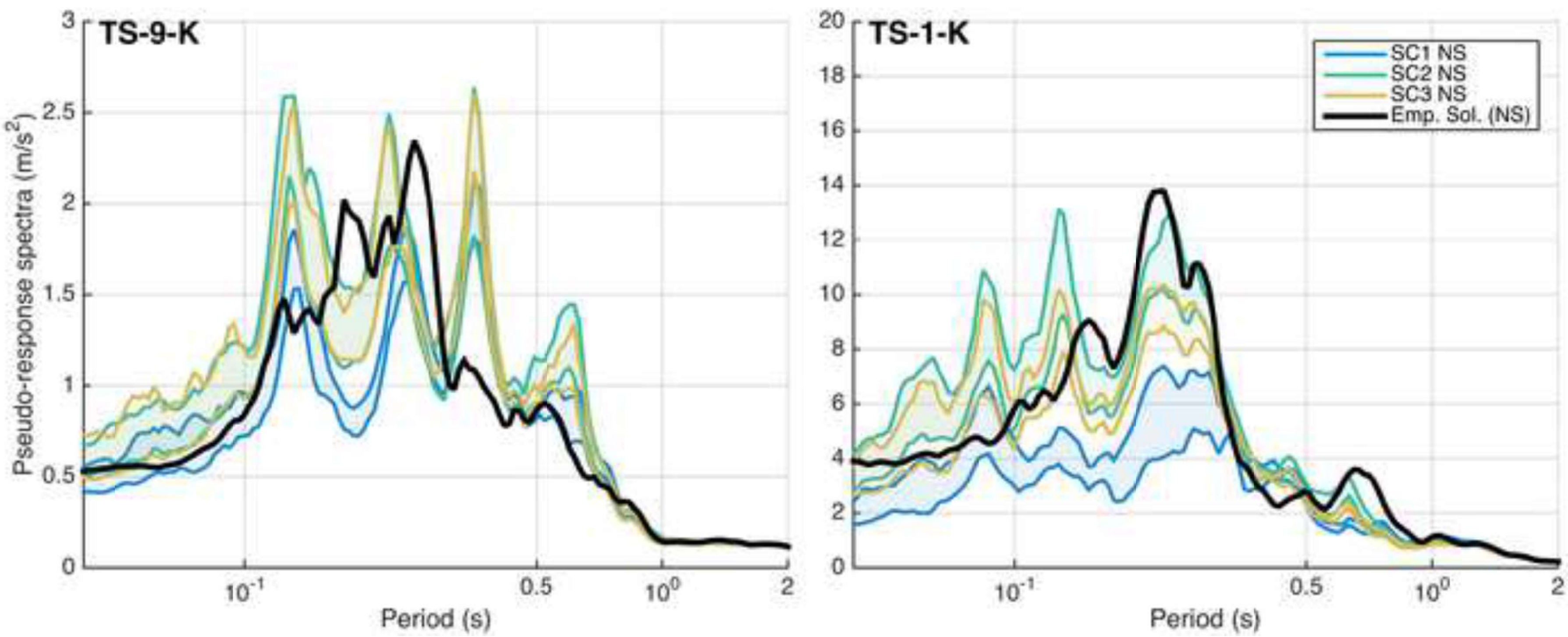
TS-9-K
TS-1-K
Pseudo-response spectra (m/s²)
Period (s)
Period (s)
SC1 NS
SC2 NS
SC3 NS
Emp. Sol. (NS)
0
0.5
1
1.5
2
2.5
3
0
2
4
6
8
10
12
14
16
18
20
10⁻¹
0.5
10⁰
2

Figure 15

Click here to download Figure
Fig_15_Misfit_period_average_KSRH10.jpg

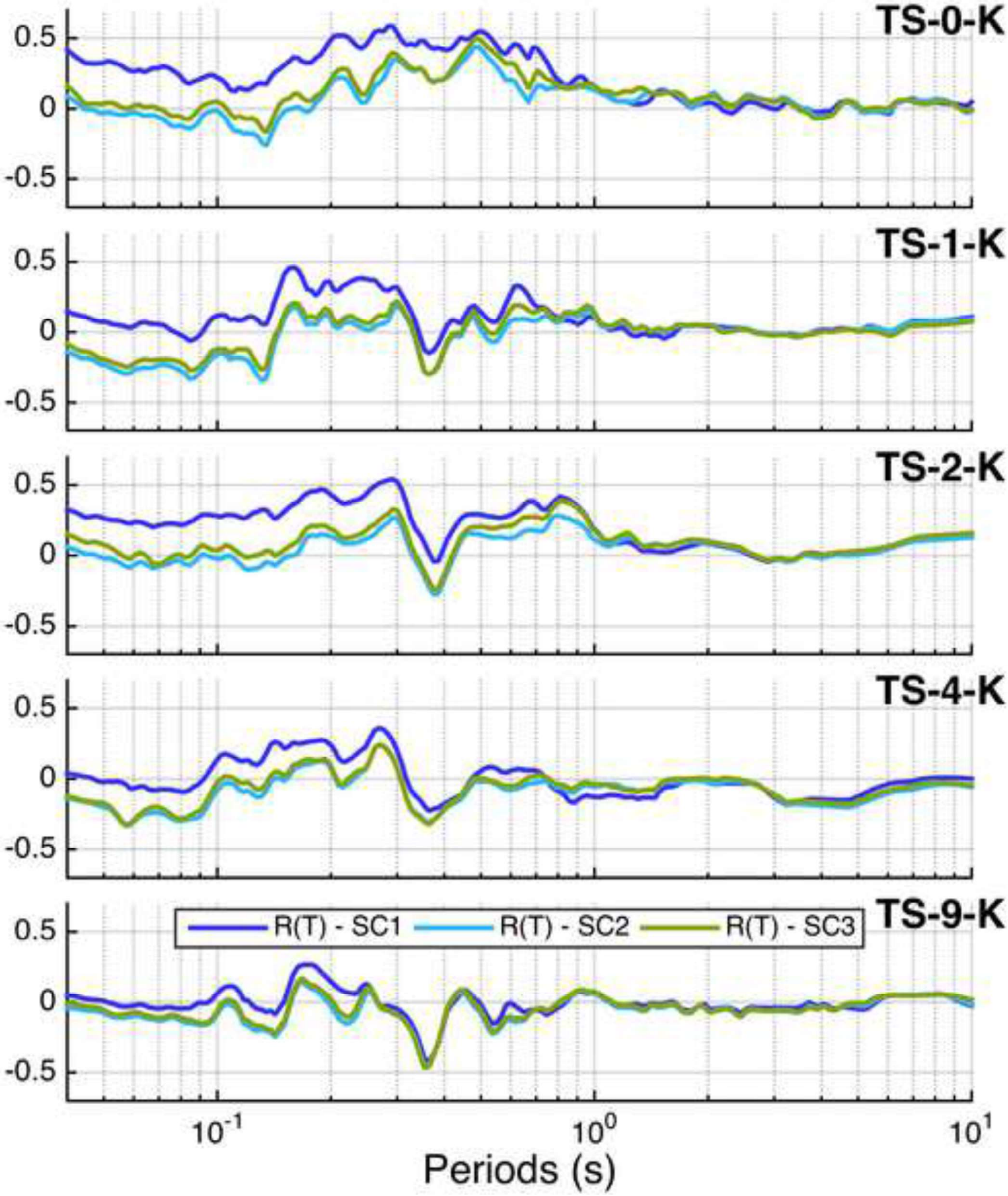

PRENOLIN: international benchmark on 1D nonlinear site response analysis – Validation phase exercise

Julie Régnier, Luis-Fabian Bonilla, Pierre-Yves Bard, Etienne Bertrand, Fabrice Hollender, Hiroshi Kawase, Deborah Sicilia, Pedro Arduino, Angelo Amorosi, Dominiki Asimaki, Daniela Boldini, Long Chen, Anna Chiaradonna, Florent DeMartin, Ahmed Elgamal, Gaetano Falcone, Evelyne Foerster, Sebastiano Foti, Evangelia Garini, George Gazetas, Céline Gélis, Alborz Ghofrani, Amalia Giannakou, Jim Gingery, Nathalie Glinsky, Joseph Harmon, Youssef Hashash, Susumu Iai, Steve Kramer, Stavroula Kontoe, Jozef Kristek, Giuseppe Lanzo, Annamaria di Lernia, Fernando Lopez-Caballero, Marianne Marot, Graeme McAllister, E.Diego Mercerat, Peter Moczo, Silvana Montoya-Noguera, Michael Musgrove, Alex Nieto-Ferro, Alessandro Pagliaroli, Federico Passeri, Aneta Richterova, Suwal Sajana, Maria Paola Santisi d'Avila, Jian Shi, Francesco Silvestri, Mahdi Taiebat, Giuseppe Tropeano, Didrik Vandeputte and Luca Verrucci.

Electronic supplement

The electronic supplement contains elements that provide details on: (1) the codes used during the benchmark with the table of the participants and codes used (Table S1) (2) the analysis performed on the accelerometric data to determine the angle of incidence of seismic waves at KSRH10 and Sendai site (Figure S1). (3) A figure that indicate the location of the soil sampling performed to characterize Sendai and KSRH10 sites (Figure S2 from S5) and (4) Figures on applicability of the numerical methods (Figure S6 and Figure S7).

A detailed presentation of the Polarization analysis for verification of the verticality of the incident propagating input motions is given below:

Since P- and S-waves show a high degree of linear polarization (contrary to Rayleigh waves which are generally elliptically polarized (i.e. Montalbetti and Kanasewich, 1970), the direction of propagation for P-waves is parallel to the particle motion trajectory (hodograph) and perpendicular to the direction of propagation for S-waves. Rayleigh wave particle motion is within the vertical-radial plane, and Love waves are polarized in a horizontal plane perpendicular to the propagation direction. Due to reflections and scattering, a rather a complex particle motion trajectory is observed in real seismograms instead of pure polarization states. The hodograph can therefore be fitted to an ellipsoid in a least-squares sense by means of a covariance analysis (Flinn, 1965; Jurkevics, 1988).

The 3x3 covariance matrix is symmetric, has real non-negative eigenvalues, and its eigenvectors are the principal axes of an ellipsoid that represents the best fit to the data in a least-squares sense. The eigenvector associated with the largest eigenvalue points into the main polarization direction, i.e. the long axis of the ellipsoid. The direction of polarization is calculated from the components (direction cosines) of this eigenvector. The direction can be described by a horizontal azimuth angle ϕ and by the deviation from the vertical direction or apparent incidence angle θ as (Maercklin, 1999):

$$\theta = arctan\left(\frac{\sqrt{x^2+y^2}}{z}\right)$$

Eq S1

$$\varphi = \arctan\left(\frac{x}{y}\right)$$

Eq S2

Here, x and y denote the two horizontal components of the principal eigenvector V and z its vertical component.

The choice of the time window length and the frequency bandwidth are subject to trade-offs between resolution and variance (e.g. Wang & Teng, 1997). A short time window and a narrow bandwidth avoid averaging over different phases allow for the resolution of frequency-dependent polarization, whereas a longer window and a wider frequency band yield more stable polarization estimates. Besides that, any filtering before the polarization analysis has to be applied in the same way to all three components and should not distort the signal significantly. In our analysis we whose a time window of 1s and we filtered the data unsing a low-pass filter with a cut-off frequency of 2Hz.

After the main polarization direction is determined, the degree of linear or planar polarization is evaluated. The rectilinearity RL is a measure of the degree of linear polarization of an event (Flinn, 1965). Montalbetti & Kanasewich (1970) and Kanasewich (1981) define RL as:

$$RL = 1 - \left(\frac{\lambda_2}{\lambda_1}\right)$$

Eq S3

with the two largest eigenvalues λ_1 and λ_2. With this definition the range of values is between RL = 0 for elliptical or undetermined polarization, and RL = 1 for exactly linear polarization. In **Error! Reference source not found.**, we potted the incidence in stereographic projection for the two sites (left KSRH10 and right Sendai) of the wave at the borehole station (bottom stereonet) and at the surface (top stereonet).

References

Aubry, D., Modaressi, A., 1996. GEFDYN, Manuel scientifique. Éc. Cent. Paris LMSS-Mat.

Bardet, J.P., Ichii, K., Lin, C.H., 2000. EERA: a computer program for equivalent-linear earthquake site response analyses of layered soil deposits. University of Southern California, Department of Civil Engineering.

Benz, T., 2006. Small strain stiffness of soils and its consequences. Dr. Thesis IGS Univ. Stuttg.

Benz, T., Vermeer, P.A., Schwab, R., 2009. A small-strain overlay model. Int. J. Numer. Anal. Methods Geomech. 33, 25–44.

Flinn, E.A., 1965. Signal analysis using rectilinearity and direction of particle motion. Proc. IEEE 53, 1874–1876.

Gerolymos, N., Gazetas, G., 2006. Winkler model for lateral response of rigid caisson foundations in linear soil. Soil Dyn. Earthq. Eng. 26, 347–361.

Gerolymos, N., Gazetas, G., 2005. Constitutive model for 1-D cyclic soil behaviour applied to seismic analysis of layered deposits. Soils Found. 45, 147–159.

Hashash, Y.M.A., Groholski, D.R., Phillips, C.A., Park, D., Musgrove, M., 2012. DEEPSOIL 5.1. User Man. Tutor. 107.

ITASCA, F., 2011. 7.0: User Manual. Licence Number 213-039-0127-18973. Sapienza—Univ Rome Earth Sci. Dep.

Jurkevics, A., 1988. Polarization analysis of three-component array data. Bull. Seismol. Soc. Am. 78, 1725–1743.

Kontoe, S., 2006. Development of time integration schemes and advanced boundary conditions for dynamic geotechnical analysis. Imperial College London (University of London).

Li, W., Assimaki, D., 2010. Site-and motion-dependent parametric uncertainty of site-response analyses in earthquake simulations. Bull. Seismol. Soc. Am. 100, 954–968.

Maercklin, N., 1999. Polarisationsanalyse refraktionsseismischer Daten vom Vulkan Merapi, Indonesien.

Matasović, N., Ordóñez, G., 2007. D-MOD2000. GeoMotions, LLC, Computer Software.

Matasovic, N., vucetic, M., 1993. Analysis of seismic records obtained on november 24, 1987 at the Wildlife liquefaction array. University of California, Los Angeles.

Mercerat, E.D., Glinsky, N., 2015. A nodal discontinuous Galerkin method for non-linear soil dynamics. 6th Int. Conf. Earthq. Geotech. Eng.

Modaressi, H., Foerster, E., 2000. CyberQuake. User's Man. BRGM Fr.

Montalbetti, J.F., Kanasewich, E.R., 1970. Enhancement of teleseismic body phases with a polarization filter. Geophys. J. Int. 21, 119–129.

Potts, D.M., Zdravkovic, L., 1999. Finite element analysis in geotechnical engineering: theory. Imperial College of Science, Technology and Medicine. Thomas Telford Publishing, Thomas Telford Ltd, ISBN 0-7277-2783-4.

Santisi d'Avila, M.P., Lenti, L., Semblat, J.-F., 2012. Modelling strong seismic ground motion: three-dimensional loading path versus wavefield polarization. Geophys. J. Int. 190, 1607–1624.

Santisi d'Avila, M.P., Semblat, J.-F., 2014. Nonlinear seismic response for the 2011 Tohoku earthquake: borehole records versus one-directional three-component propagation models. Geophys. J. Int. 197, 566–580.

Santisi d'Avila, M.P., Semblat, J.-F., Lenti, L., 2013. Strong Ground Motion in the 2011 Tohoku Earthquake: A One-Directional Three-Component Modeling. Bull. Seismol. Soc. Am. 103, 1394–1410.

Shi, J., Asimaki, D., 2017. From Stiffness to Strength: Formulation and Validation of a Hybrid Hyperbolic Nonlinear Soil Model for Site-Response Analyses. Bull. Seismol. Soc. Am.

Susumu Iai, T.K., Yoasuo Matsunaga, 1990. Strain space plasticity model for cyclic mobility (No. 4). port and harbour reasearch insitute.

Taborda, D.M.., Zdravkovic, L., Kontoe, L., Potts, D.M., 2010. Alternative formulations for cyclic nonlinear models: parametric study and comparative analyses. Numer. Methods Geotech. Eng. NUMGE 2010 Benz Nord. Eds CRC Press, 423–428.

Tropeano, G., Chiaradonna, A., d'onofrio, A., Silvestri, F., 2016. An innovative computer code for 1D seismic response analysis including shear strength of soils. 101680geotSIP 15-P-017.

1. List of table caption

2. List of Figure caption

Figure S1

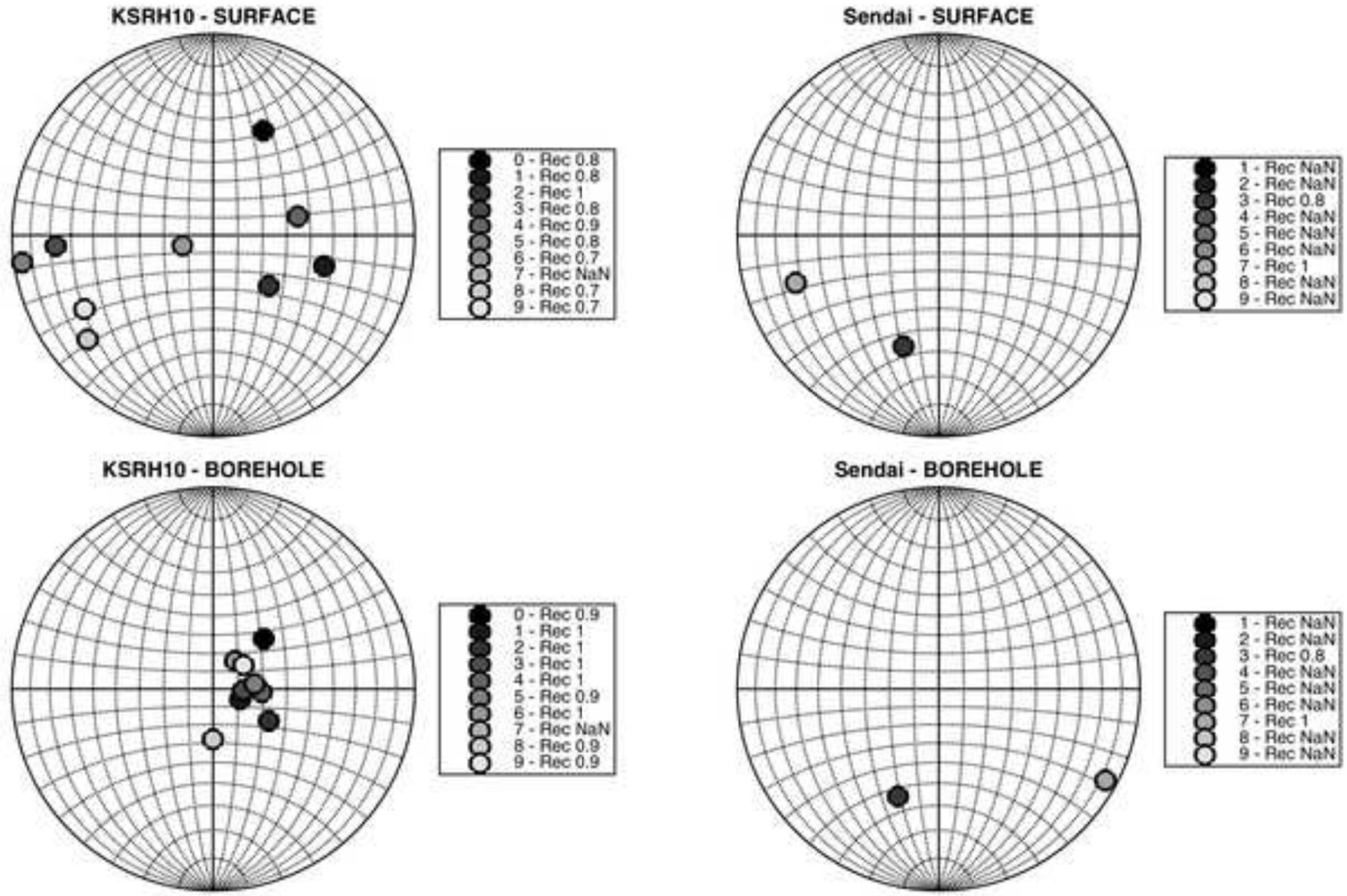
KSRH10 - SURFACE
0 - Rec 0.8
1 - Rec 0.8
2 - Rec 1
3 - Rec 0.8
4 - Rec 0.9
5 - Rec 0.8
6 - Rec 0.7
7 - Rec NaN
8 - Rec 0.7
9 - Rec 0.7
Sendai - SURFACE
1 - Rec NaN
2 - Rec NaN
3 - Rec 0.8
4 - Rec NaN
5 - Rec NaN
6 - Rec NaN
7 - Rec 1
8 - Rec NaN
9 - Rec NaN
KSRH10 - BOREHOLE
0 - Rec 0.9
1 - Rec 1
2 - Rec 1
3 - Rec 1
4 - Rec 1
5 - Rec 0.9
6 - Rec 1
7 - Rec NaN
8 - Rec 0.9
9 - Rec 0.9
Sendai - BOREHOLE
1 - Rec NaN
2 - Rec NaN
3 - Rec 0.8
4 - Rec NaN
5 - Rec NaN
6 - Rec NaN
7 - Rec 1
8 - Rec NaN
9 - Rec NaN

Figure S2

Measurements quantities (SENDAI(2))

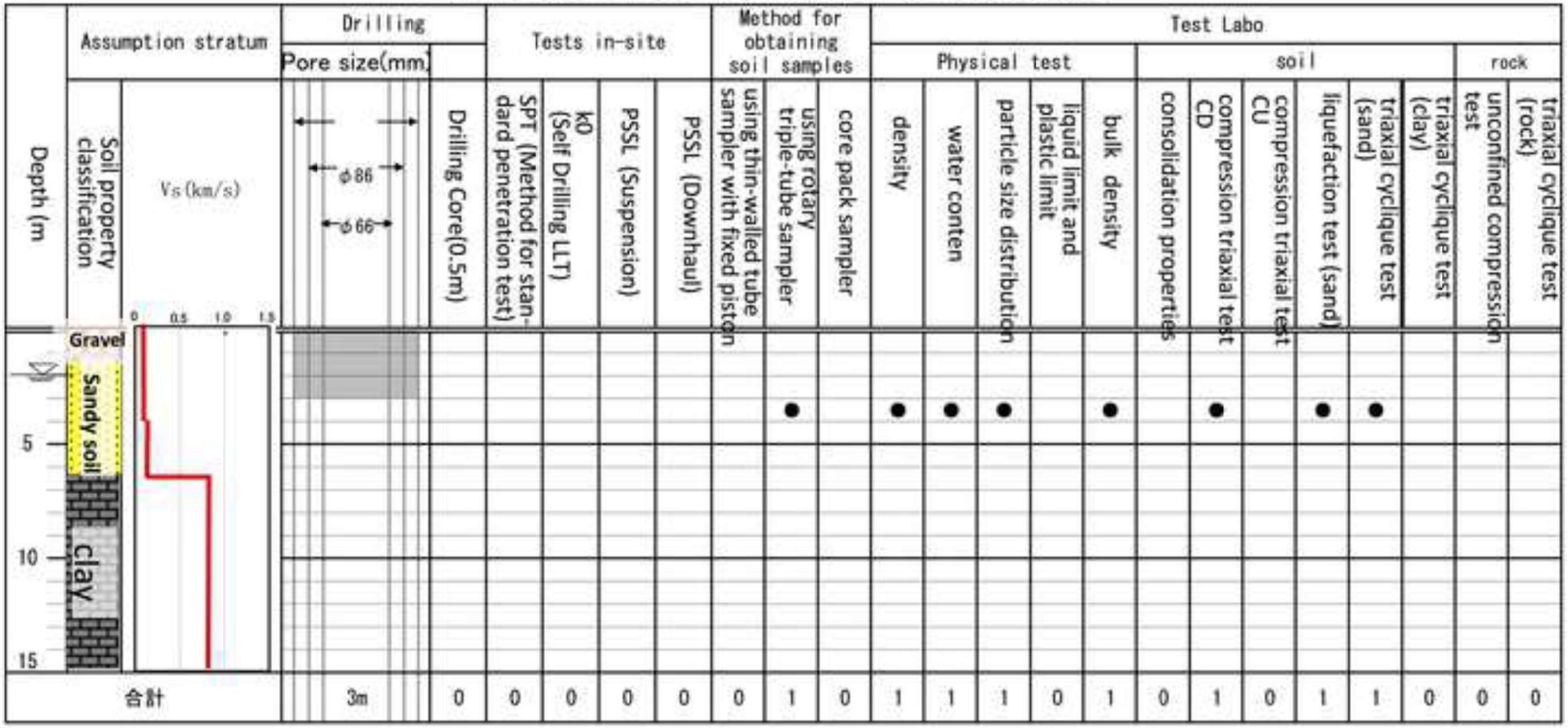

Figure S3

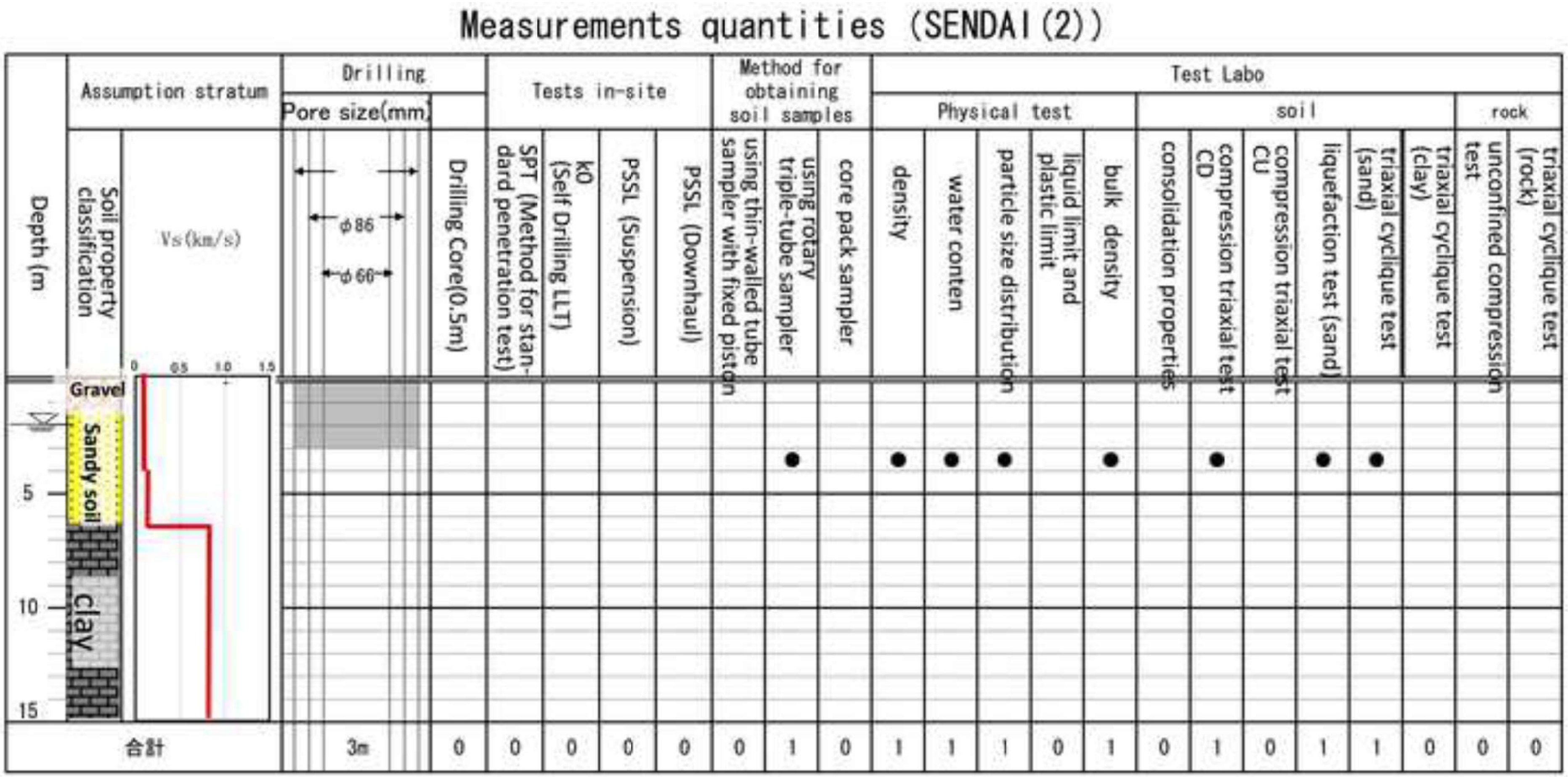
Measurements quantities (SENDAI (2))
Depth (m
Assumption stratum
Soil property classification
Vs (km/s)
0
0.5
1.0
1.5
Gravel
Sandy soil
clay
5
10
15
Drilling
Pore size(mm)
φ86
φ66
Drilling Core(0.5m)
Tests in-site
SPT (Method for standard penetration test)
k0 (Self Drilling LLT)
PSSL (Suspension)
PSSL (Downhaul)
Method for obtaining soil samples
using thin-walled tube sampler with fixed piston
using rotary triple-tube sampler
core pack sampler
Test Labo
Physical test
density
water conten
particle size distribution
liquid limit and plastic limit
bulk density
soil
consolidation properties
compression triaxial test CD
compression triaxial test CU
liquefaction test (sand)
triaxial cyclique test (sand)
triaxial cyclique test (clay)
rock
unconfined compression test
triaxial cyclique test (rock)
合計
3m
0
0
0
0
0
0
1
0
1
1
1
0
1
0
1
0
1
1
0
0
0

Figure S4

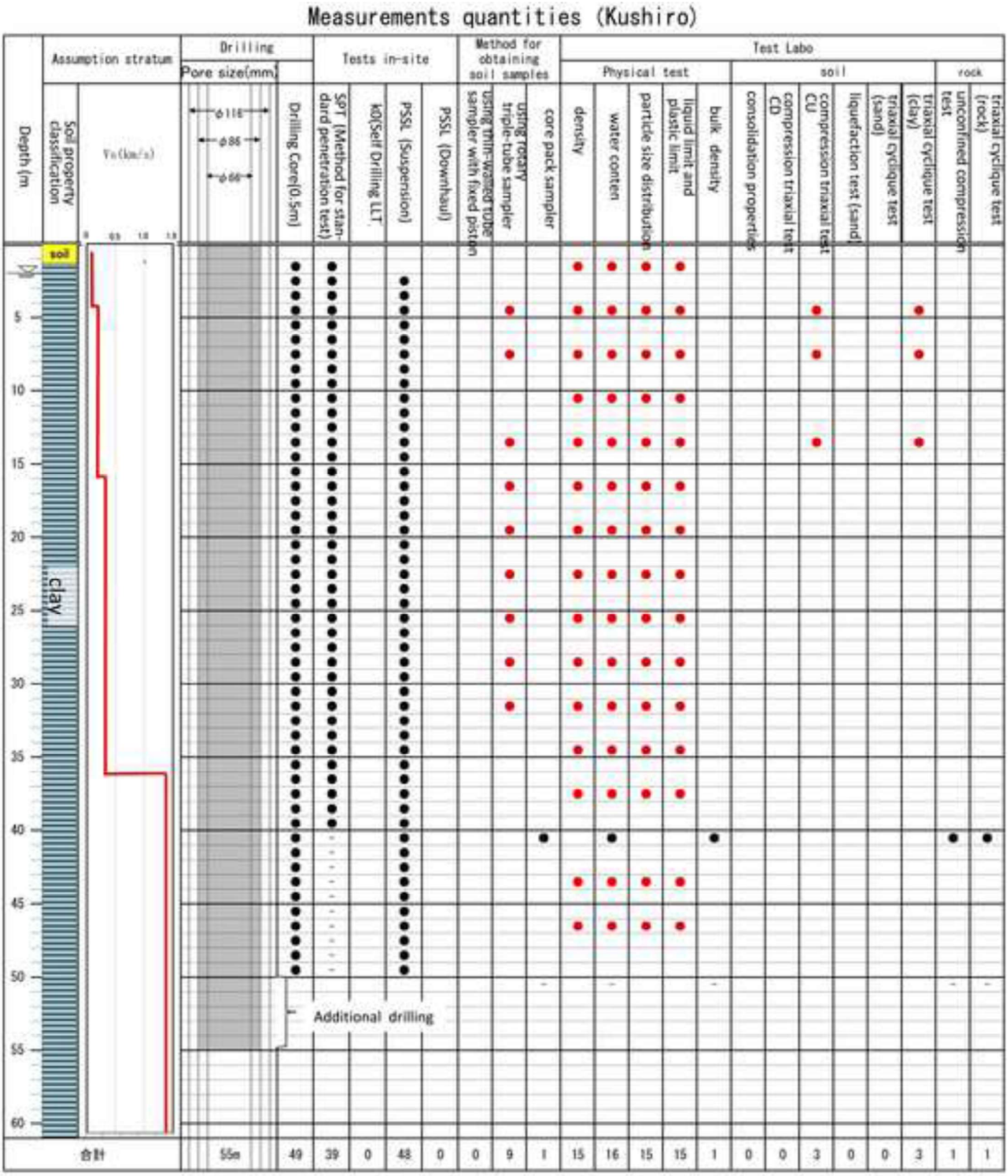
Measurements quantities (Kushiro)
Depth (m)
Assumption stratum
Soil property classification
Vs (km/s)
soil
clay
Drilling
Pore size(mm)
φ116
φ86
φ66
Tests in-site
Drilling Core(0.5m)
SPT (Method for standard penetration test)
k0(Self Drilling LLT)
PSSL (Suspension)
PSSL (Downhole)
Method for obtaining soil samples
using thin-walled tube sampler with fixed piston
using rotary triple-tube sampler
core pack sampler
Test Labo
Physical test
density
water content
particle size distribution
liquid limit and plastic limit
bulk density
soil
consolidation properties
compression triaxial test CD
compression triaxial test CU
liquefaction test (sand)
triaxial cyclique test (sand)
triaxial cyclique test (clay)
rock
unconfined compression test
triaxial cyclique test (rock)
Additional drilling
合計
55m
49
39
0
48
0
0
9
1
15
16
15
15
1
0
0
3
0
0
3
1
1

Figure S5

Click here to download Supplemental Material (Main Page, Tables, Figures) Fig_S5.jpeg

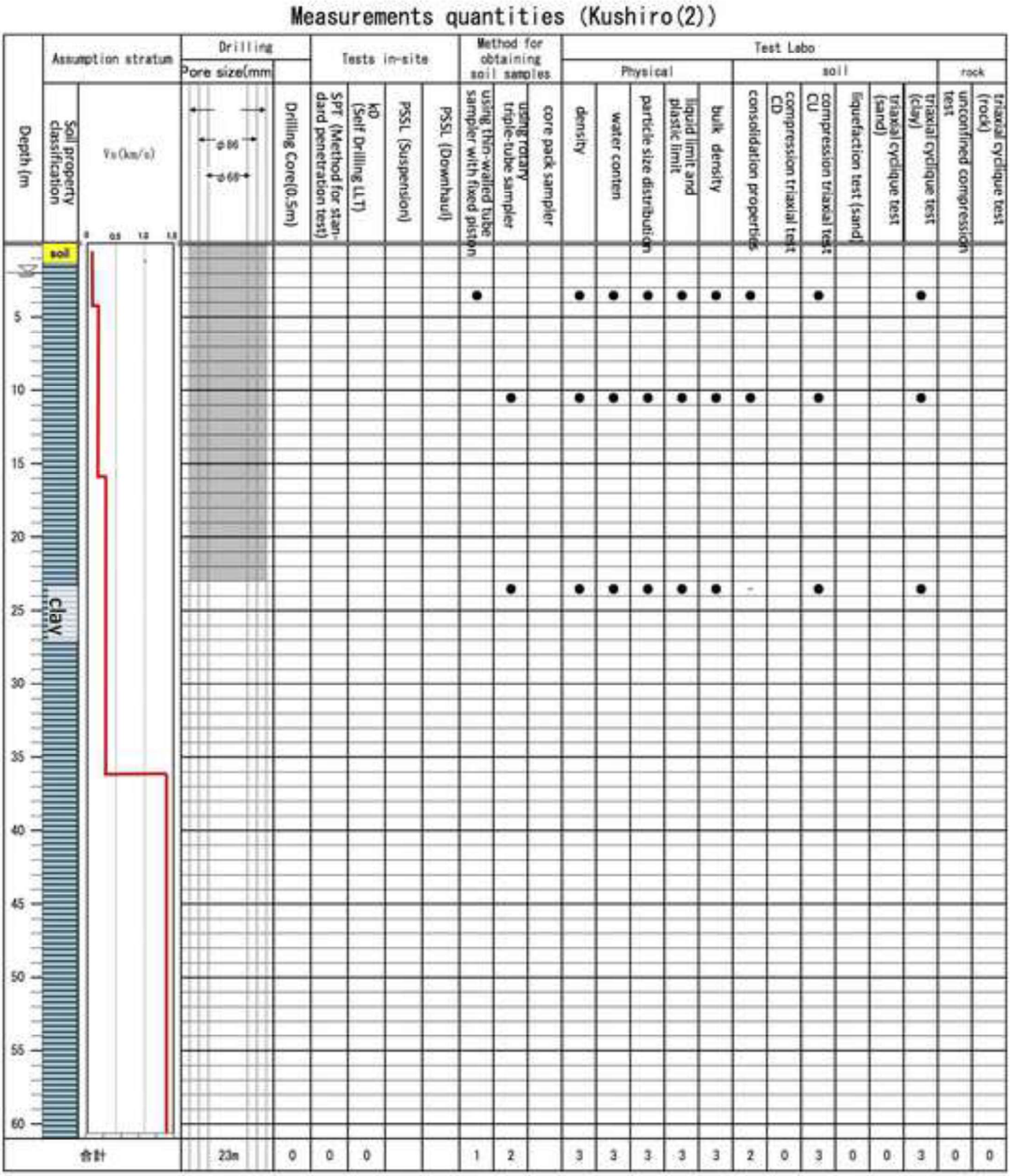

Figure S6

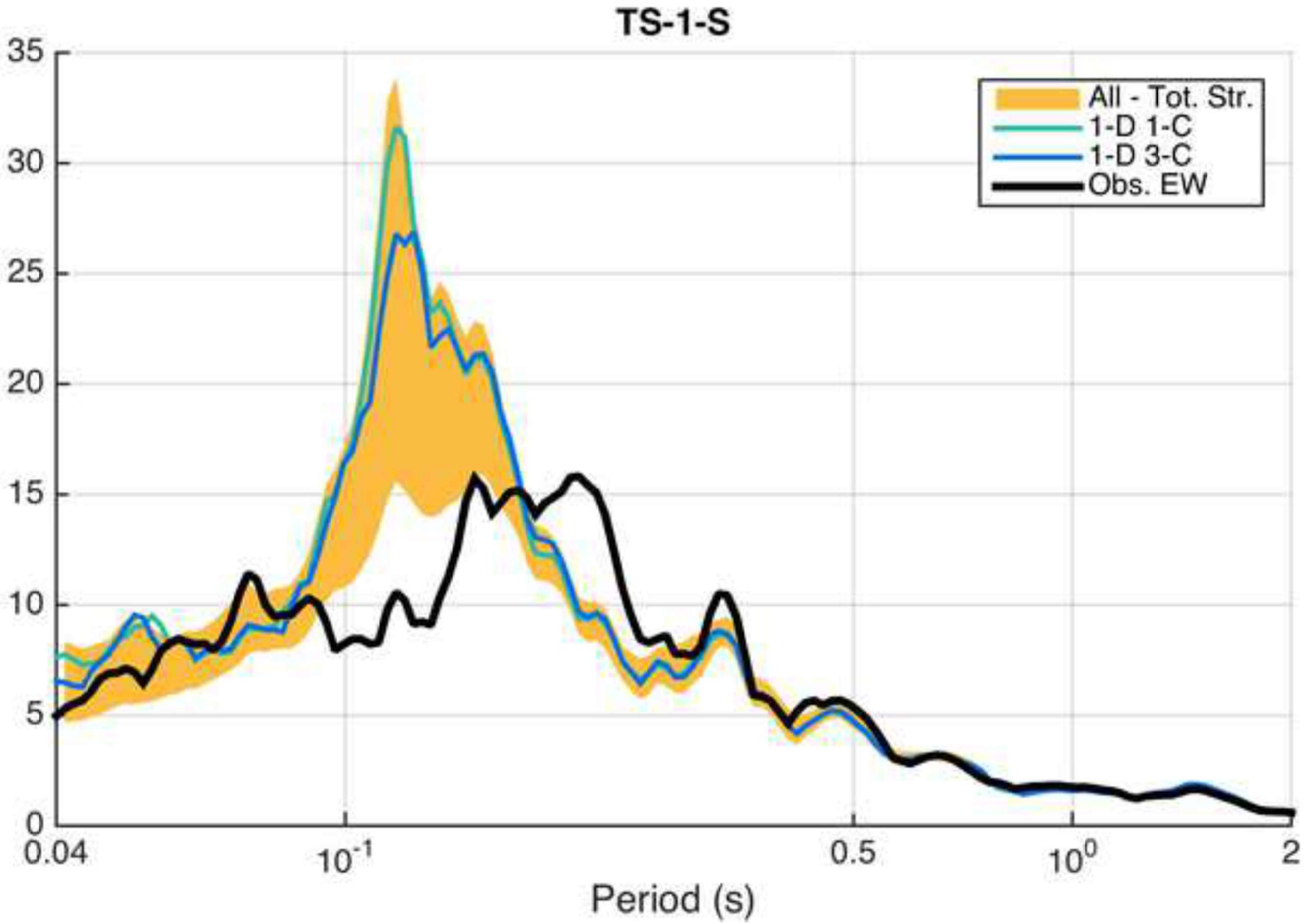
TS-1-S
35
30
25
20
15
10
5
0
0.04
10^-1
0.5
10^0
2
Period (s)
All - Tot. Str.
1-D 1-C
1-D 3-C
Obs. EW

Figure S7

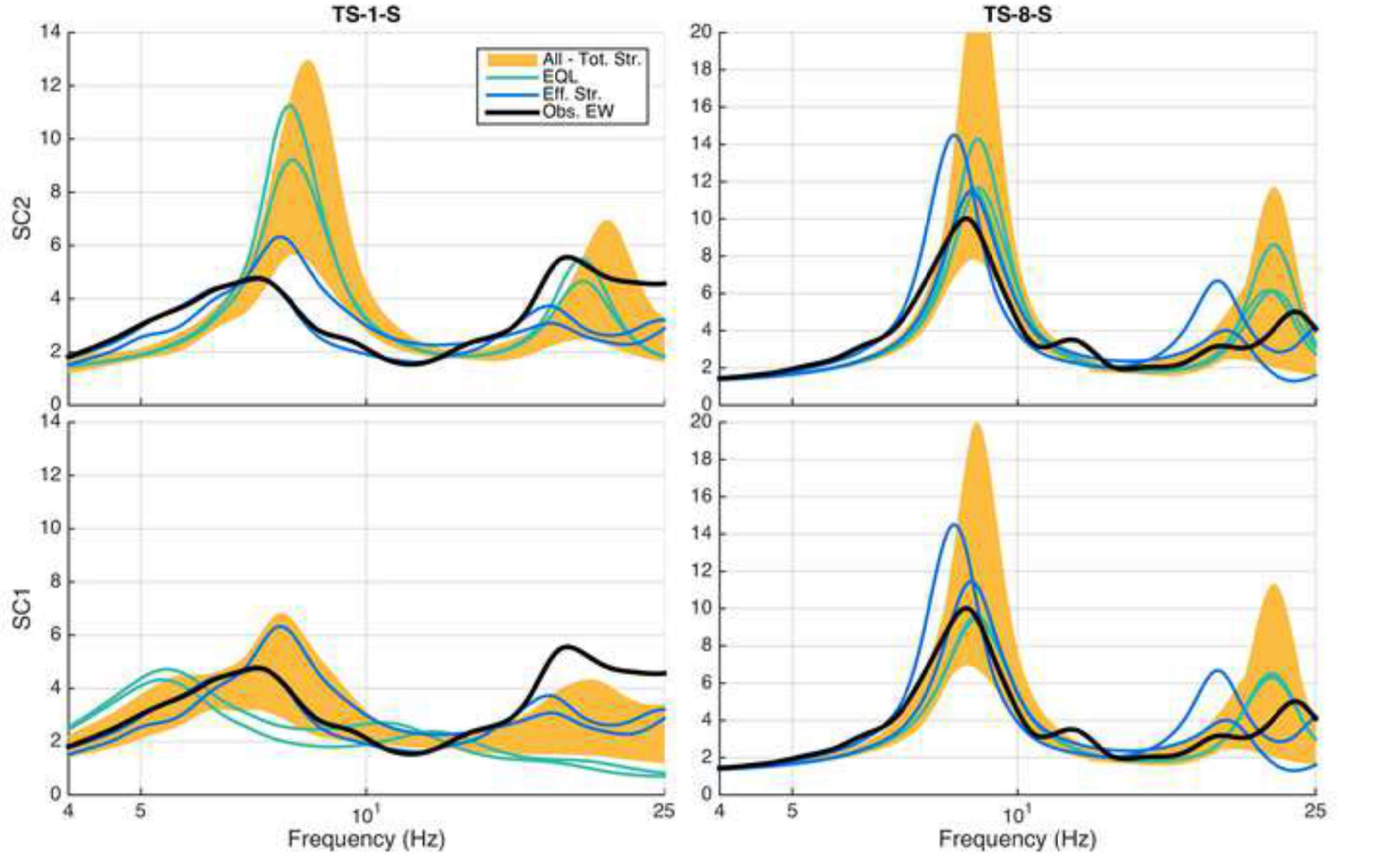
TS-1-S
TS-8-S
All - Tot. Str.
EQL
Eff. Str.
Obs. EW
SC2
SC1
Frequency (Hz)
Frequency (Hz)
4
5
10^1
25
0
2
4
6
8
10
12
14
16
18
20

Table S1: List of the teams that participate to the PRENOLIN benchmark with references on the code used.

Team Name	Affiliation	Team Index		Code Name	*Code Reference*
D. Asimaki & J. Shi	Caltech, Pasadena, California	**A**	**0**	SeismoSoil	(Li and Assimaki, 2010; Matasovic and vucetic, 1993; Shi and Asimaki, 2017)
S. Iai	DPRI, Kyoto University, Kyoto, Japan	**B**	**0**	FLIP	(Iai, 1990)
S. Kramer	University of Washington, Seattle, Washington	**C**	**0**	PSNL	(In development)
E. Foerster	CEA, France	**D**	**0**	CYBERQUAKE	(Modaressi and Foerster, 2000)
C. Gelis	IRSN, France	**E**	**0**	NOAH-2D	(Iai, 1990)
A. Giannakou	Fugro, Nanterre Cedex, France	**F**	**0**	DEEPSOIL 5.1	(Hashash et al., 2012)
G. Gazetas, E. Garini & N. Gerolymos	NTUA, Greece	**G**	**0**	NL-DYAS	(Gerolymos and Gazetas, 2006, 2005)5)
J. Gingery & A. Elgamal	UCSD, La Jolla, California	**H**	**0**	OPENSEES-UCSD-SOIL-MODEL	See Data and Resources
Y. Hashash & J. Harmon	Univ, Illinois,US	**J**	**0**	DEEPSOIL-NL 5.1	(Hashash et al., 2012)
		J	**1**	DEEPSOIL-EL 5.1	(Hashash et al., 2012)
P. Moczo, J. Kristek & A. Richterova	CUB, Comenius University, Bratislava, Slovakia	**K**	**0**	1DFD-NL-IM	
S. Foti & S. Kontoe	Politecnico di Torino, Torino, Italy and Imperial College, United Kingdom	**L**	**1**	ICFEP	(Kontoe, 2006; Potts and Zdravkovic, 1999; Taborda et al., 2010)
		L	**2**	DEEPSOIL-NL 5.1	(Hashash et al., 2012)
G. Lanzo, S. Suwal, A. Pagliaroli & L. Verrucci	University of Rome La Sapienza and University of Chieti-Pescara, Italy	**M**	**0**	FLAC_7,00	(ITASCA, 2011)
		M	**1**	DMOD2000	(Matasović and Ordóñez, 2007)
		M	**2**	DEEPSOIL 5.1	(Hashash et al., 2012)
F. Lopez-Caballero & S. Montoya-Noguera	CentraleSupélec, Paris-Saclay University, Châtenay-Malabry, France	**N**	**0**	GEFDyn	(Aubry and Modaressi, 1996)
F. De-Martin	BRGM, France	**Q**	**0**	EPISPEC1D	(Iai, 1990) See Data and Resources
B .Jeremić , F. Pisanò & K. Watanabe	UCD, LBLN, TU Delft & Shimizu Corp	**R**	**0**	real ESSI Simulator	See Data and Resources
A. Nieto-Ferro, D. Vandeputte	EDF, Paris & Aixen-Provence, France	**S**	**0**	ASTER	See Data and Resources
A. Chiaradonna, F. Silvestri & G. Tropeano	UNICA and University of Naples, Naples, Italy	**T**	**0**	SCOSSA_1,2	(Tropeano et al., 2016)
		T	**1**	STRATA	
M.P. Santisi d'Avila	University of Nice Sophia Antipolis, Nice, France	**U**	**0**	SWAP_3C	(Santisi d'Avila et al., 2012, 2013; Santisi d'Avila and Semblat, 2014)
D. Mercerat and N. Glinsky	CEREMA, France	**Y**	**0**	DGNL	(Mercerat and Glinsky, 2015)
D. Boldini, A. Amorosi, A. di Lernia & G. Falcone	Unversity of Bologna, Sapienza University of Rome, and Politecnico di Bari, Italy	**Z**	**0**	EERA	(Bardet et al., 2000)
		Z	**1**	PLAXIS	(Benz, 2006; Benz et al., 2009)
M. Taiebat & P. Arduino	UBC, British Columbia, Canada and University of Washington, Seattle, Washington	**W**	**0**	Opensees	See Data and Resources

DPRI, Disaster Prevention Research Institute; CEA, Commissariat à l'Energie Atomique; IRSN, Institut de Radioprotection et de Sûreté Nucléaire; NTUA, National Technical University of Athens; UCSD, University of California, San Diego; ECP, Eclode Centrale Paris-Supelec; BRGM, Bureau De Recherches Géologiques et Minières; UCD, University of California, Davis; LBLN, Lawrence Berkeley National Laboratory; EDF, Electricité de France; UNICA, University of Calgari; CEREMA, centre d'études et d'expertise sur les risques, l'environnement, la mobilité et l'aménagement; UBC, University of British Columbia.